

BIOMEDICAL POLYMERS FROM TYROSOL:  
THE INFLUENCE OF CARBONATE ISOMER  
SEQUENCE AND PHASE BEHAVIOR ON  
EROSION AND MECHANICAL  
PERFORMANCE

By

SVEN DANIEL SOMMERFELD

A dissertation submitted to the  
Graduate School—New Brunswick  
Rutgers, The State University of New Jersey  
in partial fulfillment of the requirements

for the degree of

Doctor of Philosophy

Graduate Program in Chemistry and Chemical Biology

written under the direction of

Joachim Kohn

and approved by

---

---

---

---

New Brunswick, New Jersey

October, 2014

## **ABSTRACT OF THE DISSERTATION**

# **Biomedical Polymers from Tyrosol: The Influence of Carbonate Isomer Sequence and Phase Behavior on Erosion and Mechanical Performance**

**By SVEN DANIEL SOMMERFELD**

**Dissertation Director:**

**Joachim Kohn**

Polycarbonates are a class of degradable polymers used in biomedical applications including vehicles for drug-delivery and scaffolds for tissue engineering. They can be classified into two groups i.e. aliphatic and aromatic polycarbonates, each with distinctive mechanical properties and degradation mechanisms.

Aliphatic polycarbonates are soft and flexible materials most suitable for cartilage or blood vessel repair. Aromatic polycarbonates are strong and stiff, useful for hard-tissue applications such as bone regeneration. While aliphatic polycarbonates may undergo a surface erosion process mediated by biological activity, aromatic polycarbonates as for example tyrosine-derived compositions undergo hydrolytic degradation and slow mass erosion.

In this thesis, aromatic-aliphatic polycarbonates from natural (hydroxyalkyl)phenols such as tyrosol were explored with the rationale of combining the advantages of both



classes of polycarbonates.

Copolymers of tyrosol and homovanillyl alcohol had high tensile strength, and showed enzymatic surface erosion by lipase, *in vitro*. During erosion, mechanical properties were retained for at least 18 weeks: The wet modulus of  $E_T = 0.9 \pm 0.1$  GPa was retained at 65% (w/w) mass loss (rate =  $0.14 \pm 0.01$  mg cm<sup>-2</sup> d<sup>-1</sup>).

The aromatic–aliphatic polycarbonates from (hydroxyalkyl)phenols showed sequence isomerism of diaryl, dialkyl, and aryl alkyl carbonate bonds. In order to control the carbonate isomer sequence, a selective synthesis methodology for diaryl and dialkyl carbonate diols as pre-programmed monomers was developed.

An alternating sequence (*alt*) of diaryl and dialkyl carbonates demonstrated dramatic changes of the phase behavior and erosion as compared to the scrambled sequence (*scr*): A faster erosion rate of  $0.36 \pm 0.01$  mg cm<sup>-2</sup> d<sup>-1</sup> for amorphous *alt* was observed. When heated, *alt* readily attained a 3-dimensional crystalline order, whereas *scr* showed sluggish transition into a 1-dimensional mesophase. Oriented and annealed films of *alt* had improved stiffness with  $E_T = 5.4 \pm 0.3$  GPa as compared to *scr* and poly(l-lactic acid) with  $E_T = 3.8 \pm 0.2$  GPa and  $E_T = 3.8 \pm 0.3$  GPa, respectively.

The *in vivo* subcutaneous implantation of polymer discs resulted in slow mass loss after 3 months. However, the surface morphology appeared strikingly similar to *in vitro* samples. Further investigation into implant location and specimen dimensions may help to identify conditions for the *in vivo* resorbability.

## Acknowledgments

I would like to acknowledge my thesis advisor Dr. Joachim Kohn for giving me the opportunity to work in his laboratory, his support and mentorship.

My committee members, Dr. Ralf Warmuth, Dr. Gene S. Hall and Dr. Michael Jaffe who were wonderful co-advisors.

A special thank you to Dr. Zheng Zhang as a great mentor, discussion partner and friend as well as to Dr. Jared Bushman for encouraging persistence and curiosity.

Dr. Sanjeeva Murthy for the great mentorship in material sciences and polymer physics, Dr. Das Bolikal and Barry Cunningham for mentorship in polymer synthesis, Dr. Arnold Luk for introduction into QCM-D, Dr. Lauren Macri for mentorship in project management, Dr. Murat Guvendiren for advice on manuscript writing.

For assistance with parts of the experimental work: Dr. Sanjeeva Murthy, Koustubh Dube, Dr. Zheng Zhang, Courtney Yurecko, Yangmin Chen.

For help in editing and proof reading: Koustubh Dube, Dr. Murat Guvendiren, Dr. Zhang Zheng, Dr. Vinod Damodaran, Barry Cunningham. My helpful and collegial co-workers: Ganesan Subramanian, Dr. Carole Kantor, Dr. Dave Devore, Dr. Loreto Valenzuela, Dr. Aniq Darr, Carmine Iovine, Dr. Marius Costache, Matt Laughland, Richard Farias, Dr. Jenny Raynor, Dr. Hanshella Magno, Veena Bolikal, Dr. Larisa Sheihet, Dr. Pallasana Narayanan, Edward Phillips. My collaborators, Dr. Helena Felgueiras, Rene O'cuto, Dr. Jędrzej Skrobot, Dr. Prabhas Moghe, Dr. Jocie Cherry, Dr. Sebastian Vega, Dr. Jim Kaduk, Dr. Adriana Martin. The office: John Bushby, Valentina Petrenko, Shah Shrey, Kristen Ryan, Carmen Castro, John Watkins, Carol Lenardson, Allison Larkin. Financial support: RESBIO (P41EB001046), AFIRM (W8IXWH-05-2-0034), REVA Medical Inc., NJCBM.

# Dedication

For my parents, Marie-Luise Sommerfeld and Klaus-Dieter Sommerfeld.

My brother, Benjamin Isermann.

# Table of Contents

<b>Abstract</b> . . . . .	ii
<b>Acknowledgments</b> . . . . .	iv
<b>Dedication</b> . . . . .	v
<b>List of Tables</b> . . . . .	ix
<b>List of Figures</b> . . . . .	xi
<b>List of Abbreviations</b> . . . . .	xix
<b>1. Introduction</b> . . . . .	1
1.1. Polymeric Systems for Biomedical Applications . . . . .	1
1.2. Polymer Synthesis . . . . .	8
1.3. Rationale and Hypotheses . . . . .	11
1.4. Research Objective and Organization . . . . .	12
<b>2. Materials and Methods</b> . . . . .	13
2.1. Materials . . . . .	13
2.2. Methods . . . . .	14
<b>3. Enzymatic Surface Erosion of High Tensile Strength Polycarbonates Based on Natural Phenols</b> . . . . .	18
3.1. Abstract . . . . .	18
3.2. Introduction . . . . .	19

3.3. Experimental . . . . .	22
3.4. Results and Discussion . . . . .	24
3.5. Conclusion . . . . .	40
<b>4. Highly Chemoselective Phosgenation of (Hydroxyalkyl)phenols for Pre-Programmed Carbonate Diols . . . . .</b>	<b>41</b>
4.1. Abstract . . . . .	41
4.2. Introduction . . . . .	42
4.3. Experimental . . . . .	43
4.4. Results and Discussion . . . . .	50
4.5. Conclusions . . . . .	58
<b>5. Physicochemical Properties of Degradation Intermediates . . . . .</b>	<b>60</b>
5.1. Abstract . . . . .	60
5.2. Introduction . . . . .	61
5.3. Experimental . . . . .	62
5.4. Results and discussion . . . . .	64
5.5. Conclusion . . . . .	75
<b>6. Sequence Structure in Degradable, Aromatic–aliphatic Polycarbon- ates from Tyrosol Provides Control Over Phase Transitions and Bio- erosion . . . . .</b>	<b>76</b>
6.1. Abstract . . . . .	76
6.2. Introduction . . . . .	77
6.3. Experimental . . . . .	79
6.4. Results and Discussion . . . . .	82
6.5. Conclusion . . . . .	104

<b>7. The <i>In Vivo</i> Behavior of Polycarbonates from Tyrosol and 1,3-propanediol</b>	105
7.1. Abstract	105
7.2. Introduction	106
7.3. Experimental	108
7.4. Results and Discussion	109
7.5. Conclusion	119
<b>Appendices</b>	138
Supporting Information Chapter 3	139
Supporting Information Chapter 4	140
Supporting Information Chapter 6	154
Supporting Information Chapter 7	162

## List of Tables

3.1. Chemical shift assignment from $^1\text{H}$ -NMR spectra . . . . .	26
3.2. Distribution of sequence isomers in polycarbonate backbone . . . . .	27
3.3. Physical properties of polycarbonates from Ty and Hva . . . . .	29
3.4. Mechanical properties of polycarbonates from Ty and Hva . . . . .	30
3.5. Mechanical properties of poly(tyrosol carbonate) during erosion . . . .	34
3.6. Temperature-dependent erosion behavior of QCM-D and macroscopic films . . . . .	37
4.1. Optimization study for biphasic diaryl carbonate diol synthesis . . . .	51
4.2. Substrate scope for diaryl carbonate diols of (hydroxyalkyl)phenols from biphasic reactions . . . . .	52
4.3. Solvent optimization for aliphatic chlorocarbonyl . . . . .	54
4.4. Substrate scope for aliphatic chlorocarbonyl . . . . .	56
4.5. Substrate scope for aliphatic dialkyl carbonate diol . . . . .	57
5.1. Half-lives of pH-dependent hydrolysis and rate constants $k_{OH}$ in aque- ous solution for carbonate diols from tyrosol. . . . .	69
5.2. Temperature-dependent solubility of carbonate diols from tyrosol and tyrosol in PBS at pH = 7 . . . . .	70
6.1. Summary of thermal and crystalline properties of <i>scr</i> and <i>alt</i> . . . . .	90
6.2. Bioerosion rates of <i>scr</i> and <i>alt</i> . . . . .	101
7.1. Physical properties of polycarbonates from Ty and PD . . . . .	110
7.2. Mechanical properties of polycarbonates from Ty and PD . . . . .	111
7.3. Comparison of <i>in vivo</i> and <i>in vitro</i> erosion . . . . .	117

4.	Summary of Thermal and crystalline properties of <i>scr</i> and <i>alt</i> , controls powder and ambient cooled films. . . . .	155
----	---	-----



## List of Figures

1.1. Structures of aromatic and aliphatic polycarbonates: (A) poly(ethylene carbonate), (B) poly(trimethylene carbonate), (C) poly(tetramethylene carbonate), (D) poly(BPA carbonate), (E) poly(DTE carbonate). . .	1
1.2. Co- and terpolycarbonates for biomedical applications: (A) Random, block terpolymer of DTE, DT and PEG, (B) random copolymer of TMC and CL, (C) tri-block copolymer of DTR-diester and mPEG, (D) triblock copolymer of TMC. . . . .	4
1.3. Examples of current innovations in polycarbonate technology: (A) Poly(1,3-glycerol carbonate), (B) poly(1,2-glycerol carbonate), (C) allyl functionalized polycarbonate, (D) poly(cyclohexene carbonate), (E) poly(limonene carbonate), (F) poly(D-glucose carbonate), (G) poly-(ferrulic acid- <i>co</i> -tyrosyl ester carbonate). . . . .	6
1.4. Reaction schemes for polycarbonates synthesis: (A) Interfacial polymerization using phosgene equivalent, (B) anhydrous, organic solvent with phosgene equivalent and organic base, (C) ring-opening polymerization using stannous octoate with TMC, (D) direct polymerization of carbon dioxide with epoxide using catalyst. . . . .	8
1.5. Structures of phosgene and equivalents: (A) Phosgene, (B) diphosgene (trichloromethylchloroformate), (C) triphosgene (bis(trichloromethyl)-carbonate, BTC), (D) diethyl carbonate, (E) diphenyl carbonate. . .	10
3.1. Chemical structures of (A) tyrosol, (B) homovanillyl alcohol, (C) poly-(tyrosol- <i>co</i> -homovanillyl carbonate). . . . .	24

3.2.	Results of $^1\text{H}$ NMR spectroscopy on polycarbonate compositions of Ty/Hva (mol %) 100/0, 90/10, 75/25, 50/50, and 0/100 with notations of respective peak assignments referenced to DMSO- $d^6$ : (A) Overlay spectra, (B) polymer sequence isomers at carbonate bond: head-to-head, tail-to-tail, head-to-tail. . . . .	25
3.3.	$^{13}\text{C}$ -NMR spectrum (126 MHz, DMSO- $d^6$ ) of poly(tyrosol carbonate): Zoom into chemical shift of aromatic ring carbon $\text{C}_4$ ( $\delta$ 135–136 ppm) with assignments of triads A, B, C, D. . . . .	28
3.4.	(A) Relative mass retention of specimens with compositions of Ty/Hva (mol %) 100/0, 90/10, 75/25, 50/50, and 0/100 incubated in lipase solution at 37 °C, (B) correlation between relative mass and thickness loss of poly(tyrosol carbonate). . . . .	32
3.5.	Relative $M_w$ retention of (A) polycarbonate specimens with compositions of Ty/ Hva (mol %) 100/0, 90/10, 75/25, 50/50, 0/100 incubated in lipase solution, (B) 100/0 and 90/10 in lipase and PBS control at 37 °C. . . . .	32
3.6.	SEM morphology of surfaces of disc shaped specimens from poly(tyrosol carbonate) after incubation in lipase: (A) 0 weeks, (B) 1 week, (C) 4 weeks, (D) 6 weeks, (E) 9 weeks, (F) 9 weeks, PBS control. . .	33
3.7.	(A) QCM-D temperature dependent frequency plots of thin films from compositions of Ty/Hva (mol %) 100/0, 90/10, 75/25, 50/50, and 0/100, (B) lipase adsorption at 20 °C, (C) rate of mass loss per area in dependence of temperature, (D) illustration of lipase adsorption, erosion and end behavior. . . . .	36

3.8. Cell viability of hMSCs on polycarbonate substrates of Ty/Hva (mol %)	
100/0, 90/10, 50/50 after 4 h, 4 days, and 7 days: (A) Representative images from epifluorescence microscopy on hMSC morphology,	
(B) cell density determined by AlamarBlue assay relative to standards on TCPS. . . . .	39
5.1. UV absorption spectra (200–300 nm, acetonitrile): (A) Diaryl carbonate diol <b>2a</b> , (B) dialkyl carbonate diol <b>4a</b> , tyrosol <b>1a</b> . . . . .	65
5.2. Reaction scheme for the hydrolytic degradation of carbonate diols <b>2a</b> and <b>4a</b> in aqueous solution with rate constant $k_{obs}$ . . . . .	66
5.3. Kinetic plots for the hydrolysis of carbonate diols ( <b>2a</b> , pH = 10): (A) Decay curve (area under peak from HPLC), (B) logarithmic concentration change over time. . . . .	67
5.4. Logarithmic plots of hydrolysis rate constant ( $k_{obs}$ ) over the pH for carbonate diols <b>2a</b> and <b>4a</b> . . . . .	68
5.5. QCM-D comparison of lipase erosion of thin films from poly(tyrosol-carbonate): (A) Flow = 24 $\mu\text{L min}^{-1}$ , (B) stopped-flow at 37 °C in PBS, (C) illustration of thin film erosion by lipase. . . . .	71
5.6. SEM images of surface layers of poly(tyrosol carbonate): (A) and (C) aqueous rinse, (B) rinse with 70% (w/v) ethanol, after lipase incubation, (D) PBS control, <i>in vitro</i> incubation at 37 °C. . . . .	73
6.1. Fabrication of oriented polymer films: (A) Quenched (B) annealed, (C) stretched above $T_g$ from quenched, (D) stretched and annealed. . . .	80
6.2. Synthesis and structure of polycarbonates from tyrosol with controlled carbonate isomer sequences: (A) Alternating sequence ( <i>alt</i> ), (B) scrambled sequence ( <i>scr</i> ), (C) directional sequence ( <i>dir</i> ). . . . .	82
6.3. $^{13}\text{C}$ NMR spectra (126 MHz, $\text{CDCl}_3$ ), poly(tyrosol carbonate): (top) <i>alt</i> , (middle) <i>dir</i> , (bottom) <i>scr</i> , zoom into carbonate chemical shift ( $\delta$ 151–156 ppm) with assignments of HH, TT, HT. . . . .	83

6.4.	$^1\text{H}$ NMR (500 MHz, $\text{CDCl}_3$ ), poly(tyrosol carbonate): (top) <i>alt</i> , (middle) <i>dir</i> , (bottom) <i>scr</i> , zoom into $\text{C}_\alpha\text{H}_2$ chemical shift ( $\delta$ 4.2–4.5 ppm) with assignments of HH, TT, HT. . . . .	84
6.5.	DSC scans of quenched and annealed polycarbonate films of <i>scr</i> and <i>alt</i> : (A) First heating, overview, (B) first heating, zoom into $T_g$ , (C) cooling, (D) second heating. Rate = $10\text{ }^\circ\text{C min}^{-1}$ , exotherm up. . . .	85
6.6.	Powder X-ray diffraction patterns of films from poly(tyrosol carbonate): (Top) <i>alt</i> , (bottom) <i>scr</i> , (A) and (C) quenched, (B) and (D) annealed. . . . .	87
6.7.	(A) SAXS and (B) WAXS scans of <i>alt<sub>q</sub></i> , simultaneous experiment during heating. (C) Interpretation of phase behavior of <i>alt<sub>q</sub></i> during heating in DSC. . . . .	88
6.8.	X-ray diffraction patterns in 2-D of films from poly(tyrosol carbonate): (Top) <i>alt</i> , (bottom) <i>scr</i> , (A) and (E) quenched, (B) and (F) annealed, (C) and (G) quenched and stretched, (D) and (H) quenched, annealed and stretched. . . . .	92
6.9.	A 3-dimensional structural model for <i>alt</i> derived from the diffraction pattern of the highly oriented and crystalline film (quenched, stretched and annealed): (A) Side view of the unit cell, (B) top view, (C) zoom into the diaryl carbonate, (D) unit cell parameters. . . . .	93
6.10.	Stress-strain curves of films from poly(tyrosol carbonate) <i>alt</i> and <i>scr</i> : (A) Unoriented, (B) oriented. . . . .	95
6.11.	Mechanical properties of films from poly(tyrosol carbonate) <i>alt</i> and <i>scr</i> in comparison to PLLA and poly(DTE carbonate): (A) and (B) Tensile Modulus, (C) and (D) stress at yield. . . . .	96

6.12. Bioerosion of poly(tyrosol carbonate) <i>alt</i> and <i>scr</i> : (A) Mass loss per area, (B) thickness loss, (C) correlation between relative mass and thickness loss. Disc shaped specimens incubated in lipase solution at 37 °C. . . . .	98
6.13. SEM morphology of surfaces of compression molded discs of poly(tyrosol carbonate): (Left) <i>scr</i> , (right) <i>alt</i> , (A), (B), (C) and (D) 3 months <i>in vivo</i> , (E) and (F) 3 weeks <i>in vitro</i> , incubation in lipase solution at 37 °C. . . . .	103
7.1. Chemical structures of (A) poly(tyrosol carbonate), (B) 85/15, (C) 76/24 molar ratios of Ty/PD in poly(tyrosol- <i>co</i> -1,3-propanediol carbonate). . . . .	109
7.2. Explant overview images: (Top) 3 weeks, (bottom) 3 months, (A) and (D) 100/0, copolymers with molar ratios of Ty/PD of (B) and (E) 85/15, (C) and (F) 76/24. . . . .	112
7.3. SEM morphology of explant surfaces of polycarbonates from Ty/PD of (left) 100/0, (middle) 85/15, (right) 76/24 molar ratios, (A), (B), (C) 3 weeks detail, (D), (E), (F) 3 months detail, (G), (H), (I) 3 months overview. . . . .	114
7.4. <i>In vitro</i> erosion: (A) Mass loss per area, (B) thickness loss of polycarbonates from Ty/PD with molar ratios of 100/0, 85/15 and 76/24 incubated in lipase solution at 37 °C. . . . .	116
7.5. Microscopic images from histological slides of polycarbonates from Ty/PD with molar ratios of (left) 100/0, (middle) 85/15, (right) 76/24, (A), (B), (C) 3 weeks, (D), (E), (F) 3 months, (G) scale bar. . . . .	118
S1. (A) Stress-strain curves of compositions of Ty/ Hva (mol %) 100/0, 90/10, 75/25, 50/50, 0/100 in the wet state, PBS at 37 °C, (B) stress-strain curves for poly(tyrosol carbonate) in the dry state at ambient temperature and wet state, PBS at 37 °C. . . . .	139

S2.	NMR spectra, bis(4-(2-hydroxyethyl)phenyl) carbonate <b>2a</b> . . . . .	140
S3.	NMR spectra, bis(4-(3-hydroxypropyl)phenyl) carbonate <b>2b</b> . . . . .	141
S4.	NMR spectra, bis(4-(2-hydroxyethyl)-2-methoxyphenyl) carbonate <b>2c</b> . . . . .	142
S5.	NMR spectra, bis(4-(2-hydroxymethyl)phenyl) carbonate <b>2e</b> . . . . .	143
S6.	NMR spectra, bis(4-(3-hydroxymethyl)phenyl) carbonate <b>2f</b> . . . . .	144
S7.	<sup>1</sup> H NMR (400 MHz, CDCl <sub>3</sub> ): Global spectral deconvolution of chloro- formate and trichloromethyl carbonate species formed <i>in situ</i> . . . . .	145
S8.	NMR spectra, 4-hydroxyphenethyl carbonochloridate <b>3a</b> and 4-hy- droxyphenethyl(trichloromethyl)carbonate <b>3a*</b> . . . . .	146
S9.	NMR spectra, 3-(4-hydroxyphenyl)propyl carbonochloridate <b>3b</b> and 3-(4-hydroxyphenyl)propyl(trichloromethyl)carbonate <b>3b*</b> . . . . .	147
S10.	NMR spectra, 4-hydroxy-3-methoxyphenethyl carbonochloridate <b>3c</b> and 4-hydroxy-3-methoxyphenethyl(trichloromethyl)carbonate <b>3c*</b> . . . . .	148
S11.	NMR spectra, 2-hydroxyphenethyl carbonochloridate <b>3d</b> and 2-hy- droxyphenethyl(trichloromethyl)carbonate <b>3d*</b> . . . . .	149
S12.	NMR spectra, bis(4-hydroxyphenethyl) carbonate <b>4a</b> . . . . .	150
S13.	NMR spectra, bis(3-(4-hydroxyphenyl)propyl) carbonate <b>4b</b> . . . . .	151
S14.	NMR spectra, bis(4-hydroxy-3-methoxyphenethyl) carbonate <b>4c</b> . . . . .	152
S15.	NMR spectra, bis(2-hydroxyphenethyl) carbonate <b>4d</b> . . . . .	153
S16.	<sup>13</sup> C NMR spectra (126 MHz, CDCl <sub>3</sub> ) of poly(tyrosol carbonate): (Top) <i>alt</i> , (middle) <i>dir</i> , (bottom) <i>scr</i> . Full spectrum overlay. . . . .	154
S17.	DSC scans of polymer powder and ambient cooled polycarbonate films of <i>scr</i> and <i>alt</i> : (A) First heating, (B) cooling, (C) second heating. Rate = 10 °C min <sup>-1</sup> , exotherm up. . . . .	155
S18.	DSC scans of oriented polycarbonate films: (A) <i>alt</i> , (B) <i>scr</i> . First heating scans of quenched, stretched, stretched & annealed films, rate = 10 °C min <sup>-1</sup> , exotherm up. . . . .	156

S19. DSC slow scans of quenched polycarbonate films: (A) <i>alt</i> , (B) <i>scr</i> . First heating, cooling and second heating, rate = 1 °C min <sup>-1</sup> , exotherm up. . . . .	156
S20. Powder X-ray diffraction patterns of poly(tyrosol carbonate): (Top) <i>alt</i> , (bottom) <i>scr</i> , (A) and (C) polymer powder, (B) and (D) ambient cooled films. . . . .	157
S21. (A) Stress-strain curve of films of <i>alt</i> and <i>scr</i> at T <sub>g,wet</sub> , (B) X-ray diffraction in 2-D of <i>alt</i> , quenched and stretched. . . . .	157
S22. X-ray diffraction in 2-D of films of control polymers: (Top) PLLA, (bottom) poly(DTE carbonate), (A) and (D) quenched, (B) and (E) quenched and stretched, (C) quenched, annealed and stretched. . . .	158
S23. X-ray diffraction in 2-D of quenched films from poly(tyrosol carbonate) over time: (A) <i>alt</i> , 2 months in PBS (B) <i>scr</i> , 2 months in lipase (C) <i>scr</i> , 2 months in PBS. . . . .	158
S24. Bioerosion of <i>alt</i> or <i>scr</i> at high and low M <sub>w</sub> , control in PBS . . . . .	159
S25. Bioerosion of <i>alt</i> or <i>scr</i> at quenched, stretched and annealed or ambient cooled in lipase solution . . . . .	159
S26. Bioerosion control of quenched, compression molded films from PLLA and poly(DTE carbonate) . . . . .	160
S27. Dimensional stability of <i>alt</i> and <i>scr</i> polymer films . . . . .	160
S28. Relative cell viability of polycarbonate films with <i>alt</i> or <i>scr</i> sequence	161
S29. (A) SAXS and (B) WAXS scans of <i>alt</i> <sub>q</sub> , simultaneous experiment dur- ing heating, rate = 10 °C min <sup>-1</sup> , exotherm up. . . . .	161
S30. <sup>1</sup> H NMR (500 MHz, DMSO- <i>d</i> <sup>6</sup> ) spectrum: poly(tyrosol- <i>co</i> -1,3-propane- diol carbonate) with 75/15 molar ratio of Ty/PD. . . . .	162
S31. <sup>1</sup> H NMR (500 MHz, DMSO- <i>d</i> <sup>6</sup> ) spectrum: poly(tyrosol- <i>co</i> -1,3-propane- diol carbonate) with 76/24 molar ratio of Ty/PD. . . . .	163

S32. Bioerosion of Ty/PD: (A) Mass loss per area, (B) thickness loss, incubation in PBS at 37 °C. . . . .	163
---	-----



## List of Abbreviations

ACN acetonitrile

*alt* alternating

DI deionized

BTC bis(trichloromethyl) carbonate

BPA bisphenol A

DCM dichloromethane

*dir* directional

DMF *N, N*-dimethylformamide

DMSO dimethylsulfoxide

DSC differential scanning calorimetry

D dissipation factor

DT desaminotyrosyl-tyrosine

DTE desaminotyrosyl-tyrosine ethyl ester

ESI MS electrospray ionization mass-spectrometry

equiv. equivalent

FDA food and drug administration

GPC gel permeation chromatography

Hva homovanillyl alcohol

HPLC high-performance liquid chromatography

hMSCs human mesenchymal stem cells

IPA isopropanol, 2-propanol

MDAT 3-(4-methoxyphenyl)propionic acid

$M_n$  number molecular weight average

$M_w$  molecular weight average  
mPEG methyl terminated poly(ethylene glycol)  
NMR nuclear magnetic resonance  
NaOH sodium hydroxide  
PBS phosphate buffered saline  
PCL polycaprolactone  
PD 1,3-propylenediol  
PEC poly(ethylene carbonate)  
PDLLA poly(D,L-lactic acid)  
PEG poly(ethylene glycol)  
PFA paraformaldehyde  
PLA poly(lactic acid)  
PLLA poly(L-lactic acid)  
PTMC poly(trimethylene carbonate)  
Py pyridine  
QCM-D quartz crystal microbalance with dissipation  
R rest  
*scr* scrambled  
SAXS small angle x-ray scattering  
SD standard deviation  
SE standard error  
SEM scanning electron microscope  
 $T_c$  glass transition temperature  
TCPS tissue culture polystyrene  
 $T_g$  glass transition temperature  
TGA thermogravimetric analysis  
THF tetrahydrofuran  
TLL lipase from *Thermomyces lanuginosus*

TMS trimethyl silyl

$T_m$  melting temperature

Ty tyrosol

WAXS wide angle x-ray scattering

WU = water uptake

# Chapter 1

## Introduction

### 1.1 Polymeric Systems for Biomedical Applications

#### 1.1.1 Aromatic and Aliphatic Polycarbonates

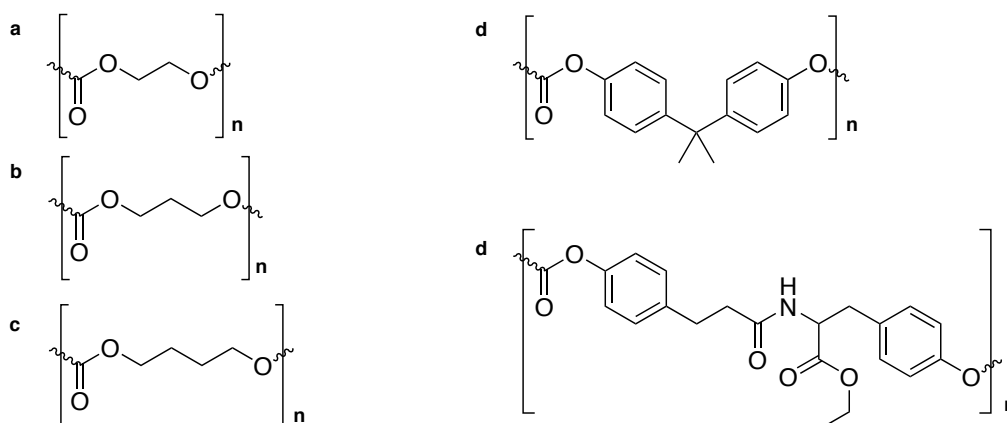


Figure 1.1: Structures of aromatic and aliphatic polycarbonates: (A) poly(ethylene carbonate), (B) poly(trimethylene carbonate), (C) poly(tetramethylene carbonate), (D) poly(BPA carbonate), (E) poly(DTE carbonate).

For biomedical applications, several fundamental structures of polycarbonates, polymers of carbon dioxide and diols, have been considered for biomedical applications (Figure 1.1). Polycarbonates can be divided into two groups, depending on the nature of the backbone linkages: Aliphatic polycarbonates (23) and aromatic polycarbonates (115). Poly(trimethylene carbonate) (PTMC) is the most extensively investigated aliphatic polycarbonate (143). While PTMC of low molecular weight is semi-crystalline featuring a low  $M_p$ , PTMC of high molecular weight is amorphous and rubbery (68). PTMC is characterized by a low tensile modulus of less than 7

MPa. Further, strain-induced crystallization occurs in PTMC resulting in relatively high ultimate tensile strength of around 17 MPa (100). PTMC is a degradable polymer that undergoes surface erosion, when implanted *in vivo*. Most likely, enzymatic activity is involved in the bioerosion. The *in vivo* erosion behavior can be simulated by incubation in lipase *in vitro*. At the same time, the hydrolytic degradation rate is negligible (143; 141). Other aliphatic polycarbonates that features longer methylene chains such as poly(tetramethylene carbonate) also shows enzymatic erosion (122). In contrast, polycarbonates with shorter chains such as poly(ethylene carbonate) (PEC) are less susceptible to an enzymatic attack. However, rapid erosion was observed *in vivo* for PEC (50). In this case, reactive oxygen species may be responsible mediating the erosion process. As a result from a radical induced unzipping mechanism cyclic degradation products were obtained (31).

The original aromatic polycarbonate derived from bisphenol A (2,2-bis(4-hydroxyphenyl)propane, BPA) is an important engineering plastic with excellent mechanical properties such as a tensile modulus of 2 GPa. However, in spite of the degradable carbonate linkage, poly(DTE carbonate) is not degradable by hydrolysis due to its low water uptake. Thus, its use for temporary biomedical applications is limited (38). In addition, scrutinization of possible adverse health effects of BPA has been growing. Already, early studies noted that BPA is able to mimic estrogen activity (34). Nonetheless, BPA-derivatives remain extremely popular in the context of restorative dental use in the clinic (26).

As an alternative to polycarbonates from BPA, polymers derived from diphenolic, pseudo-amino acid monomers were developed (74; 39; 107). To overcome the drawbacks of aromatic polycarbonates, the polycarbonates based on pseudo-amino acids contain an additional amide bond to favor degradability by increasing the water uptake. In addition, monomeric units are designed in such a way that after hydrolysis of all degradable bonds only non-toxic compounds are released. Considering scrutinization by FDA regulations, it is a minimal requirement that the end products of

degradation must be *generally considered as safe* (GRAS). The mechanical properties and processability of poly(BPA carbonate) are matched by poly(BPA carbonate), in specific. This polymer indeed showed hydrolytic degradation (49) and when implanted into bone, a benign tissue response. In this case, direct bone-material bonding was observed (54). Albeit *in vitro* degradation (125), the resorption *in vivo* was minimal within a time period of 3 years (126). In the light of the slow resorption *in vivo* several improvements of the parent poly(DTE carbonate) have been reported leading to a discussion about copolymerization continued below.

### 1.1.2 Specialty Copolymers

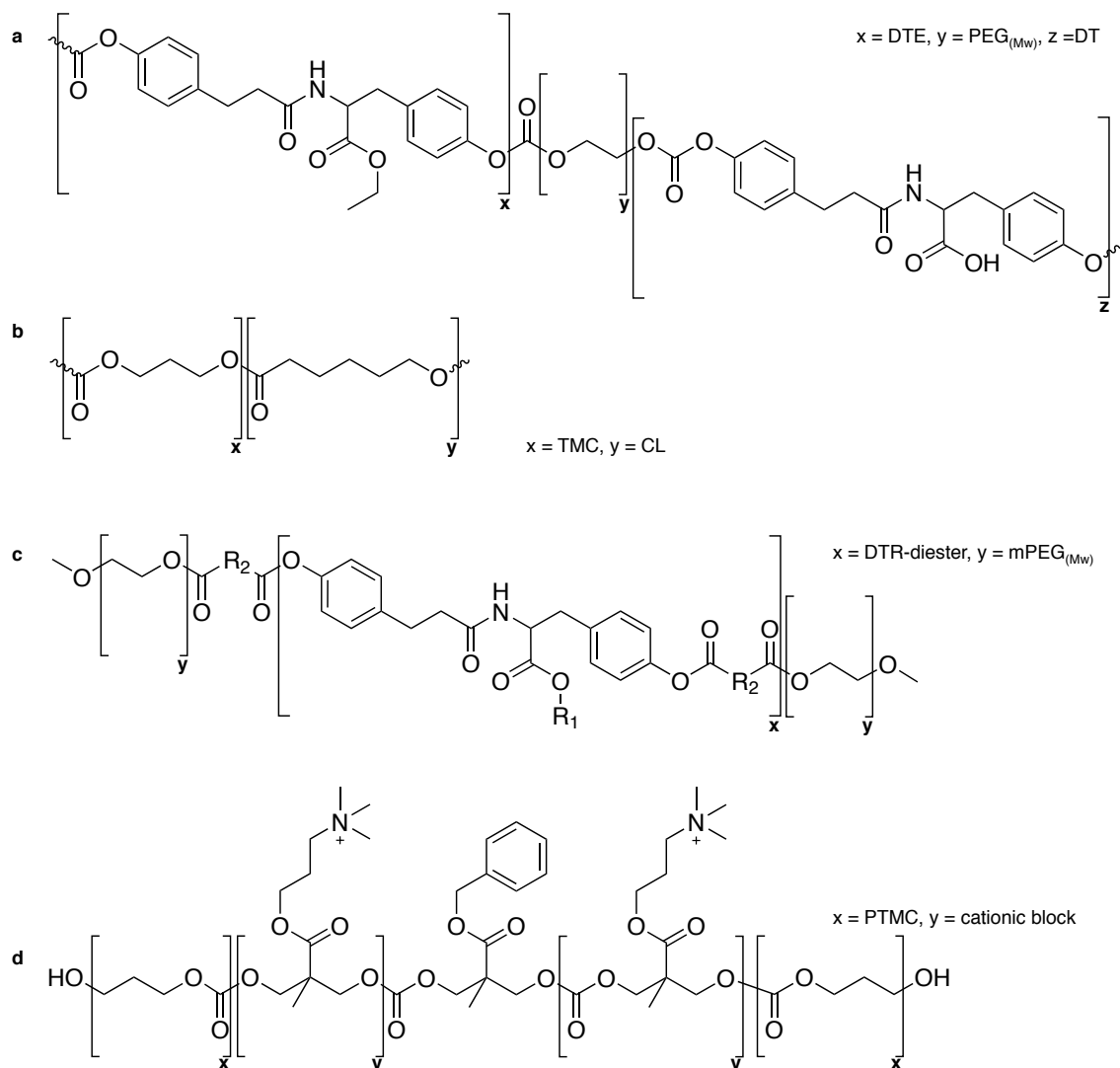


Figure 1.2: Co- and terpolycarbonates for biomedical applications: (A) Random, block terpolymer of DTE, DT and PEG, (B) random copolymer of TMC and CL, (C) tri-block copolymer of DTR-diester and mPEG, (D) tri-block copolymer of TMC. X, y, z for molar content of monomeric units.

The copolymerization of two or more monomers is a common strategy to fine tune polymer properties. In Figure 1.2 modifications of fundamental polymer structures illustrate how properties are tailored to the requirements of specific biomedical applications.

For example, terpolymers of desaminotyrosyl-tyrosine ethyl ester (DTE), desaminotyrosyl-tyrosine (DT) and poly(ethylene glycol) allow to adjust hydrolytic degradation rates over a broad period of time (82). This is achieved by adding DT with a free carboxylic acid pendant chain and hydrophilic PEG to increase the water uptake (138; 15). For example, the half-life of the molecular weight is reduced to 19 h at compositions of 35 mol % of DT and 6 mol % of PEG<sub>1k</sub>. In turn, the terpolymer is stable for weeks at lower contents of DT and PEG (72). These polymers find applications in tissue engineering as bone regeneration scaffolds (82) and polymeric coatings for implants at cortical neural interfaces (73).

Strategies to overcome drawbacks of aliphatic polycarbonates such as the rather weak mechanical performance include copolymerization of trimethylene carbonate (TMC) with common monomers such as  $\epsilon$ -caprolactone (CL) and lactide. However, statistical copolymers of TMC and CL are softer than PTMC, but the crystallinity intrinsic to PCL, is lowered by the addition of TMC (102). These materials were evaluated for soft tissue engineering applications such as nerve regeneration tubes (100; 114; 40). For drug delivery applications, amphiphilic copolymers can act as micellar nano-carriers in aqueous solution. Here, modulation of polymer properties is optimized for drug-loading or respective to the surface functionality of the nano-carrier. A micelle-forming ABA-triblock copolymers of oligomeric blocks of DTR-diester (hydrophobic) and PEG (hydrophilic) incorporated hydrophobic drugs of low solubility such as paclitaxel(117). Drug-loading capacity was maximized by optimizing the ester chain length to R = octyl (118). Paclitaxel-loaded nanospheres were evaluated for topical skin treatment of psoriasis in a controlled release system (59).

A spectacular example for the use of aliphatic polycarbonates features tri-block copolymers of PTMC and a cationic block leading to micellar nanospheres with a positive surface charge. These nanoparticles insert preferentially in prokaryotic cell membranes as compared to eukaryotic membranes e.g. blood cells. Therefore, they can act as potent and selective antimicrobial agents (94).



### 1.1.3 Current Advances in Polycarbonate Technology

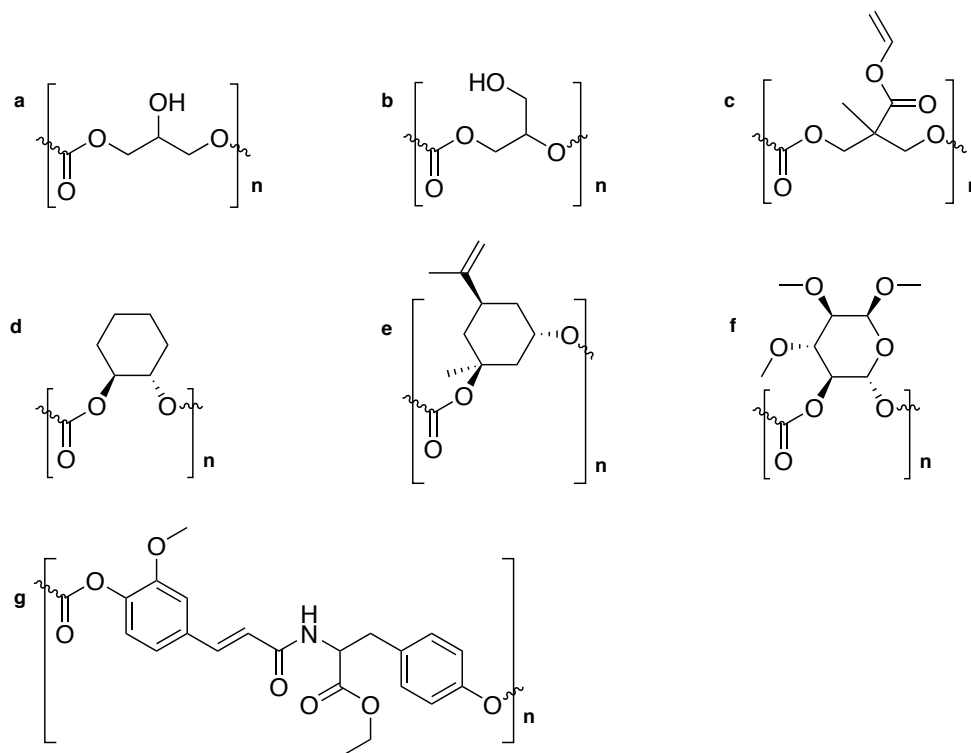


Figure 1.3: Examples of current innovations in polycarbonate technology: (A) Poly(1,3-glycerol carbonate), (B) poly(1,2-glycerol carbonate), (C) allyl functionalized polycarbonate, (D) poly(cyclohexene carbonate), (E) poly(limonene carbonate), (F) poly(D-glucose carbonate), (G) poly(ferrulic acid-*co*-tyrosyl ester carbonate).

Recently developed polycarbonates based on new fundamental structures demonstrate ongoing efforts to advance the design space for polymeric materials (Figure 1.3). These polycarbonates are mostly derived from natural, likely non-toxic compounds. For example, poly(1,3-glycerol carbonate) is an interesting example of an aliphatic polycarbonate, because it features a free hydroxyl group in the pendant chain. This hydroxyl group is potentially useful for pendant chain functionalization (109). In comparison, the synthesis of poly(1,2-glycerol carbonate) featuring a primary hydroxyl group is more challenging. Using chiral, organometallic catalysts, it was possible to obtain isotactic poly(1,2-glycerol carbonate) (140). Noteworthy, the degradation rate was faster for the respective polycarbonate with the primary as compared to

the secondary alcohol (140). Alternatively, allyl functionalized polycarbonate enable pendant chain modifications by radical addition or click chemistry (127).

Several approaches highlight the introduction of six-membered rings such as cyclohexane (60), limonene, a natural compound from lemon peel oil (22) and glucose in poly(D-glucose carbonate) (45; 89) to the aliphatic polycarbonate backbone.

Clearly, recent advances in the synthesis of aliphatic polycarbonates were driven by the progress in homogeneous metal catalysts (28). From a materials design perspective it is interesting only few recent examples report on new aromatic polycarbonates. Novel aromatic polycarbonates based on ferrulic acid and tyrosine derivatives (95) resemble previously reported work on tyrosine-derived polycarbonates (107).

In perspective, major advances in synthetic methodology entice the growth of a variety of new aliphatic polycarbonates, while there is a lack in the development of new polycarbonates with aromatic functionality.

## 1.2 Polymer Synthesis

### 1.2.1 Synthesis of Polycarbonates

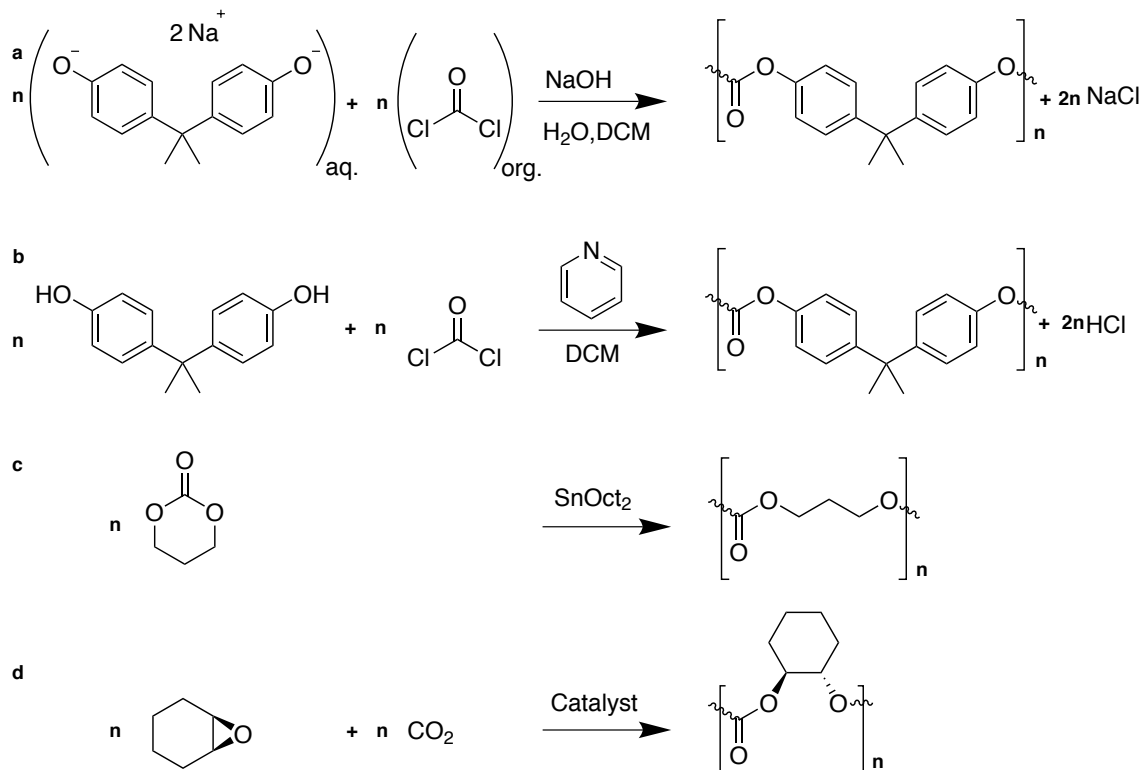


Figure 1.4: Reaction schemes for polycarbonates synthesis: (A) Interfacial polymerization using phosgene equivalent, (B) anhydrous, organic solvent with phosgene equivalent and organic base, (C) ring-opening polymerization using stannous octoate with TMC, (D) direct polymerization of carbon dioxide with epoxide using catalyst.

Figure 1.4 summarizes the most important synthesis approaches for polycarbonates. The classic synthesis of an aromatic polycarbonate from a diphenolic monomer and phosgene features a biphasic reaction system comprised of an aqueous phase and an organic phase such as DCM or chloroform. The aqueous phase contains a strong inorganic base such as  $\text{NaOH}$  and the diphenolic monomer in its anionic form. The organic phase serves as reservoir for phosgene that is applied to the reaction mixture in gaseous form. The reactants interact at the interface of the organic and aqueous phases to form polycondensation product. As the reaction proceeds product either appears in the organic phase, while acid generated during the reaction is neutralized

by base in the aqueous phase.(Figure 1.4 A) (115; 64).

As an alternative to the interfacial polymerization, polycarbonates from a diol and phosgene equivalent can also be formed in dry, organic solvents containing an organic base.(Figure 1.4 B) Here, the choice of the organic base is important as pyridine provides high  $M_w$  product (66). This method was also reported to provide polycarbonates from aliphatic diols such as isosorbide (25). Interestingly, such polycondensations have been unsuccessful with modified pseudo-amino acid monomers containing aliphatic groups such as serine and threonine ester due to  $\beta$ -elimination as shown by Kohn and Bolikal (unpublished results) as well as by the group of Wooley (95).

Poly(trimethylene carbonate), an aliphatic polycarbonate is synthesized by ring-opening polymerization from cyclic carbonates under metal catalysis. High molecular weight PTMC can be obtained when stannous octoate ( $\text{SnOct}_2$ ) is used (68). The original ring-opening polymerization of PTMC achieved only low molecular weight species, when potassium carbonate was used as a catalyst (23).

Polycarbonates can be directly synthesized from carbon dioxide and an epoxide using a heterogeneous catalyst such as diethylzinc and water (51; 52). The low reactivity of carbon dioxide has posed a challenge to this intriguing way to obtain a polycarbonate without phosgene. Recently, advances in the developments of new single-site homogeneous catalysts have sought to replace the old heterogenous catalysts. These new approaches provide better control over carbon dioxide reactivity and add features such as stereoselectivity into the polymerization reaction (28).

### 1.2.2 Phosgene and Equivalents

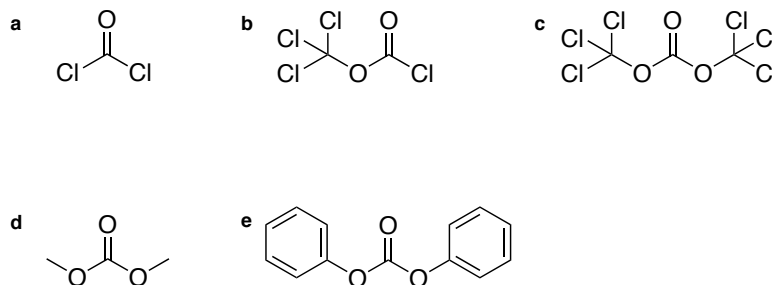


Figure 1.5: Structures of phosgene and equivalents: (A) Phosgene, (B) diphosgene (trichloromethylchloroformate), (C) triphosgene (bis(trichloromethyl)carbonate, BTC), (D) diethyl carbonate, (E) diphenyl carbonate.

Phosgene and alternatively phosgene equivalents are common reagents in the synthesis of polycarbonates (Figure 1.5). Phosgene is considered as a highly dangerous substance due to its gaseous state at ambient temperature in combination with high toxicity and a pleasant smell (35). Despite its toxicity, the usefulness and versatility of phosgene as a reagent was well elaborated in reactions such as chlorinations or carbonylations (5). In turn, trichloromethylchloroformate or diphosgene (DPG) is a liquid with similar reactivity to phosgene (30; 36). For a long time, the crystalline bis-(trichloromethyl)carbonate was known (30), but its utility as substitute for gaseous phosgene was only popularized until much later (36).

Alternatively, organic carbonates have been employed as eco-friendly alternatives such as dimethyl carbonate (DMC) with a low toxicity showing in a high LD50 (rat, oral)  $13.8 \text{ g kg}^{-1}$  (129). However, reactivity of DMC is low and transesterification into diphenyl carbonate is required to make organic carbonates useful as highly reactive phosgene substitutes (61).

### 1.3 Rationale and Hypotheses

Aliphatic polycarbonates are suited as materials for resorbable devices in biomedical applications because they can exhibit surface erosion behavior mediated by biological activity. However, aromatic polycarbonates often supersede the mechanical performance of aliphatic polycarbonates, but the resorption is slow.

The rationale of this thesis is that aromatic–aliphatic polycarbonates based on (hydroxyalkyl)phenols may combine good mechanical performance and the desired surface erosion behavior. The development of a novel class of polycarbonates may overcome the limitations posed on the previously known polycarbonate families. In this context, the following hypotheses will be discussed in detail.

- Aromatic-aliphatic polycarbonates combine the bulk properties of strong and stiff aromatic polycarbonates with the surface erosion behavior of soft aliphatic polycarbonates, when the glass transitions ( $T_g$ ) are in a range near physiological temperatures.
- Parameters in biphasic, interfacial phosgenation reactions can be tailored to selectively obtain diaryl, dialkyl and aryl alkyl carbonate diols from (hydroxyalkyl)phenols, useful as pre-programmed monomers for polymerization.
- Controlled sequences of carbonate isomers in the backbone of aromatic-aliphatic polycarbonates enable control over erosion behavior and mechanical properties through the physical polymer state.
- The surface erosion process found *in vitro* is fundamentally relevant to the *in vivo* environment of implanted polymer species.

## 1.4 Research Objective and Organization

The objective of this study is the development of a degradable polymer platform that expands the available technology for materials in temporary biomedical devices. Resorbability is sought to be merged with optimal retention of mechanical performance throughout the erosion process.

This thesis is divided into seven chapters introducing degradable aromatic–aliphatic polycarbonates derived from natural (hydroxyalkyl)phenols as mechanically strong and erodible polymers for potential biomedical applications. In **Chapter 1**, a literature overview of polycarbonate technologies and the current progress in the field were presented. In **Chapter 2** the materials and experimental methods are summarized. To avoid redundancies, this chapter will be referred to considering general experimental methods in later parts. In **Chapter 3** the synthesis of aromatic–aliphatic polycarbonates from tyrosol and homovanillyl alcohol is introduced. Further, the enzymatic surface erosion of mechanically strong polycarbonates is described. In **Chapter 4** selective synthesis methods are reported to control the carbonate isomer formation of (hydroxyalkyl)phenols to create pre-programmed carbonate diols polymerization reactions. In **Chapter 5** the physicochemical properties of diaryl and dialkyl carbonate diols are reported respective to the function as degradation intermediates and pre-programmed polymerizable units. In **Chapter 6**, the synthesis and properties of polycarbonates from tyrosol with controlled carbonate isomer sequences are introduced. Further, the effects of the sequence on erosion and mechanical performance respective to orientation and phase behavior is reported. Finally, the *in vivo* behavior of aromatic–aliphatic polycarbonates from tyrosol and softer copolymers is described in **Chapter 7**.

## Chapter 2

### Materials and Methods

This chapter serves the purpose to give the reader a broader overview of the general reagents used such as solvents, standard procedures followed and the lab equipment applied throughout this thesis. Conditions and procedures specific to a certain scientific investigation or application are described in detail in the respective chapters.

#### 2.1 Materials

All chemicals used were ACS reagent grade or better. Solvents dichloromethane (DCM), tetrahydrofuran (THF), 1,4-dioxane, 2-propanol (IPA), methanol (MeOH) were obtained from Fisher Scientific Thermo Fisher Scientific (Waltham, MA). Bis-(trichloromethyl) carbonate (BTC), pyridine (Py), deuterated dimethyl sulfoxide (DMSO-d<sup>6</sup>), 1,3-propanediol, phosphate buffered saline (PBS), hydrochloric acid (37%), 4-hydroxybenzyl alcohol, 3-(4-methoxyphenyl)propionic acid, 4-(3-hydroxypropyl)-phenol, 4-(2-Hydroxyethyl)-2-methoxyphenol (homovanillyl alcohol), 3-hydroxybenzyl alcohol, 2-(2-hydroxyethyl)phenol and lipase from *Thermomyces lanuginosus* (EC3.1.1.3, minimum 10<sup>5</sup> units g<sup>-1</sup>) were obtained from Sigma-Aldrich (St. Louis, MO). Hexane and N,N-dimethylformamide (DMF) were obtained from Thermo Fisher Scientific (Waltham, MA). Tyrosol (4-(2-hydroxyethyl)phenol) was obtained from TCI (Tokyo, Japan).



## 2.2 Methods

### 2.2.1 General Procedure for Polycarbonate Synthesis

CAUTION: Bis(trichloromethyl) carbonate (triphosgene) used in the following procedure is a hazardous material. Triphosgene can release deadly phosgene, a gas that can be lethal before it can be recognized by its smell. All procedures using triphosgene need to be performed in a closed fume hood and under supervision of an experienced and well-trained operator. A monitor and alarm system for accidental exposure to phosgene is required.

Generally, polycarbonates were synthesized by condensation polymerization using diol monomer (1 equiv.) dissolved in DCM and Py with BTC in DCM added drop wise over the course of 2 h at ambient temperature.

### 2.2.2 Polymer Characterization

The polymers were purified by cycles of precipitation in 2-propanol and dissolution in dichloromethane. The chemical composition was confirmed by analysis of  $^1\text{H}$  and decoupled  $^{13}\text{C}$  nuclear magnetic resonance spectra (500 MHz NMR, Varian, U.S.A.). As a solvent DMSO- $\text{d}_6$  was used and all spectra were referenced to the solvent signal. The number and weight average molecular weights ( $M_n$  and  $M_w$ ) of the copolymers were determined relative to polystyrene standards using gel permeation chromatography (GPC, Waters, Milford, MA) equipped with two PL gel columns of 100.000 and 1.000 Å (Polymer Laboratories, Amherst, MA). DMF with 0.1% TFA was applied as eluting solvent. Thermal properties were analyzed using differential scanning calorimetry (DSC 2520, Mettler Toledo, Columbus, OH). The heating rate was  $10\text{ }^\circ\text{C min}^{-1}$  and the glass transition temperature ( $T_g$ ) was calculated using the ASTM mid-point method. The first and second heat scans were used to determine  $T_g$  of fully hydrated and dry specimens, respectively.

### 2.2.3 Compression Molding

Polymer films were compression molded at around  $T_g + 40\text{ }^{\circ}\text{C}$  or  $T_m + 20\text{ }^{\circ}\text{C}$ , respectively, using a Carver press (model 4122, Carver, Wabash, IN) with a thickness of 250  $\mu\text{m}$  for water uptake and degradation studies and a thickness of 400  $\mu\text{m}$  thick for mechanical testing, respectively.

### 2.2.4 Water Uptake

Specimens from compression-molded films, cut to a sample size of approximately 10 mg, were incubated in PBS at  $37\text{ }^{\circ}\text{C}$  until the equilibrium water uptake was reached. The specimens were blotted with paper and immediately subjected to thermo gravimetric analysis (TGA, Mettler-Toledo, Columbus, OH). Specimens were heated from  $25\text{--}150\text{ }^{\circ}\text{C}$  at a heating rate of  $10\text{ }^{\circ}\text{C min}^{-1}$ .

### 2.2.5 Mechanical Properties

Mechanical properties of polymers were characterized using a mechanical tensile testing apparatus equipped with a 10 N submersible load cell (Bose Electroforce, Eden Prairie, MN). The initial grip-to-grip separation was 8 mm and the maximal strain was 150% due to instrument limitation. The crosshead speed was  $0.1\text{ mm s}^{-1}$ . Alternatively, a mechanical tensile testing apparatus equipped with a 100 N load cell (MTS systems, Eden Prairie, MN) was used to achieve up to 500% strain. In both instruments, the crosshead speed was  $0.1\text{ mm s}^{-1}$ . Rectangular-shaped specimens were cut to a width of 2–6 mm from compression-molded films of 100–400  $\mu\text{m}$  thickness. Mechanical properties in the dry state were determined at room temperature. To measure the mechanical properties in the wet state, specimens were preconditioned in PBS at  $37\text{ }^{\circ}\text{C}$  for 24 h, and then immersed in PBS at  $37\text{ }^{\circ}\text{C}$  for testing. To follow the mechanical properties during degradation (see below), specimens were incubated in lipase solution as well as in PBS (as control) and retrieved at respective time

points. The tensile tests were performed in the wet state. The tensile modulus was determined from the initial, linear part of the stress-strain curve, using the grip-to-grip distance to measure elongation. The stress and strain at yield ( $\sigma_{yield}$  and  $\epsilon_{yield}$ ) values were determined from the upper yield point. The analyses were performed in triplicate.

### 2.2.6 Degradation Experiments

Polymer discs with a diameter of 6 mm and thickness of approximately 25  $\mu\text{m}$  were immersed in 3 mL of lipase solution from *Thermomyces lanuginosus* as a model enzyme with an activity of 5 kU  $\text{mL}^{-1}$ . For control experiments, specimens were immersed in PBS. All solutions contained 0.02% (w/w) of sodium azide to prevent bacterial growth. The incubation temperature was 37 °C and the solutions were replaced twice per week. Samples in triplicate were removed at respective time points and rinsed with deionized water and 70% (v/v) ethanol. The mass and thickness of the samples were measured after drying *in vacuo* for 72 h at ambient temperature.

### 2.2.7 Spin-coating of Polymer Thin Films

Polymer thin films were prepared by spincoating from 1–1.25% (w/v) polymer solution in dry dioxane at 3000 rpm using a spin-coater (Headway Research, Garland, TX) in a humidity-controlled atmosphere (less than 10% relative humidity). For contact angle measurements 15 mm glass coverslips (Fisher Scientific Pittsburgh, PA) and for QCM-D gold-coated quartz crystal QSX100 (Q-sense, Glen Burnie, MD) were used as substrates. The samples were dried *in vacuo* for at least 12 h.

### 2.2.8 Scanning Electron Microscopy (SEM)

Dried specimens subjected to degradation media or PBS control were sputter coated (SCD 004, Leica Microsystems, Liechtenstein) with gold/palladium, and then the

morphology of the specimens was studied by SEM (1830I, Amray, USA, Voltage = 20 kV).

### **2.2.9 Quartz Crystal Microbalance with Dissipation (QCM-D)**

In a Q-sense E4 (Q-sense, Glen Burnie, MD), the surfaces of sensor crystals coated with polymer thin films were equilibrated with PBS buffer at  $24\text{ }\mu\text{l min}^{-1}$ . A temperature program was executed between 20–29 °C with lipase (or PBS control) preadsorbed at 20 °C. The interval time between temperature steps was 30 min while frequency was recorded for overtones  $n = 3, 5, 7, 9$ . The frequency change ( $\Delta f_n$ ) and the dissipation change were recorded over time. The change of mass per area was obtained using the Sauerbrey equation with  $\Delta m = C\Delta f_n$ ; ( $C = 17.7\text{ ng cm}^{-2}\text{ s}^{-1}\text{ Hz}^{-1}$ ) with negligible dissipation changes during erosion (113). The rate of mass loss for each temperature step was obtained by linear regression after equilibration.

## Chapter 3

# Enzymatic Surface Erosion of High Tensile Strength Polycarbonates Based on Natural Phenols

Previously published with minor alterations: Sven D Sommerfeld, Zheng Zhang, Marius C Costache, Sebastian L Vega, and Joachim Kohn. Enzymatic surface erosion of high tensile strength polycarbonates based on natural phenols.

*Biomacromolecules*, 15(3):830–836, 2014.

### 3.1 Abstract

Surface erosion has been recognized as a valuable design tool for resorbable biomaterials within the context of drug delivery devices, surface coatings, and when precise control of strength retention is critical. Here we report on high tensile strength, aromatic–aliphatic polycarbonates based on natural phenols, tyrosol (Ty) and homovanillyl alcohol (Hva), that exhibit enzymatic surface erosion by lipase. The Youngs moduli of the polymers for dry and fully hydrated samples are 1.0 to 1.2 GPa and 0.8 to 1.2 GPa, respectively. Typical characteristics of enzymatic surface erosion were confirmed for poly(tyrosol carbonate) films with concomitant mass loss and thickness-loss at linear rates of  $0.14 \pm 0.01 \text{ mg cm}^{-2} \text{ d}^{-1}$  and  $3.0 \pm 0.8 \text{ } \mu\text{m d}^{-1}$  respectively. The molecular weight and the mechanical properties of the residual films remained constant. Changing the ratio of Ty and Hva provided control over the glass transition temperature ( $T_g$ ) and the enzymatic surface erosion: increasing the Hva

content in the polymers resulted in higher  $T_g$  and lower enzymatic erosion rate. Polymers with more than 50 mol % Hva were stable at 37 °C in enzyme solution. Analysis on thin films using quartz crystal microbalance with dissipation (QCM-D) demonstrated that the onset temperature of the enzymatic erosion was approximately 20 °C lower than the wet  $T_g$  for all tested polymers. This new finding demonstrates that relatively high tensile strength polycarbonates can undergo enzymatic surface erosion. Moreover, it also sheds light on the connection between  $T_g$  and enzymatic degradation and explains why few of the high strength polymers follow an enzyme-mediated degradation pathway.

## 3.2 Introduction

Surface eroding polymers as compared to bulk eroding polymers have distinct advantages for the design of resorbable medical implants (124). Typically, during bulk erosion a decrease in molecular weight of the polymer occurs before any mass loss is observed. This leads to unfavorable changes in polymer characteristics such as diminishing mechanical strength and lack of control over long-term drug release. By contrast, surface erosion leads to mass loss with only negligible molecular weight decrease throughout the bulk of the polymer. Surface erosion is advantageous in applications requiring a controlled retention of mechanical properties during degradation and in drug delivery applications where the rate of drug release can be controlled by the erosion of surface layers of the polymeric matrix. However, hydrolytic surface erosion is only observed when the rate of polymer degradation is faster than the rate of water penetration into the bulk of the polymer (42; 21). Hence, for small medical implants, hydrolytic surface erosion is limited to extremely fast degrading polymers such as some polyanhydrides and some poly(ortho esters) (46). In the clinic, a surface eroding device (Gliadel) made from polyanhydrides is used to

release a chemotherapeutic agent in the brain over 2–3 weeks (16). Most degradable polymers used in the design of medical and drug release devices are materials such as polyesters that invariably undergo bulk erosion (1). Interestingly, Pitt et al. reported that poly(trimethylene carbonate) (PTMC), an aliphatic polycarbonate, showed surface erosion behavior *in vivo*, while the hydrolytic degradation was slow *in vitro* (143). It was later demonstrated that PTMC underwent enzymatic degradation by hydrolytic enzymes *in vitro*, mimicking surface erosion characteristics found *in vivo* (141). Hence, hydrolytic enzymes are likely to play a significant role in the degradation of PTMC. Further, the involvement of reactive oxygen species in the erosion of aliphatic polycarbonates was recently suggested by Amsden et al., similar to previous findings by Anderson et al. in poly(carbonate urethane)s (24; 29; 27) studies have evaluated the suitability of devices from surface eroding, aliphatic polycarbonates for antibiotic delivery, and implantation in a soft tissue environment for vascular and cardiac tissue engineering (62; 32; 6; 120). Since the material properties of these aliphatic polycarbonates are characterized as flexible and rubbery ( $T_g$  lower than 37 °C), it was previously postulated that enzymatic surface erosion requires a flexible polymer backbone that can comply with the enzymes active site (106). Therefore, it is accepted that aromatic polycarbonates and most other currently available biodegradable polymers with Young's moduli in the GPa range are not susceptible to enzymatic surface erosion, even though amorphous poly(lactic acid) is degradable by Proteinase K (135; 136). Likewise, a wide range of tyrosine-derived polycarbonates were extensively studied by Kohn et al., but were not found to degrade by enzyme-mediated processes (125; 126; 39). Heretofore, few efforts have been made to discover new polymers of high strength that undergo enzymatic surface erosion.

In this contribution, we report on the preparation and characterization of a series of aromatic–aliphatic polycarbonates based on tyrosol and homovanillyl alcohol. Both monomers are readily available from natural resources such as olive oil mill waste waters and products of fermentation processes (79; 55). Tyrosol and hydroxytyrosol are

assessed as GRAS (generally recognized as safe) substances by the FDA. Homovanillyl alcohol is a metabolite of hydroxytyrosol and has an  $LD_{50}$  of  $3200 \text{ mg kg}^{-1}$  (oral, rabbit; data from the Material Safety Data Sheet provided by the supplier). As antioxidants they have been credited with benign biological activities(43). The structures of the monomers contain both a phenol and an alcohol group: After polycondensation, polymers with both aromatic and aliphatic carbonate functionalities were obtained. Remarkably, we found enzymatic surface erosion behavior resembling the degradation of soft, aliphatic polycarbonates, while the mechanical properties were strong, similar to aromatic polycarbonates. QCM-D analysis on thin films demonstrated the connection between  $T_g$  and enzymatic surface erosion; this finding explains why amorphous poly(lactic acid) and the polycarbonates based on tyrosol and homovanillyl alcohol with  $T_g$  below  $60^\circ\text{C}$  can undergo surface erosion, while most of the other high tensile strength polymers with significantly higher  $T_g$  cannot.



### 3.3 Experimental

In brief, **Chapter 2** generally described the herein used materials and procedures followed such as polymer characterization, compression molding, water uptake, mechanical properties by Bose Electroforce (Eden Prairie, MN), degradation experiments in lipase solution and PBS control, spin-coating of polymer thin films, SEM, QCM-D. It is be noted that the general procedure for the synthesis of polycarbonates was followed using tyrosol and homovanillyl alcohol as diol monomers.

The experimental procedures below are considered specific to this chapter.

#### 3.3.1 Static Contact Angle Measurement

To measure the contact angle, a drop of water was applied to the polymer-coated surface and the static contact angle was determined using a goniometer (Rame-Hart, Succasunna, NJ) with at least five independent measurements per composition.

#### 3.3.2 Attachment and Proliferation of Human Mesenchymal Stem Cells (hMSCs) on Polymer Films

Bone marrow derived hMSCs of passage numbers between 2 and 5 (Texas A&M University, College Station, TX) were cultured in MSC basal medium supplemented with SingleQuots (Lonza, Walkersville, MD). Compression-molded discs (approximate thickness = 250  $\mu\text{m}$ ) of (co)polymers from Ty and Hva were cut to fit wells of a 48-well tissue culture polystyrene (TCPS) plate (Corning, Corning, NY). Cells were seeded at a density of  $5 \times 10^3$  cells  $\text{cm}^2$ . The hMSCs were cultured at 37 °C in an incubator supplemented with 5% (v/v) of CO<sub>2</sub>. Cell viability and proliferation were evaluated at time points of 4 h, 4 days, and 7 days. For qualitative fluorescence microscopy imaging, cells were fixed with 4% (w/v) paraformaldehyde for 10 min and then permeabilized with 0.1% (w/v) Triton X-100 for 3 min. Staining was conducted

using Alexa Fluor 488 phalloidin for 20 min and Hoechst for 5 min. For quantification of viability, the cell culture medium containing 10% (v/v) of AlamarBlue reagent (Invitrogen, Carlsbad, CA) was added to wells of live cells after a buffer rinse. The fluorescence of the supernatant was measured after 4 h of incubation ( $\lambda_{ex} = 560$  nm,  $\lambda_{ex} = 590$  nm) (132). The total cell count on polymer substrates was calculated for each time point by comparing fluorescence readouts against a standard curve of known cell numbers. Three independent experiments were carried out ( $n = 3$ ) with three replicates for each condition.

### 3.4 Results and Discussion

#### 3.4.1 Synthesis and Chemical Structure

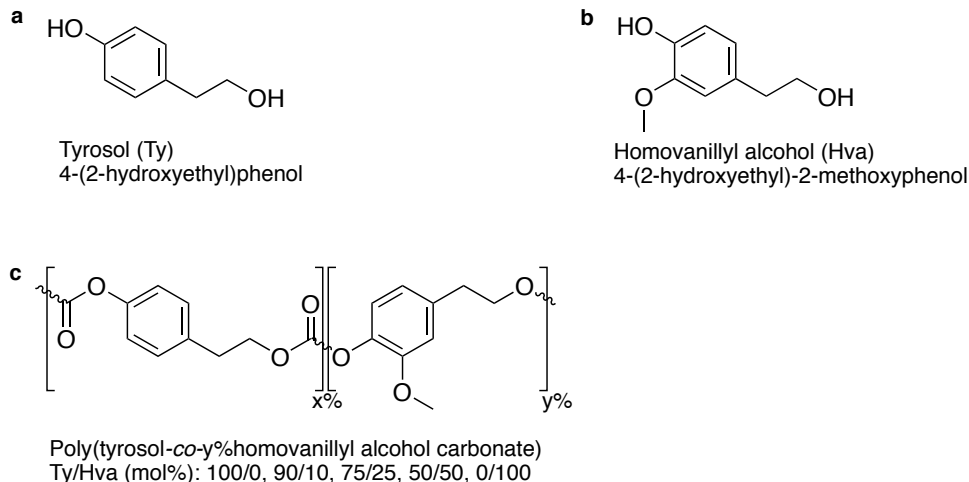


Figure 3.1: Chemical structures of (A) tyrosol, (B) homovanillyl alcohol, (C) poly-(tyrosol-co-homovanillyl carbonate).

A series of polycarbonates from tyrosol (Ty) and homovanillyl alcohol (Hva) (Figure 3.1 A–C) was prepared by condensation polymerization using triphosgene with Ty content of 100, 90, 75, 50, and 0 mol% in the feed. The polymer composition respective to Ty and Hva was confirmed using  $^1\text{H}$  NMR spectroscopy (Figure 3.2 A). As illustrated in Figure 3.2 B, the backbone structure featured sequence isomers with diaryl (head-to-head, HH), dialkyl (tail-to-tail, TT) and aryl alkyl (head-to-tail, h/t) carbonates. Chemical shifts of protons in head-to-head, tail-to-tail isomers (aromatic: a1 and b1, aliphatic: d1 and e1) were distinguished from those in head-to-tail isomers at corresponding positions (aromatic: a2 and b2, aliphatic d2 and e2) for Ty and Hva. Additional protons exclusive to Hva units were annotated accordingly (aromatic: c1 and c2, methoxy: f1 and f2).

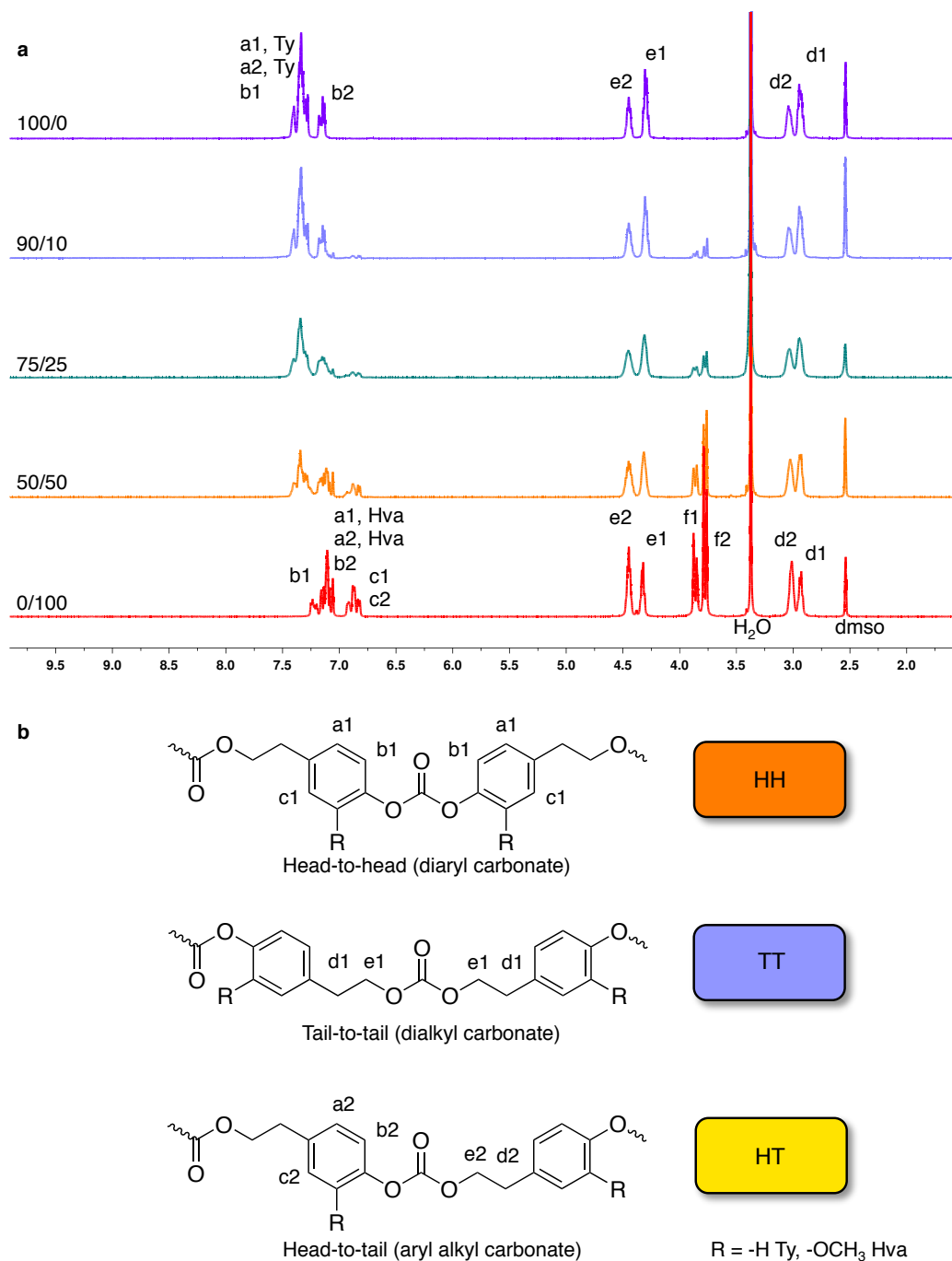


Figure 3.2: Results of  $^1\text{H}$  NMR spectroscopy on polycarbonate compositions of Ty/Hva (mol %) 100/0, 90/10, 75/25, 50/50, and 0/100 with notations of respective peak assignments referenced to DMSO- $d_6$ : (A) Overlay spectra, (B) polymer sequence isomers at carbonate bond: head-to-head, tail-to-tail, head-to-tail.

A detailed tabulation of the chemical shift assignments with signals that arose from Ty and Hva contributions is provided in Table 3.1.

Table 3.1: Chemical shift assignment from  $^1\text{H}$ -NMR spectra]

Head-to-head (diaryl)/tail-to-tail (dialkyl)			Head-to-tail (aryl alkyl)		
Proton	Chemical shift		Proton	Chemical shift	
	[ppm]			[ppm]	
a1 (aryl, Ty)	7.3(m)		a2 (aryl, Ty)	7.3 (m)	
a1 (aryl, Hva)	7.1(m)		a2 (aryl, Hva)	7.1 (m)	
b1 (aryl)	7.3 (m)		b2 (aryl)	7.1 (m)	
c1 (aryl, Hva)	6.9, 6.8 (m)		c2 (aryl, Hva)	6.7, 6.8 (m)	
d1 (alkyl)	2.9 (m)		d2 (alkyl)	3.0 (m)	
e1 (alkyl)	4.3 (m)		e2 (alkyl)	4.4 (m)	
f1 (methoxy, Hva)	3.8 (s, s)		f2 (methoxy, Hva)	3.7 (s, s)	

s = singlet, m = multiplet.

The distribution of carbonate sequence isomers was determined by integration of the  $^1\text{H}$ -NMR signals of the aliphatic  $\text{H-C}_\alpha$  e1 and e2. Further, the aliphatic methylene protons d1 and d2 as well as the aromatic ring protons a1, a2 and b1, b2 were quantified. The distribution of carbonate sequence isomers is shown in Table 3.2.

In poly(tyrosol carbonate) (100/0), the experimentally determined ratios of HH : TT : HT were 1 : 1 : 1.3, while the theoretical, statistical distribution for HH : TT : HT was 1 : 1 : 2. Therefore, the polycondensation reaction of tyrosol and triphosgene showed modest selectivity towards carbonates of HH and TT connectivity. This is most likely due to a faster reaction rate of the phenolate versus the aliphatic hydroxyl in the beginning of the phosgenation reaction. When the phenolate was consumed, the reaction rate for the aliphatic hydroxyl increased and leading the formation of HT. Increasing Hva content in the feed lead to a shift in the sequence isomer distributions

towards the HT isomer. In 50/50, the statistical distribution was obtained, while in poly(Hva carbonate) ratios for HH : TT : HT of 1 : 1 : 2.8 were determined. The effects of the compositional changes from Ty to Hva and the backbone structure on the properties of these aromatic–aliphatic polycarbonates are subject of detailed studies in this chapter.

Table 3.2: Distribution of sequence isomers in polycarbonate backbone

Ty/ Hva (mol %)	Head-to-head (Diaryl carbonate)	Tail-to-tail (Dialkyl carbonate)	Head-to-tail (Aryl alkyl carbonate)
100/0	1	1	1.3
90/10	1	1	1.4
75/25	1	1	1.6
50/50	1	1	2.0
0/100	1	1	2.8
Statistical ratios	1	1	2

<sup>a</sup>Calculated from integrated <sup>1</sup>H-NMR Spectra

In addition to <sup>1</sup>H-NMR spectra, the <sup>13</sup>C-NMR spectroscopy on poly(tyrosol carbonate) (100/0) yields detailed information of the sequence microstructure. A zoom into the chemical shift of the aromatic ring carbon C<sub>4</sub> in the <sup>13</sup>C-NMR spectrum reveals structured triads of the tyrosol units (Figure 3.3).

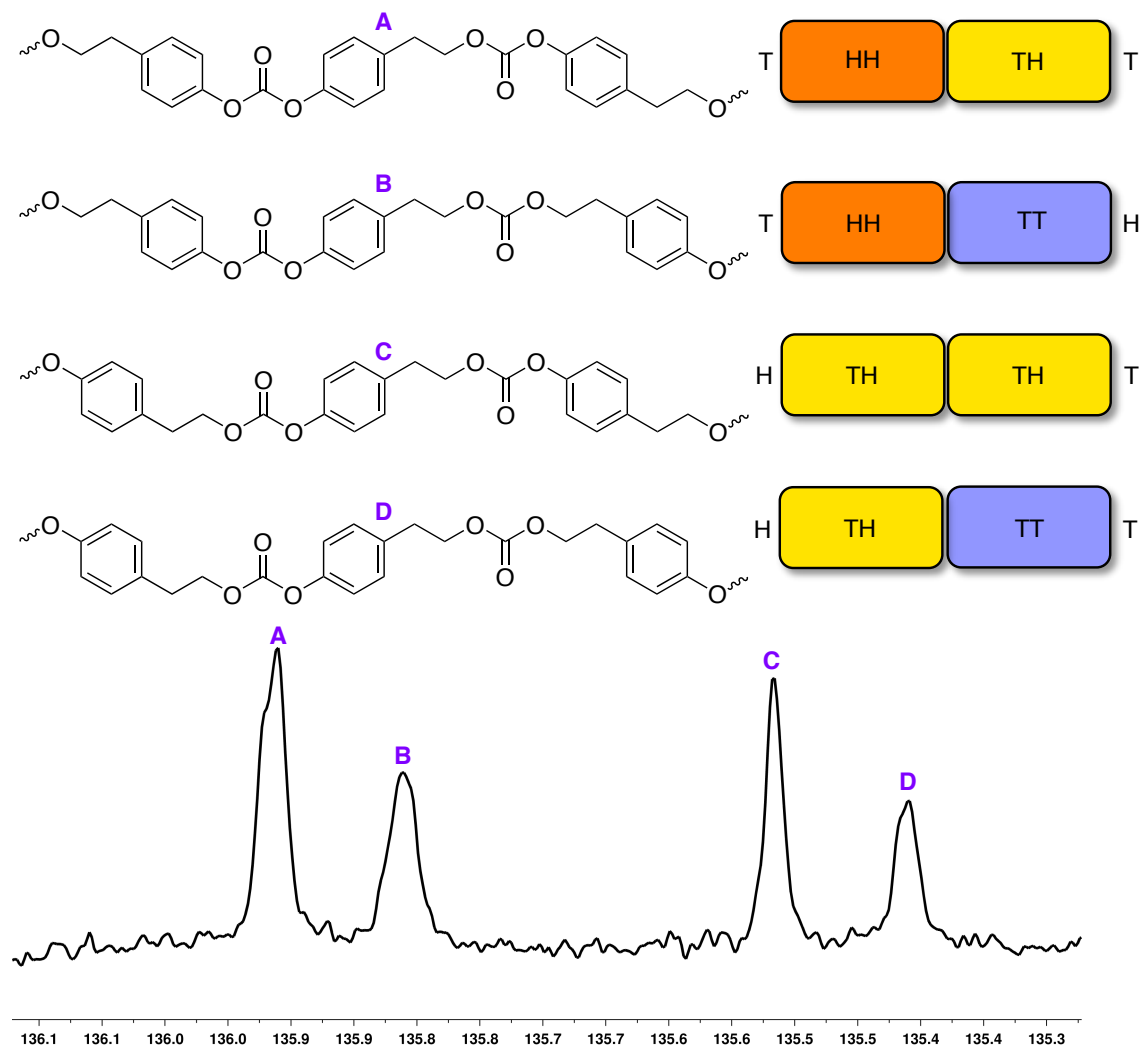


Figure 3.3:  $^{13}\text{C}$ -NMR spectrum (126 MHz,  $\text{DMSO}-d^6$ ) of poly(tyrosol carbonate): Zoom into chemical shift of aromatic ring carbon  $\text{C}_4$  ( $\delta$  135–136 ppm) with assignments of triads A, B, C, D.

The signals revealed information about the triads spanning three consecutive tyrosol units, two full carbonate bonds and two halves of carbonate bonds. Indeed, the four theoretically possible triad orientations were identified experimentally. The assignment for the respective signals of the  $\text{C}_4$  atoms are noted A–D. It must be noted that the relative peak intensities are not indicative of the actual ratios of triads found in the polycarbonate backbone.

### 3.4.2 Physical Polymer Properties

The physical properties in the series of polycarbonates from Ty and Hva are listed in Table 3.3.

Table 3.3: Physical properties of polycarbonates from Ty and Hva

Ty/ Hva (mol %)	Mn (10 <sup>3</sup> g/mol)	Mw /Mn	$T_g$ (°C)		Contact angle (°) <sup>a</sup>
			dry	wet	
100/0	174	1.49	60	50	80 ± 2
90/10	227	1.46	63	54	81 ± 1
75/25	212	1.42	65	57	82 ± 2
50/50	183	1.45	69	60	80 ± 2
0/100	117	1.52	74	63	80 ± 2

<sup>a</sup>Mean ± standard deviation (SD), n = 5.

All polymers were of high molecular weight with Mn values ranging from 117 to 227 g mol<sup>-1</sup>. In the dry state, the  $T_g$  increased with the content of Hva in the composition from 60 to 74 °C in accordance with the Fox equation (14). This  $T_g$  increase may be explained by reduced polymer chain flexibility due to the methoxyl substituent of Hva. As reported elsewhere, additional steric barriers to chain rotations raised  $T_g$  in polystyrenes and polymethacrylates (83). In the wet state, the  $T_g$  of preconditioned polycarbonates from Ty and Hva was reduced by approximately 10 °C for all compositions; the equilibrium water uptake of the polymer specimens throughout the series was less than 1 % (w/w), thus explaining the moderate reduction of the  $T_g$  upon hydration. Under physiological conditions all polymers were in the glassy, amorphous state. The polymer surfaces throughout the series were characterized as moderately hydrophobic with water contact angles around 81°.

To evaluate the applicability of the polycarbonates from Ty and Hva in the fabrication of biodegradable load-bearing devices, the tensile moduli as well as stress and



Table 3.4: Mechanical properties of polycarbonates from Ty and Hva

Ty/ Hva (mol %)	Modulus [GPa]		Yield Stress [MPa]		Yield strain <sup>c</sup>	
	Dry <sup>a</sup>	Wet <sup>b</sup>	Dry <sup>a</sup>	Wet <sup>a</sup>	Dry <sup>a</sup>	Wet <sup>a</sup>
100/0	1.1 $\pm$ 0.2	0.8 $\pm$ 0.2	38 $\pm$ 2	27 $\pm$ 2	6%	5%
90/10	1.0 $\pm$ 0.1	1.0 $\pm$ 0.1	42 $\pm$ 5	27 $\pm$ 1	6%	6%
75/25	1.0 $\pm$ 0.1	0.9 $\pm$ 0.1	42 $\pm$ 2	32 $\pm$ 1	6%	6%
50/50	1.2 $\pm$ 0.1	0.9 $\pm$ 0.1	57 $\pm$ 3	34 $\pm$ 2	8%	6%
0/100	1.2 $\pm$ 0.1	1.2 $\pm$ 0.2	54 $\pm$ 2	43 $\pm$ 2	7%	6%

<sup>a</sup>Tested at RT; <sup>b</sup>Preconditioned for 24 h and tested in PBS at 37 °C; <sup>c</sup>SD < 1%.

strain at the yield point were determined by tensile testing (see Table 3.4 and Figure S2, Supporting Information). Changing the ratio of Ty and Hva provided control over the glass transition temperature ( $T_g$ ) while the mechanical properties remained similar. In the dry state at room temperature, all polymers were characterized as strong and stiff materials with tensile moduli in the range from 1.0  $\pm$  0.1 GPa to 1.2  $\pm$  0.1 GPa and the yield stress ( $\sigma_{yield}$ ) ranging from 38  $\pm$  2 MPa to 57  $\pm$  3 MPa. The yield strain ( $\epsilon_{yield}$ ) was approximately 6% for all compositions. The polymers were ductile and did not break at 150% strain, which was the maximal elongation that could be measured by our experimental setup. Under simulated physiological conditions at 37 °C, lower tensile moduli ranging between 0.8  $\pm$  0.2 GPa to 1.2  $\pm$  0.2 GPa and 27  $\pm$  2 MPa to 43  $\pm$  2 MPa values of the copolymers were recorded; the  $\epsilon_{yield}$  was not affected. The moderate reduction of mechanical performance in the wet state is expected due to hydration and higher temperature during testing. The physical properties and the mechanical performance of the reported polymers were comparable to other resorbable, aromatic polycarbonates. For example, poly(DTE carbonate) (DTE = desaminotyrosyl tyrosine ethyl ester), suitable for biomedical applications, has a modulus of 1.5 GPa in both the dry and the wet states at 22 °C (12). In

particular, copolymers of DTE and PEG(5 mol % of PEG,  $M_n = 5 \text{ g mol}^{-1}$ ) with 1.2 GPa in the dry state and 0.6 GPa in the wet state match the performance range of polycarbonates from Hva and Ty (138). By contrast, aliphatic polycarbonates, e.g., PTMC, are much more flexible and possess lower moduli in the low megapascal range under physiologically relevant conditions (100).

### 3.4.3 Enzyme-Mediated Surface Erosion *In Vitro* and Retention of Mechanical Properties

To explore the in vitro degradation behavior, compression-molded specimens of polycarbonates from Hva and Ty were immersed in lipase solution and in PBS as a control. The pH of the degradation medium remained around  $\text{pH} = 7$  for all the tested groups measured after 1 week before replacement with fresh solution. At  $37^\circ\text{C}$  in lipase solution, the molecular weight remained unchanged, while linear mass loss was observed for poly(tyrosol carbonate) and compositions with 90 and 75 mol % Ty (Figure 3.4 A). For poly(tyrosol carbonate) a rate of mass loss of  $0.14 \pm 0.01 \text{ mg cm}^{-2} \text{ d}^{-1}$  was demonstrated. At this rate, only about half of the mass was retained at a 6-week time point. The last structurally intact specimens were retrieved after 9 weeks with a relative mass loss of around 80%. The lipase dependent erosion was slower for compositions with 90 and 75 mol % Ty showing rates of  $0.07 \pm 0.01 \text{ mg cm}^{-2} \text{ d}^{-1}$  and  $0.03 \pm 0.01 \text{ mg cm}^{-2} \text{ d}^{-1}$ , respectively. However, the mass loss of compositions with lower than 50 mol % Ty was too slow to be quantified accurately. Poly(homovanillyl carbonate) was stable in lipase solution at  $37^\circ\text{C}$ . In accordance with the mass loss results, concomitant thickness-loss was observed for poly(tyrosol carbonate) specimens at a rate of  $3.0 \pm 0.8 \mu\text{m d}^{-1}$  (Figure 3.4 B).

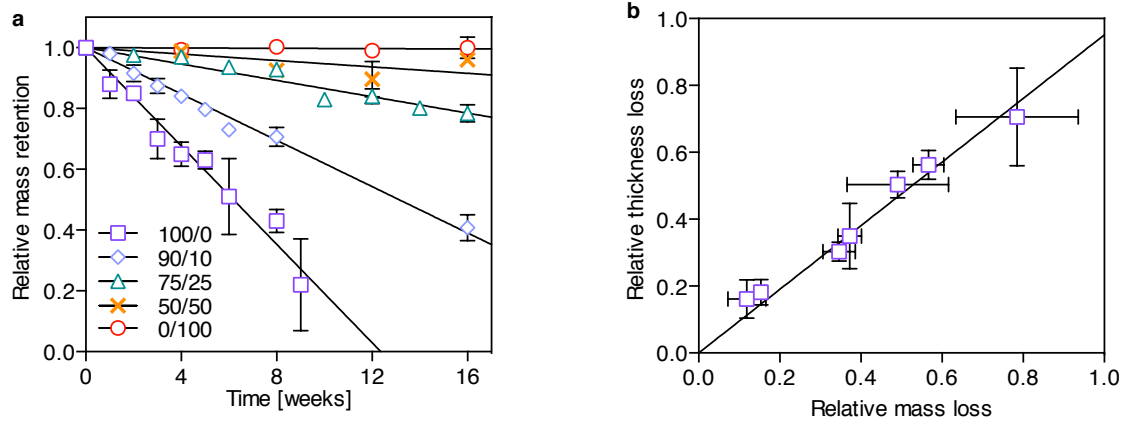


Figure 3.4: (A) Relative mass retention of specimens with compositions of Ty/Hva (mol %) 100/0, 90/10, 75/25, 50/50, and 0/100 incubated in lipase solution at 37 °C, (mean  $\pm$  SD,  $n = 3$ ). (B) Correlation between relative mass and thickness loss of poly(tyrosol carbonate) specimens incubated in lipase solution at 37 °C, (mean  $\pm$  SD,  $n = 3$ ). The linear regression lines were plotted.

Likewise, the thickness of specimens containing 90 and 75 mol % Ty decreased over time as well, while no change was observed for compositions with 50 mol % Ty and poly(homovanillyl carbonate). No surface erosion was observed for any composition incubated in PBS, while the long-term stability of poly(tyrosol carbonate) was evaluated for a period of 1 year showing no significant changes in molecular weight (Figure 3.5).

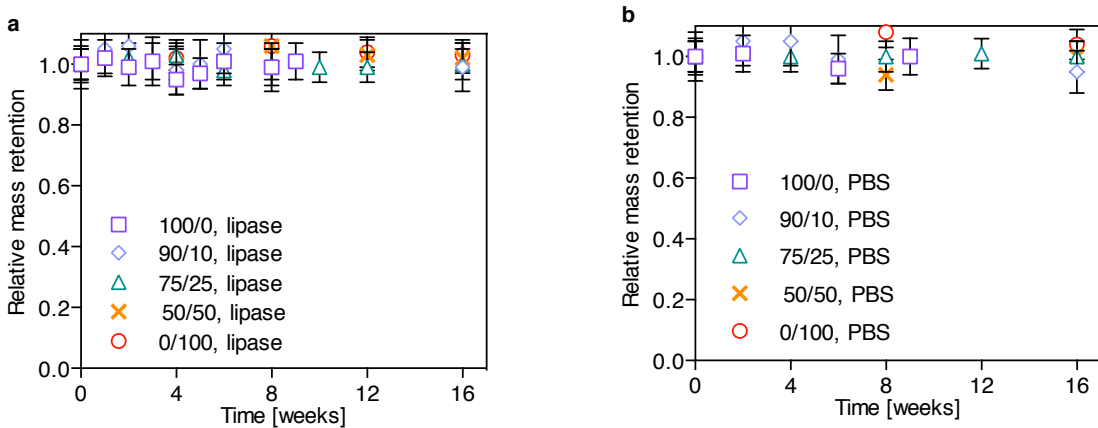


Figure 3.5: Relative  $M_w$  retention of (A) polycarbonate specimens with compositions of Ty/ Hva (mol %) 100/0, 90/10, 75/25, 50/50, 0/100 incubated in lipase at 37 °C, and (B) 100/0 and 90/10 in lipase solution and PBS control at 37 °C.

A unique morphology of partially eroded poly(tyrosol carbonate) specimens was revealed in SEM images: while the untreated poly(tyrosol carbonate) specimens showed a smooth surface (Figure 3.6 A), pits and cavities were seen on surfaces when incubated in lipase solution after rinsing with 70% (v/v) ethanol and drying (Figure 3.6 B–E). Over time, pits evolved into regular patterned cavities. The surfaces of specimens were progressively eroded by lipase while control specimens incubated in PBS maintained a smooth surface (Figure 3.6 F).

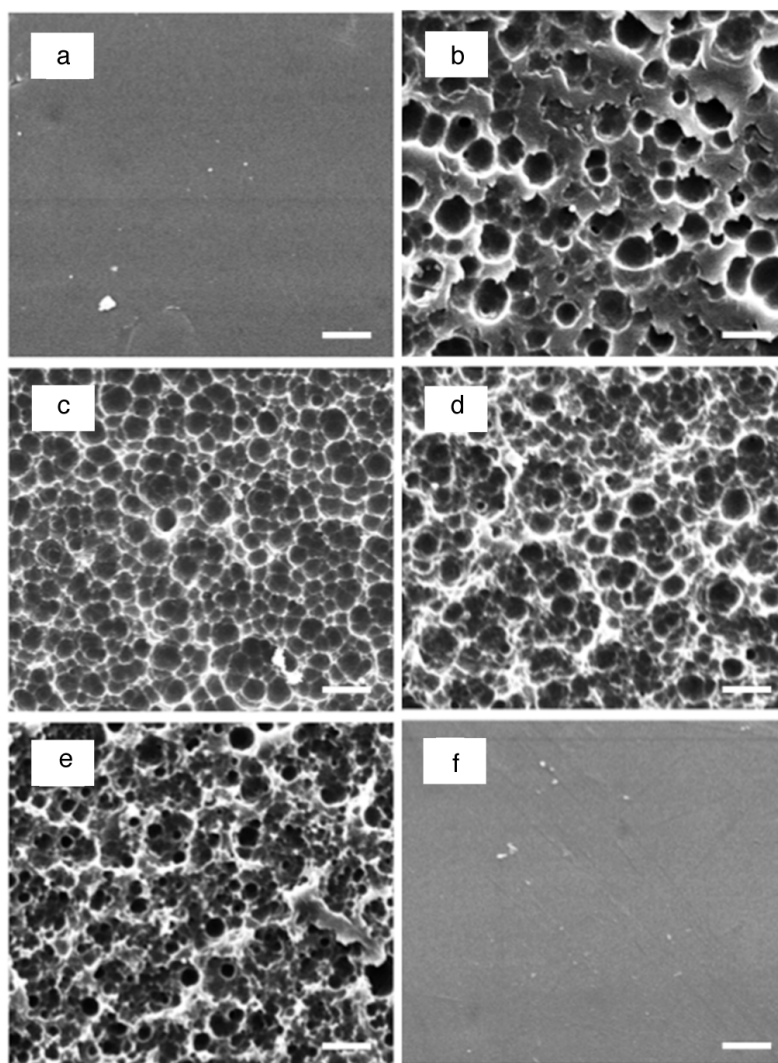


Figure 3.6: SEM morphology of disc shaped specimens from poly(tyrosol carbonate) after incubation in lipase solution: (A) 0 weeks, (B) 1 week, (C) 4 weeks, (D) 6 weeks, (E) 9 weeks, (F) 9 weeks, PBS control, after rinse with 70% (v/v) ethanol. Scale bar =10  $\mu\text{m}$ .

The mechanical properties of poly(tyrosol carbonate), the fastest eroding composition, were evaluated over time in lipase solution and PBS as a control. In both conditions, the modulus,  $\sigma_{yield}$ , and  $\epsilon_{yield}$  values were retained for a period of at least 18 weeks, as shown in Table 3.5.

Table 3.5: Mechanical properties of poly(tyrosol carbonate) during erosion. (Mean  $\pm$  SD, n = 4)

Time	Modulus (GPa)		$\sigma_{yield}$ (MPa)		$\epsilon_{yield}^c$		Mass loss <sup>b,c</sup>	
	Lipase	PBS	Lipase	PBS	Lipase	PBS	Lipase	PBS
24 h	0.9 <sup>d</sup>	0.8 <sup>e</sup>	25 $\pm$ 2	27 $\pm$ 2	4%	5%	1%	-
1 wk	0.8 <sup>d</sup>	0.8 <sup>d</sup>	21 $\pm$ 2	34 $\pm$ 5	4%	6%	7%	-
4 wk	0.8 <sup>d</sup>	0.9 <sup>e</sup>	26 $\pm$ 1	26 $\pm$ 2	6%	5%	17%	-
18 wk	0.9 <sup>d</sup>	0.8 <sup>d</sup>	22 $\pm$ 1	27 $\pm$ 1	4%	6%	65%	-

<sup>a</sup>Tested in PBS at 37 °C; <sup>b</sup>Mass loss 400  $\mu$ m thick specimens; SD <sup>c</sup><10%; <sup>d</sup> $\pm$  0.1; <sup>e</sup> $\pm$  0.3 GPa

When engineering surface eroding devices, however, it has to be considered that due to changes in the specimens dimensions the force required to deform the specimens will decrease with time. Nevertheless, the change is predictable, and may be adjusted for by setting the design parameters. In comparison, for bulk-degrading devices, mechanical properties decline in a less controllable manner. For example, poly(DL-lactic acid) specimens are weakened by the possible formation of hollow structures in the bulk with only the retention of an outer shell (44).

#### 3.4.4 Glass Transition Temperature and Onset of Enzymatic Erosion

We studied the temperature dependence of enzymatic erosion on thin films of polycarbonates from Ty and Hva using QCM-D (Figure 3.7). The experiment was conducted by stepwise increasing the temperature in a range between 20 and 49 °C as shown in the QCM-D frequency traces of Figure 3.7A. Lipase was adsorbed at the beginning of the experiments, showing comparable adsorption isotherms for all compositions with frequency changes ( $\Delta f$ ) of -22 Hz and -26 Hz (mass adsorption of 290 460 ng cm<sup>-2</sup>) at 20 °C(Figure 3.7B). At this temperature all polycarbonate thin films were stable against enzymatic degradation. Then, at specific, polymer composition-dependent onset temperatures ( $T_{onset}$ ), a transition in the frequency traces upon raising the temperature was observed for all the samples, indicating the beginning of enzymatic surface erosion.

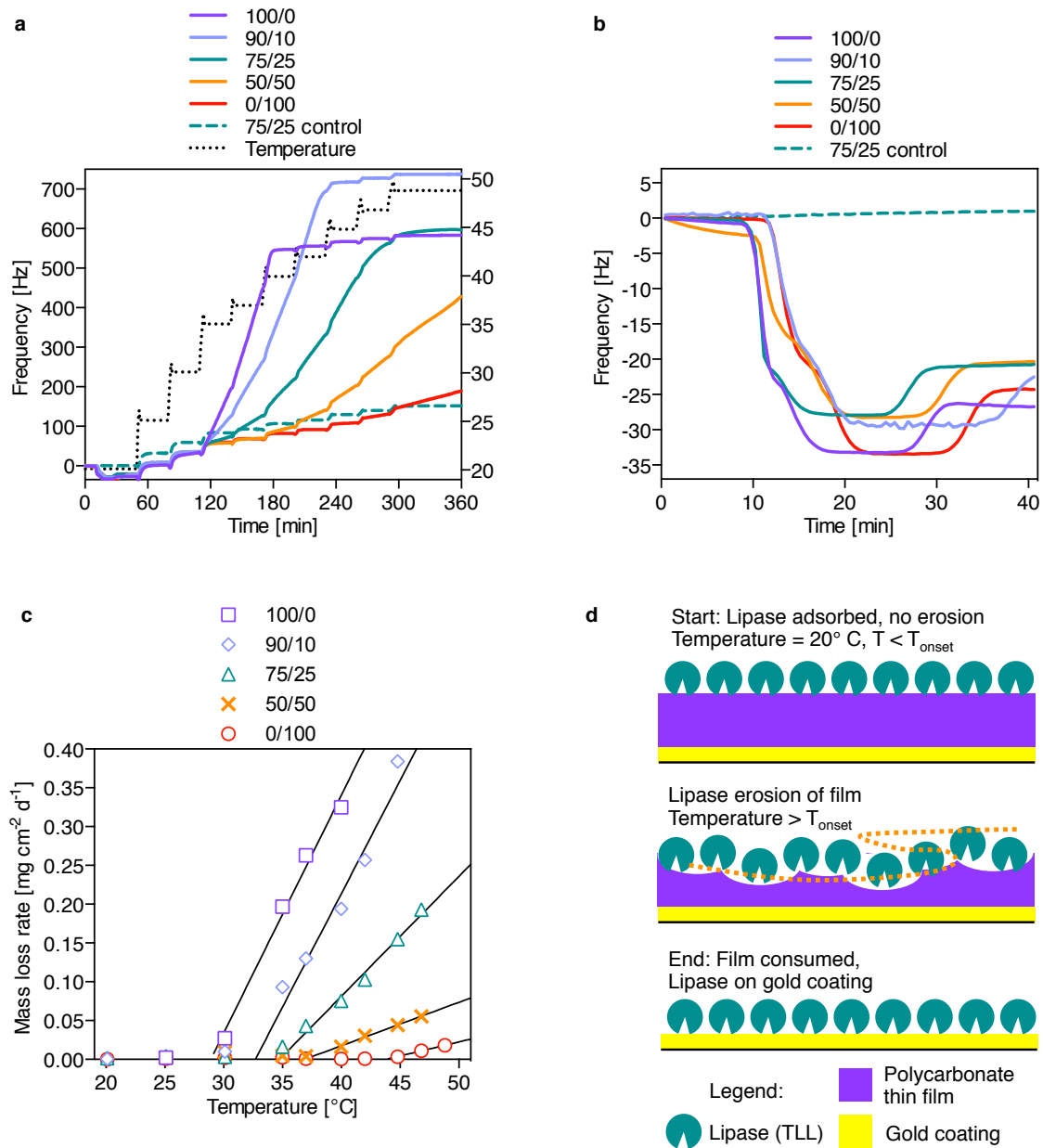


Figure 3.7: (A) QCM-D temperature dependent frequency plots of thin films from compositions of Ty/Hva (mol %) 100/0, 90/10, 75/25, 50/50, and 0/100 with preadsorbed lipase and PBS control for 75/25, (B) lipase adsorption at 20 °C), no erosion, (C) plot of rate of mass loss per area in dependence of temperature, (D) illustration of lipase adsorption at start (20 °C), erosion beyond  $T_{g(\text{wet})} - 20$  °C) and end behavior with lipase on gold.

The slope of the section in the erosion curves after equilibration in between temperature steps was used to calculate the rates of mass loss per unit area Figure 3.7C.

We observed at a certain temperature onset of mass loss for all compositions. Moreover, this onset temperature for mass loss was determined by extrapolating the linear section of the curves. The onset temperatures for mass loss, determined in such way were close to  $T_{g(wet)} - 20^\circ\text{C}$  for all compositions.

Table 3.6: Temperature-dependent erosion behavior of QCM-D and macroscopic films

Ty/ Hva (mol %)	QCM-D	$\Delta(T_{g,wet}$	QCM-D <sup>a</sup>	Macroscopic <sup>a</sup>
	$T_{onset}$ ( $^\circ\text{C}$ )	$-T_{onset}$ ) ( $^\circ\text{C}$ )	mass loss rate ( $\text{mg cm}^{-2} \text{d}^{-1}$ )	mass loss rate ( $\text{mg cm}^{-2} \text{d}^{-1}$ )
100/0	29	21	$0.20 \pm 0.02$	$0.14 \pm 0.01$
90/10	33	21	$0.12 \pm 0.01$	$0.07 \pm 0.01$
75/25	34	20	$0.03 \pm 0.01$	$0.03 \pm 0.01$
50/50	37	20	-	-
0/100	43	20	-	-

<sup>a</sup>Rate at  $37^\circ\text{C}$  as determined from linear regression.

We can therefore define the onset temperature for enzymatic surface erosion which can be expected around  $T_{onset} = T_{g(wet)} - 20^\circ\text{C}$ , where  $T_{g(wet)}$  stands for the glass transition temperature of fully hydrated samples (Table 3.6). Once  $T_{onset}$  was reached, frequency increased dramatically even after temperature equilibration, indicating erosion of the polymer films. In control experiments without lipase, no frequency changes beyond baseline equilibration were observed throughout the temperature range. For example, poly(tyrosol carbonate), the polymer with the lowest  $T_{g(wet)}$  in the series ( $50^\circ\text{C}$ ), has an expected  $T_{onset}$  of  $30^\circ\text{C}$  and was observed to undergo enzymatic surface erosion starting at  $29^\circ\text{C}$ . Most strikingly, even poly(Hva carbonate), which is non-erodible at  $37^\circ\text{C}$ , undergoes enzymatic erosion at  $43^\circ\text{C}$ . As expected, the rates of erosion increase upon heating, reflecting the temperature dependence of enzyme activity. Further differences in the rates of mass loss among the polymers at a given temperature may be due to structural effects such as steric hindrance at the lipase



active site caused by the methoxyaryl groups present in Hva.

Enzyme-mediated degradation of synthetic, degradable polymers is predominantly reported for flexible and rubbery polymers and not for stiff and glassy materials. In this sense, polymer chain flexibility appears to be an important determining factor. It is noteworthy that previous studies suggested increased flexibility of polymer chains in confinement as compared to the bulk: A depression of the bulk  $T_g$  value by approximately 20 °C was observed in ultrathin films (thickness below 100 nm) of polystyrene as a model system for confinement (58). We suggest that the polymer chain flexibility at the surface may be increased toward a more rubbery-like behavior compared to a glassy bulk (37). Similarly, the hydrated surface of glassy polymers, such as polycarbonates from Ty and Hva may start to behave in a rubbery manner at about 20 °C below the measured bulk  $T_{g(wet)}$  value. At that temperature, the active site of lipase adsorbed on the polymer surface is able to interact with hydrolyzable carbonate groups to mediate polymer degradation.

Interestingly, the identification of a  $T_{onset}$  for the enzymatic erosion of degradable polymers approximately 20 °C below  $T_{g(wet)}$  may also explain why amorphous poly(L-lactic acid) is susceptible to degradation by Proteinase K at 37 °C, while aromatic polycarbonates such as poly(DTE carbonate) with a  $T_g$  of 90 °C<sup>21</sup> have a glass transition out of a biologically relevant temperature range and do not exhibit enzymatic erosion under physiological conditions.

### 3.4.5 Cell Viability and Proliferation

Three polycarbonates from Ty and Hva (100, 90, and 50 mol % Ty) were evaluated as substrates for attachment and proliferation of human mesenchymal stem cells (hMSCs) relative to tissue-culture polystyrene (TCPS). Bone marrow-derived hMSCs were selected for these studies in view of the potential biomedical applications of these high-strength materials in orthopedics. In comparison, all compositions supported cell attachment and proliferation equally with no statistical differences found (Figure 3.8). After 4 days, hMSCs exhibited spread morphologies on all substrates as observed by confocal microscopy (Figure S5, Supporting Information). Confluence was reached after 7 days in culture on all substrates with cell densities of approximately  $6 \times 10^4 \text{ cells cm}^{-2}$ .

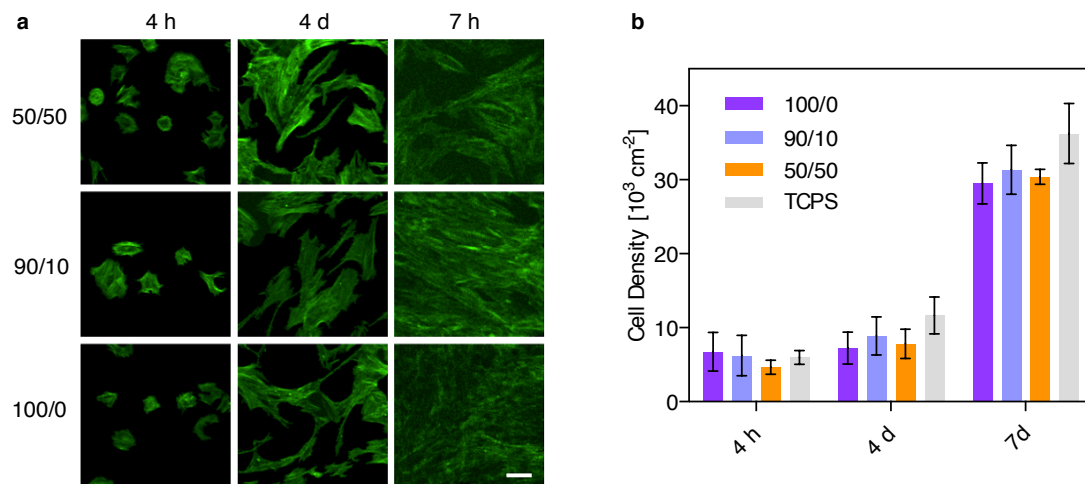


Figure 3.8: Cell viability of hMSCs on polycarbonate substrates of Ty/Hva (mol %) 100/0, 90/10, 50/50 after 4 h, 4 days, and 7 days: (A) Representative images from epifluorescence microscopy on hMSC morphology, scale bar = 100  $\mu\text{m}$ , (B) cell density determined by AlamarBlue assay relative to standards on TCPS (mean  $\pm$  SE,  $n = 3$ ).

### 3.5 Conclusion

While the phenomenon of enzymatic surface erosion has been linked to polymer chain flexibility before, it has not been recognized that a rather simple correlation with a polymers glass transition temperature can explain why some polymers undergo enzymatic surface erosion while others seem to be unaffected by enzymes. Our results demonstrate that the ability of enzymes to erode a polymer surface is not merely an intrinsic property of the polymer. Instead, it seems that the susceptibility of a polymer to undergo enzymatic surface erosion is determined by the experimental conditions and that a simple correlation ( $T_{onset} = T_{g(wet)} - 20^{\circ}\text{C}$ ) may allow one to predict if a given polycarbonate will undergo surface erosion under physiological conditions. This new understanding of enzymatic surface erosion can now be used to design innovative polymers that will exhibit enzymatic surface erosion at specific experimental conditions. This is exemplified by the system of new aromatic–aliphatic polycarbonates from the natural phenols tyrosol and homovanillyl alcohol. For selected compositions among these polymers, the hydrated surface layer of the polymer at physiological conditions (37 °C) is flexible enough to allow for enzymatic degradation, while the bulk still maintains the mechanical strength of a glassy material. In future studies, we will explore whether similar correlations can be established for other types of biomedically important polymers such as polyesters and polyamides.

## Chapter 4

# Highly Chemoselective Phosgenation of (Hydroxyalkyl)phenols for Pre-Programmed Carbonate Diols

### 4.1 Abstract

In this chapter, a new synthetic toolkit was developed for the selective phosgenation of (hydroxyalkyl)phenols respective to either alcoholic and phenolic hydroxyl groups. The resulting diaryl carbonate diols, dialkyl carbonate diols as well as hydroxyphenyl alkyl chloroformates were obtained in catalyst free conditions without use of protection groups.

The compounds constitute bifunctional polymerizable units which can serve as a new class of pre-programmed monomers for the synthesis of polycarbonates with controlled polymer backbone sequence. This is realized either by the chemoselective preformation of a carbonate in a dimer derived from (hydroxyalkyl)phenols or by creating heterobifunctional hydroxyphenyl alkyl chloroformates. For selectivity of bis(trichloromethyl) carbonate (BTC) towards the phenolic hydroxyl biphasic reactions were explored containing a basic aqueous phase loaded with the (hydroxyalkyl)phenolate and an insoluble organic phase containing the BTC. Systematically, reaction conditions were optimized to obtain bis(4-(2-hydroxyethyl))phenyl carbonate from tyrosol at high selectivity and yield. In polar, aprotic solvents such as THF the hydroxyphenyl alkyl chloroformate was formed *in situ* when a slight excess of BTC was used. After acid removal, the bis(hydroxyphenalkyl) carbonate was prepared from equivalent of (hydroxyalkyl)phenols under slow addition of pyridine as a

base.

## 4.2 Introduction

Organic carbonates are functional groups with major prominence in important industrial as well as biomedical applications. For example, dimethyl carbonate as well as diphenyl carbonates serve as fuel additives and polycondensation agents (129). Further, carbonates can provide a hydrolytically labile bond in the formation of prodrugs in medicinal chemistry (134) and in degradable polymers for biomedical implants (39). A classic synthesis of industrial polycarbonates is conducted using phosgene gas in a biphasic system comprised of alkaline aqueous and in-miscible organic phase (115). The synthetic versatility of phosgenation reactions has seen a fruitful expansion, since the use of the crystalline bis(trichloromethyl) carbonate, a reagent that was originally discovered in the nineteenth century (30), has been popularized for its safer handling properties (36). Likewise, BTC has proven useful for interfacial polymerization reactions to obtain aromatic polycarbonates (67).

In contrast, aliphatic polycarbonates such as poly(trimethylene carbonate) are best obtained by ring-opening polymerization using Stannous Octanoate as an auxiliary (143; 68). Recently, dimeric aliphatic polycarbonates were formed directly from CO<sub>2</sub> at atmospheric pressure (137).

Derivatives of (hydroxyalkyl)phenols such as tyrosol and hydroxytyrosol have drawn attention by the scientific community as they possess anti-inflammatory (10) and anti-oxidant activities (84). Chemoselective derivatization such as esterifications of (hydroxyalkyl)phenols have been explored at the alcoholic hydroxyl (13; 105) using acidic conditions, while selectivity for the phenolic hydroxyl requires formation of the phenolate under basic conditions (92). Further, selective silylation as a protection strategy is possible (116).

Surprisingly, no study has directly compared the selectivity of phosgenation reactions

for aliphatic hydroxyls and aromatic hydroxyl groups.

Previously, we have reported on the synthesis of polycarbonates from natural (hydroxyalkyl)phenols such as tyrosol and homovanillyl alcohol (119). The pyridine catalyzed polycondensation of these natural (hydroxyalkyl)phenols resulted in the formation of a distribution of diaryl, dialkyl or aryl alkyl carbonates in the polymer backbone. Herein, we report on the exploration of synthesis methods to selectively obtain diaryl and dialkyl carbonate diols by fine tuning interfacial reactivity as well as the use of auxiliaries such as Pyridine in the organic bulk. Such bifunctional carbonate diols are potentially useful in the synthesis of sequence controlled polymers using a pre-programmed monomer approach (98; 103). The potential advantages of sequence such as improvement of mechanical properties and control of the degradation rate will then be explored in the following chapters.

## 4.3 Experimental

The reagents used and the general procedures followed are described in **Chapter 2**. The synthesis procedures developed in this chapter are shown below.

### 4.3.1 Analytical Methods for Small Molecule Characterization

For  $^1\text{H}$ -NMR and  $^{13}\text{C}$  NMR spectroscopy, VNMRs (Varian, Palo Alto CA) with 400 MHz or 500 MHz were used at 25 °C with solvents  $\text{CDCl}_3$  referenced to TMS or  $\text{DMSO}-d^6$  referenced to the solvent signal. The signals are reported as chemical shift ( $\delta$ ) in parts per million; provided the multiplicity of the signals: s = singlet, d = duplet, t = triplet and m = multiplet and respective coupling constant ( $J$ ).

ESI-mass spectrometry was conducted on a Finnigan LCQ-DUO (ThermoFisher Scientific, Waltham, MA). The sample was manually injected using a syringe. Then the spectra were analyzed with the manufacturer's Xcalibur software. The most abundant ion peaks with relative intensities of isotopic patterns are annotated including

associated atoms as the mass per charge ratio ( $m/z$ ).

### 4.3.2 Synthesis

#### Optimization of biphasic phosgenation of tyrosol

Tyrosol (4-(2-hydroxyethyl)phenol) **1a** (4.45 g, 0.032 mol) was dissolved in 100 ml deionized water with NaOH (0–1.2 equiv.) as an inorganic base or an organic base such as Py or TEA. BTC (0.5–0.55 equiv.) was dissolved in 67 ml DCM. Both solutions were cooled to 5 °C in an ice/ water bath. The aqueous solution was added to the organic phase at a stirring rate of 300 rpm using an overhead stirrer. After 2 h the ice/ water bath was removed and stirring was continued for a 24h period. After separation of the phases, the organic phase was washed with HCl, then dried with MgSO<sub>4</sub> and filtered. The solvent was removed and the crude was dried *in vacuo*. After drying, the composition of the crude, the relative yield were determined by weighing. The composition of the crude was analyzed by <sup>1</sup>H-NMR spectroscopy and ESI-MS.

#### Substrate scope for biphasic phosgenation of (hydroxyalkyl)phenols

The synthesis and characterization of diaryl carbonate diols for the substrate scope of various (hydroxyalkyl)phenols such as 4-(3-hydroxypropyl)phenol **1b**, 4-(2-Hydroxyethyl)-2-methoxyphenol (homovanillyl alcohol) **1c**, 2-(2-hydroxyethyl)phenol **1d**, 4-hydroxybenzyl alcohol **1e** and 3-hydroxybenzyl alcohol **1f**, was conducted applying the conditions optimized for tyrosol.

### Selective formation of aliphatic chlorocarbonyls from (hydroxyalkyl)phenols

A oven-dried round bottom flask equipped with a magnetic stirrer was flushed with dry nitrogen gas. Then respective (hydroxyalkyl)phenol **1a–d** (1 equiv.) and BTC (1–1.2 equiv.) was added. The mixture was dissolved in dry THF added from a syringe under inert conditions. The reaction mixture was stirred for 24 h at ambient temperature. ESI-MS and NMR in CDCl<sub>3</sub> in reference to TMS were performed to confirm identity and composition of an 1 : 1 mixture of respective aliphatic chloroformate and trichloromethyl carbonate. The *insitu* mixture of equivalent chlorocarbonyl species was used for further reactions without additional purification.

### Synthesis of dialkyl carbonate diols from (hydroxyalkyl)phenols

Additional (hydroxyalkyl)phenol such as **1a–d** (1.0–1.2 equiv.) was supplemented to the respective aliphatic chlorocarbonyl. Under dry nitrogen atmosphere, Pyridine (1.0–1.2 equiv.) was added dropwise from a syringe pump over the course of 20 h at RT. Afterwards, the solution was subsequently reduced in volume and the solvent was removed *in vacuo*. The residue was dissolved in DCM (15 ml) and washed with 0.2 M HCl (7.5 ml). The organic phase was dried over MgSO<sub>4</sub> and filtered. Then the solvent removed and the product was dried *in vacuo*.

The dialkyl carbonate diols were either purified by flash chromatography or hydrolytic recrystallization in aqueous base.

### Bis(4-(2-hydroxyethyl)phenyl) carbonate **2a**

Tyrosol (4-(2-hydroxyethyl)phenol) (30.00 g, 0.22 mol) was dissolved in 675 ml deionized water with NaOH (10.42 g, 0.26 mol, 1.2 equiv.), BTC (11.81 g, 0.119 mol, 0.55 equiv.) was dissolved in DCM. Both solutions were cooled to 5 ice/water bath. The



two ice cold solutions were combined under a stirring rate of 300 rpm with an overhead stirrer. After 2 h the ice/water bath was removed and the mixture stirred until 24h were completed. 5 °C ice/water bath. The aqueous solution was added to the organic phase at a stirring rate of 300 rpm using an overhead stirrer. After 2 h the ice/water bath was removed and stirring was continued after a 24 h period was completed. After separation, the organic phase was washed subsequently with acidified HCl, then drying with MgSO<sub>4</sub>, filtering. Solvent was removed in vacuo. The product (crude yield: 29.4 g, 89%; selectivity: 99%) as a white solid. Isomeric byproducts were removed by recrystallization from DCM and hexane; white, crystalline solid (yield: 16.8 g, 57%, purity: 99.5%). Mp = 106 °C. <sup>1</sup>H-NMR (500 MHz, CDCl<sub>3</sub>) δ 7.29–7.23 (m, 4H), 7.23–7.17 (m, 4H), 3.84 (t, J = 6.5 Hz, 4H), 2.86 (t, J = 6.5 Hz, 4H), 1.61 (s, 2H). <sup>13</sup>C NMR (126 MHz, CDCl<sub>3</sub>) δ 152.62, 149.90, 137.13, 130.44, 121.26, 63.80, 38.83.

#### **Bis(4-(3-hydroxypropyl)phenyl) carbonate 2b**

<sup>1</sup>H-NMR (500 MHz, CDCl<sub>3</sub>) δ 7.26–7.14 (m, 4H), 3.66 (t, J = 6.4 Hz, 2H), 2.75–2.67 (m, 2H), 1.92–1.84 (m, 2H), 1.53 (s, 1H). <sup>13</sup>C-NMR (126 MHz, CDCl<sub>3</sub>) δ 152.57, 149.38, 140.14, 129.66, 120.97, 62.25, 34.33, 31.63. LRMS (ESI+) m/z Calcd. for C<sub>19</sub>H<sub>22</sub>O<sub>5</sub>Na [M+Na]<sup>+</sup> 353.36, found 353.3.

#### **Bis(4-(2-hydroxyethyl)-2-methoxyphenyl) carbonate 2c**

<sup>1</sup>H-NMR of crude (500 MHz, DMSO-*d*<sup>6</sup>) δ 7.17–7.06 (m, 1H), 7.02 (d, J = 1.8 Hz, 1H), 6.81 (dd, J = 8.1, 1.9 Hz, 1H), 3.81 (s, 3H), 3.61 (t, J = 7.0 Hz, 2H), 2.71 (t, J = 6.9 Hz, 2H). <sup>13</sup>C-NMR (126 MHz, DMSO-*d*<sup>6</sup>) δ 151.70 (s), 150.97 (s), 140.06 (s), 138.39 (s), 122.32 (s), 121.54 (s), 114.45 (s), 62.62 (s), 56.56 (s). LRMS (ESI+) m/z Calcd. for C<sub>19</sub>H<sub>22</sub>NaO<sub>7</sub> [M+Na]<sup>+</sup> 385.36, found 385.3.

**Bis(4-(2-hydroxymethyl)phenyl) carbonate 2e**

$^1\text{H}$ -NMR (500 MHz,  $\text{CDCl}_3$ )  $\delta$  7.44 (t,  $J = 12.7$  Hz, 2H), 7.27 (dd,  $J = 11.1, 1.6$  Hz, 2H), 4.65 (d,  $J = 72.3$  Hz 2H), 1.55 (s, 2H).

**Bis(4-(3-hydroxymethyl)phenyl) carbonate 2f**

$^1\text{H}$ -NMR (500 MHz,  $\text{CDCl}_3$ )  $\delta$  (td,  $J = 7.8, 3.5$  Hz, 1H), 7.30 (s, 1H), 7.25 (d,  $J = 7.6$  Hz, 1H), 7.23–7.19 (m, 1H), 4.53 (s, 2H).  $^{13}\text{C}$ -NMR (126 MHz,  $\text{DMSO-}d^6$ )  $\delta$  152.44 (s), 151.34 (s), 145.53 (s), 130.02 (s), 124.95 (s), 120.07 (s), 119.63 (s), 62.92 (s).

**4-hydroxyphenethyl carbonochloridate 3a and 4-hydroxyphenethyl(trichloromethyl)carbonate 3a\***

$^1\text{H}$  NMR (500 MHz,  $\text{CDCl}_3$ )  $\delta$  7.13–6.97 (m, 4H), 6.83–6.66 (m, 4H), 5.01 (s, 2H), 4.48–4.44 (m, 4H), 2.97–2.96 (m, 4H). (3a) LRMS (ESI-)  $m/z$  Calcd. for  $\text{C}_9\text{H}_9\text{Cl}_2\text{O}_3$   $[\text{M}+\text{Cl}]^-$  234.99 (100.0%), 236.99 (63.9%), 238.99 (10.6%), 236.00 (10.0%), 237.99 (6.3%) found 353.28 (100%), 237.19 (64.9%), 238.9 (8%), 236.12 (23.8%), 237.96 (11.2%). (3a\*) LRMS (ESI-)  $m/z$  Calcd. for  $\text{C}_{10}\text{H}_9\text{Cl}_4\text{O}_4$   $[\text{M}+\text{Cl}]^-$  334.92 (100.0%), 332.93 (78.2%), 336.92 (47.9%), 335.93 (11.1%), 338.92 (10.6%), 333.93 (8.7%), 337.92 (5.3%) found 334.91 (100%), 333.26 (75.5%), 336.80 (62.4%), 335.95 (8.4%), 338.81 (13.44%), 334.16 (5.88%), 337.91 (5.17%).

**3-(4-hydroxyphenyl)propyl carbonochloridate 3b and 3-(4-hydroxyphenyl)-propyl(trichloromethyl)carbonate 3b\***

$^1\text{H}$  NMR (400 MHz,  $\text{CDCl}_3$ )  $\delta$  7.09–7.00 (m, 4H), 6.83–6.68 (m, 4H), 4.71 (d,  $J = 1.0$  Hz, 2H), 4.35–4.30 (m, 2H), 4.30–4.26 (m, 2H), 2.70–2.64 (m, 4H), 2.08–1.95 (m, 4H). (3b) LRMS (ESI-)  $m/z$  Calcd. for  $\text{C}_{10}\text{H}_{11}\text{Cl}_2\text{O}_3$   $[\text{M}+\text{Cl}]^-$  249.01 (100%), 251.01 (64.5%), 250.01 (11.1%), 253.00 (10.2%), 252.01 (7%), 254.01 (1.2%) found 249.23 (100%), 251.14 (65.2%), 250.12 (19.7%), 253.2 (5.6%), 252.1 (8.1%), 254.55

(0.2%). (3b\*) LRMS (ESI-)  $m/z$  Calcd. for  $C_{11}H_{11}Cl_4O_4$   $[M+Cl]^-$  348.94 (100.0%), 346.94 (78.2%), 350.94 (49.4%), 349.94 (12.2%), 352.93 (10.2%), 347.94 (9.3%), 351.94 (5.8%) found 348.84 (100%), 347.07 (75.2%), 350.76 (49.1%), 349.90 (9.7%), 352.77 (6.7%), 348.12 (7.7%), 351.78 (2.5%).

**4-hydroxy-3-methoxyphenethyl carbonochloridate 3c and 4-hydroxy-3-methoxyphenethyl(trichloromethyl)carbonate 3c\***

$^1H$  NMR (400 MHz,  $CDCl_3$ )  $\delta$  6.91–6.83 (m, 4H), 6.76–6.66 (m, 4H), 4.47 (t,  $J = 7.0$  Hz, 2H), 4.45 (t,  $J = 7.2$  Hz, 2H), 3.89 (s, 6H), 2.97 (t,  $J = 7.1$  Hz, 2H), 2.96 (t,  $J = 7.1$  Hz, 2H). (3c) LRMS (ESI-)  $m/z$  Calcd. for  $C_{10}H_{11}Cl_2O_4$   $[M+Cl]^-$  265.00 (100.0%), 267.00 (63.9%), 266.01 (11.1%), 269.00 (10.7%), 268.00 (7.0%), 267.01 (1.4%), 270.00 (1.1%).

**2-hydroxyphenethyl carbonochloridate 3d**

$^1H$  NMR (400 MHz,  $CDCl_3$ )  $\delta$  7.39–7.04 (m, 2H), 7.04–6.60 (m, 2H), 5.27 (s, 1H), 4.54 (m, 2H), 3.07 (m, 2H).

**Bis(4-hydroxyphenethyl) carbonate 4a**

4-hydroxyphenethyl carbonochloridate and 4-(2-hydroxyethyl)phenol are dissolved in anhydrous tetrahydrofurane. Pyridine in DCM was added dropwise over 24 h. The solvent was evaporated and the residue dissolved in DCM. The crude was purified by subsequent aqueous washes with 1 N HCl and 5 M NaCl. Hydrolytic recrystallization was applied by heating the washed crude in  $H_2O$ / DI (15 mg  $ml^{-1}$ ) to 70 °C. Then NaOH was added drop wise (1 equiv.). The hot solution was filtered off. Immediately, HCl (1 equiv.) was added and the precipitate was filtered off when the solution cooled to RT. The product was rinsed with ice cold  $H_2O$ / DI and lyophilized for 48 h.

Yield: 54 %. White crystalline solid  $^1\text{H}$  NMR (500 MHz,  $\text{CDCl}_3$ )  $\delta$  7.07 (t,  $J = 5.5$  Hz, 1H), 6.82–6.68 (m, 1H), 4.81 (s, 1H), 4.27 (t,  $J = 7.2$  Hz, 1H), 2.89 (t,  $J = 7.1$  Hz, 1H).  $^{13}\text{C}$  NMR (126 MHz,  $\text{DMSO-}d^6$ )  $\delta$  156.6, 155.1, 130.2, 128.2, 115.8, 68.8, 34.1.  $^{13}\text{C}$ -NMR (126 MHz,  $\text{CDCl}_3$ )  $\delta$  155.48, 154.61, 130.45, 129.73, 115.75, 77.61, 77.36, 77.11, 68.86, 34.59. LRMS (ESI-)  $m/z$  Calcd. for  $\text{C}_{17}\text{H}_{18}\text{ClO}_5$   $[\text{M}+\text{Cl}]^-$  301.11 (100%), 302.11 (18.8%), 303.11(2.6%) found 301.25 (100%), 302.27 (16.3%), 303.22 (0.9%).

### **Bis(3-(4-hydroxyphenyl)propyl) carbonate 4b**

$^1\text{H}$  NMR (400 MHz,  $\text{CDCl}_3$ )  $\delta$  7.05 (d,  $J = 8.4$  Hz, 1H), 6.77 (t,  $J = 5.6$  Hz, 1H), 5.03 (s, 1H), 4.15 (t,  $J = 6.5$  Hz, 1H), 2.70–2.60 (m, 1H), 1.96 (dq,  $J = 13.4, 6.6$  Hz, 1H). LRMS (ESI+)  $m/z$  Calcd. for  $\text{C}_{19}\text{H}_{22}\text{O}_5\text{Na}$   $[\text{M}+\text{Na}]^+$  353.14 (100%), 354.14 (21.0%), 355.14 (3.1%) found 353.21(100%), 354.22(20.2%), 355.17(1.9%). LRMS (ESI-)  $m/z$  Calcd. for  $\text{C}_{19}\text{H}_{21}\text{O}_5$   $[\text{M}-\text{H}]^-$  329.14 (100%), 330.13 (20.7%), 331.15 (2.1%) found 329.4 (100%), 330.5 (19.1%), 331.66 (1.4%).

### **Bis(4-hydroxy-3-methoxyphenethyl) carbonate 4c**

$^1\text{H}$  NMR (400 MHz,  $\text{CDCl}_3$ )  $\delta$  6.84 (dd,  $J = 10.1, 5.9$  Hz, 1H), 6.75–6.69 (m, 1H), 5.54 (s, 1H), 4.30 (t,  $J = 7.2$  Hz, 1H), 3.87 (s, 1H), 2.90 (t,  $J = 7.2$  Hz, 1H). LRMS (ESI-)  $m/z$  Calcd. for  $\text{C}_{19}\text{H}_{21}\text{O}_7$   $[\text{M}-\text{H}]^-$  361.13(100%), 362.13(20.8%), 363.14(2.1%) found 360.97(100%), 362.01(18.1%), 363.01(2.0%) LRMS (ESI+)  $m/z$  Calcd. for  $\text{C}_{19}\text{H}_{22}\text{O}_7\text{Na}$   $[\text{M}+\text{Na}]^+$  385.13(100%), 386.13(21.1%), 387.13(3.5%) found 385.12(100%), 386.11(20.1%), 387.11(2.6%).

### **Bis(2-hydroxyphenethyl) carbonate 4d**

$^1\text{H}$  NMR (500 MHz,  $\text{CDCl}_3$ )  $\delta$  7.13 (ddd,  $J = 14.8, 7.4, 1.6$  Hz, 1H), 6.87 (td,  $J = 7.4, 1.1$  Hz, 1H), 6.80 (dd,  $J = 8.0, 1.0$  Hz, 1H), 4.34 (td,  $J = 7.0, 1.0$  Hz, 1H), 2.99 (t,  $J = 7.0$  Hz, 1H).  $^{13}\text{C}$ -NMR (126 MHz,  $\text{CDCl}_3$ )  $\delta$  155.8, 154.6, 131.4, 128.7,

123.7, 121.2, 116.2, 68.1, 30.44. LRMS (ESI+)  $m/z$  Calcd. for  $C_{17}H_{18}NaO_5$   $[M+Na]^+$  325.11(100%), 326.11(18.8%), 327.11(2.7%) found 325.19(100%), 326.21(16.3%), 327.2(1.8%).

## 4.4 Results and Discussion

### 4.4.1 Chemoselectivity in Biphasic Reaction Systems

We explored the chemoselectivity of the reaction of (hydroxyalkyl)phenols and triphosgene in biphasic reaction systems comprised of a basic aqueous phase containing compound **1a** and a triphosgene loaded, immiscible organic phase. As a starting point for our study, we supposed that the reactivity of the phenolate towards the chloro-carbonyl species at the interface may be favored over the reactivity of the alcoholic hydroxyl.

The results of the optimization of reaction parameters for the biphasic phosgenation of **1a** are shown in Table 4.1. The diaryl carbonate diol **2a** was selectively formed under basic conditions using NaOH. The optimized conditions required a slight excess of BTC (0.55 eq.) and sufficient base (1.2 eq. of NaOH) to obtain **2a** at 98% selectivity with a yield of 89% (entry 4). Only a slightly larger excess of base compared to BTC resulted in a reduced yield of 68 % (entry 3). This difference was most likely due to hydrolysis of partially water soluble reaction intermediates such as chloroformates and product. Interestingly, the dependence of the final yield on the equivalents of NaOH as opposed to the interfacial reaction of BPA which forms more hydrophobic phosgenation products. In latter case the outcome remained constant tolerating a range of NaOH excess (18).

As expected, no formation of **2a** was observed, without the presence of a base (entry 1.1). However, trace amounts of aliphatic chloroformate **3a** were formed indicating residual reactivity of alcoholic hydroxyl in the biphasic system.

Table 4.1: Optimization study for biphasic diaryl carbonate diol synthesis

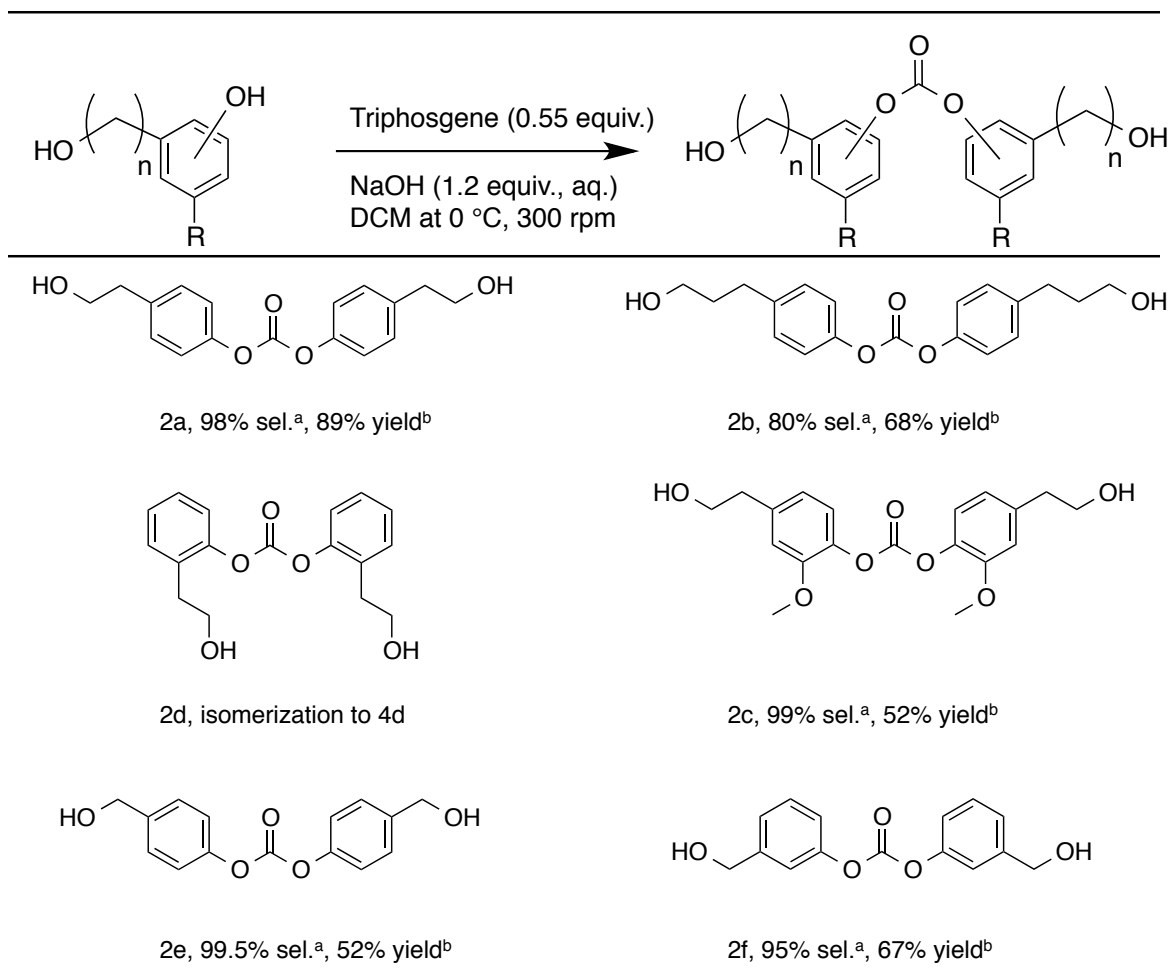
Entry	BTC (equiv.)	Base (equiv.)	Product composition (%) <sup>a</sup>				Yield <sup>b</sup> (%)
			2a	3a	4a	5a	
1.1	0.5	-	-	100	-	-	2
1.2	0.5	1.0 (NaOH)	89	10	-	1	21
1.3	0.5	1.2 (NaOH)	96	1	-	3	68
<b>1.4</b>	<b>0.55</b>	<b>1.2 (NaOH)</b>	<b>98</b>	<b>1</b>	-	<b>1</b>	<b>89</b>
1.5	0.5	1.0 (Py) <sup>c</sup>	60	-	30	10	1
1.6	0.5	1.2 (NaOH), 0.1 (TEA)	81	-	-	19	6
1.7	0.5	1.2 (NaOH), 0.1 (Py)	75 of quadrimers <sup>d</sup> , 25 of trimers <sup>d</sup>				41

<sup>a</sup>Determined by <sup>1</sup>H NMR of crude; <sup>b</sup>Overall yield; <sup>c</sup>Dropwise addition; <sup>d</sup>Identified by ESI-MS.

The use of organic base resulted in mixtures of isomeric products indicating side reactions in the organic bulk phase in competition to the interfacial reaction of the phenolic hydroxyl. While the slow addition of pyridine lead only to the formation of residual isomeric carbonates **2a**, **4a** and **5a**, a catalytic amount of pyridine in the presence of NaOH had a dramatically different effect (entry 1.7): trimers and quadrimers indicating the transition of the reaction system towards oligomerization and loss of chemoselectivity. This scenario was in accordance with the previous synthesis of polycarbonates from **1a** in DCM in the presence of pyridine showing a distribution of three possible carbonates within a polycarbonate backbone. Further, the use of TEA

as a base shifted some of the chemoselectivity towards the aryl alkyl carbonate **5a** with a merely modest yield. It is noteworthy, that we could not confirm the presence of chlorination products of **5a** which may occur in larger excess of organic base (133). Lastly, only reactant **1a** was isolated from the aqueous phase after completion of the reaction.

Table 4.2: Substrate scope diaryl carbonate diols of (hydroxyalkyl)phenols from biphasic reactions



<sup>a</sup>Determined by <sup>1</sup>H NMR analysis of crude. <sup>b</sup>Combined yield of phosgenation products.

To highlight the biphasic system for the synthesis of diaryl carbonate diols from (hydroxyalkyl)phenols, as shown for **2a**, the previously optimized conditions were applied on a range of substrates (as shown in Table 4.2). The respective products were obtained from the organic phase. As expected, the formation of a slightly more

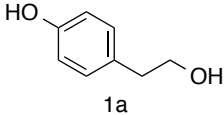
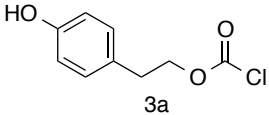
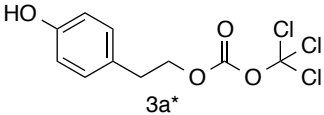
hydrophobic diaryl carbonate diol (**2b**) with an additional methylene group is also achieved with good selectivity (80%). Similarly, the reaction tolerated a methoxyl group in *ortho*-position to the phenol as in **2c**. In contrast, during the formation of **2d** isomerization into **4d** occurred. This may be attributed to facilitating effects by the *ortho*-hydroxethyl group and the formation of 7-membered cyclic carbonates, a previously reported carbonate species (17). The yield decreased significantly when more hydrophilic (hydroxyalkyl)phenols were used as observed for **2e** and **2f**. This may be explained with less hydrophobic intermediates and products hydrolyzed upon transient partitioning into the basic aqueous phase as compared to the more hydrophobic **2a** and **2b**.

#### 4.4.2 Chemoselectivity Under Acidic Conditions

It was rationalized that acidic reaction conditions without the presence of a base may selectively favor formation of aliphatic phosgenation products of (hydroxyalkyl)phenols. Accordingly, we focused primarily on the exploration of solvent choices as the main handle to optimize the formation of aliphatic chlorocarbonyls exemplified on **1a** as shown in Table 4.3.



Table 4.3: Optimization of aliphatic chlorocarbonyl formation

<div style="display: flex; align-items: center; justify-content: space-around;"> <div style="text-align: center;">  <p>1a</p> </div> <div style="text-align: center;"> <p>Triphosgene</p> <p>→</p> <p>Solvent (anhydrous), RT</p> </div> <div style="text-align: center;">  <p>3a</p> </div> <div style="text-align: center;">  <p>3a*</p> </div> </div>				
Entry	Solvent	Base (equiv.)	Selectivity (%) <sup>a</sup>	Conversion (%) <sup>a,b</sup>
3.1	Chloroform		50	<4
3.2	DCM		-	<1
3.3	Dioxane		96	99
3.4	THF		98	99
3.5	THF	Py (0.3)	95	99
3.5	THF	Py (1.0)	81	99
3.6	Toluene		-	<1

<sup>a</sup>Determined by <sup>1</sup>H NMR and ESI-MS of crude; <sup>b</sup>Combined n(3a) and 2n(3a\*)

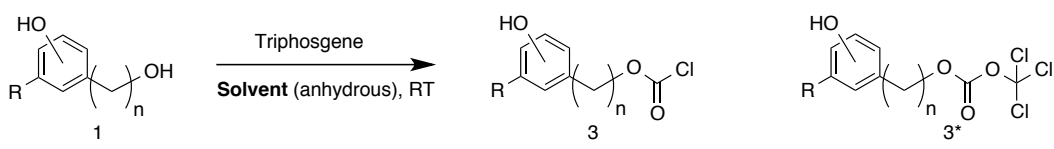
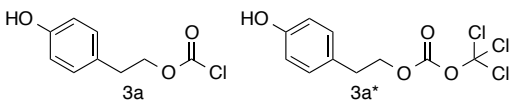
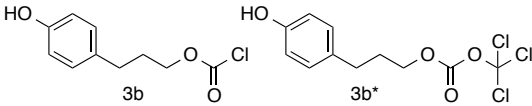
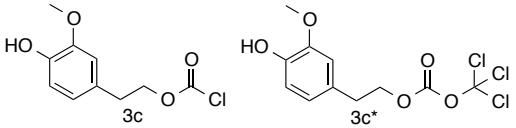
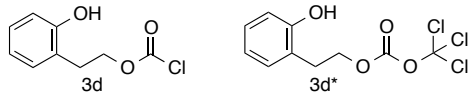
The use of anhydrous THF as a solvent for the reaction of BTC with (hydroxymethyl)phenol **1a** provided aliphatic chlorocarbonyls at high chemoselectivity (98%) and conversion (99%). Chloroformate **3a** and trichloromethyl carbonate **3a\*** formed a pair of corresponding aliphatic chlorocarbonyls in an 1 : 1 mixture; as identified by ESI-MS due to their respective *m/z* and the isotopic pattern revealing the chlorine atom content; and quantified by profile fitting the integrals of respective overlapping <sup>1</sup>H NMR triplets (Supplementary information). This finding is in accordance with the observations in a report describing the chlorocarbonyl species present during the methanolysis of BTC (99). In comparison to the methanolysis of BTC, however, only residual conversion into carbonate species was observed even after a prolonged period of 7 d reaction time.

An earlier study reported on the conversion of the chlorocarbonyl pair into chloroformate by addition of pyridine in the case of the secondary alcohol 4-penten-2-ol

(131). In contrast, our results suggested formation of dialkyl carbonate diol **4a** from **3a**<sup>\*</sup> and the primary alcohol **1a**, when pyridine was added over the course of 20 h while maintaining acidic conditions. This scenario was derived from changes in the profile fitted integrals from the <sup>1</sup>H NMR spectra, respective to pairs of **3a** and **3a**<sup>\*</sup> with an increasing ratios of 1.1 : 1 (Entry 3.5), 1.8 : 1.0 (Entry 3.6) upon Pyridine addition. Noteworthy, the slow addition of pyridine to the aliphatic chlorocarbonyl in the presence of (hydroxyalkyl)phenol may provide a way towards aliphatic carbonate diols such as **4a**.

Alternatively to THF, the use of 1,4-dioxane as a solvent resulted in an equally efficient conversion (99%) as compared to the use of THF; while only a slight loss of selectivity was observed (96%) due to the occurrence of dialkyl carbonate diol formation as a minor side reaction. In contrast, the use of chlorinated solvents Chloroform and DCM as well as toluene did not result into a relevant conversion of the reactants.

Table 4.4: Substrate scope for for aliphatic chlorocarbonyl

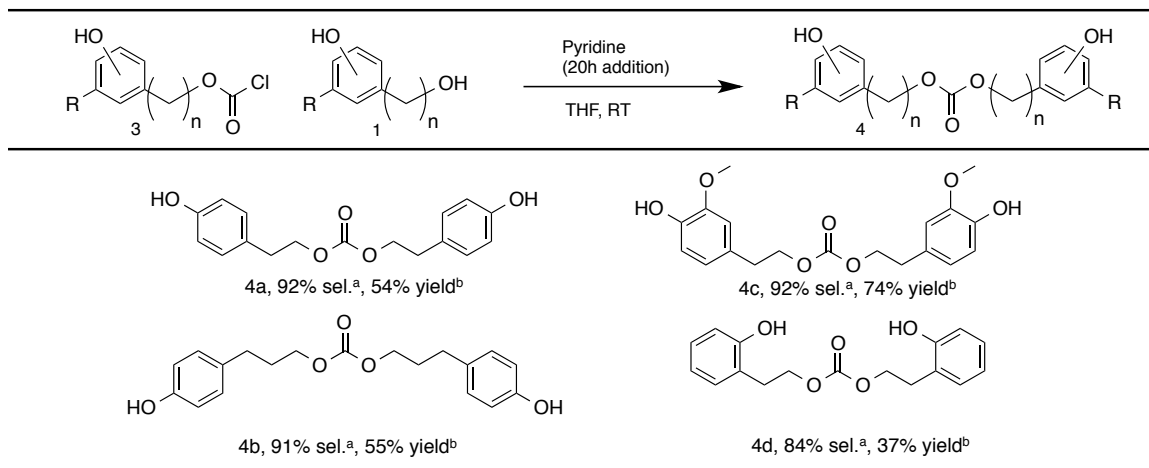
			
Chlorocarbonyl	Selectivity (%) <sup>a</sup>	Ratio 3 : 3*	Conversion (%) <sup>a,b</sup>
	> 99	1 : 1	83
	> 99	1: 1	95
	> 99	1 : 1	> 99
	97	1.1 : 1	86

<sup>a</sup>By <sup>1</sup>H NMR and ESI-MS; <sup>b</sup>Equiv. 3n, 3n\*

The chemoselective formation of aliphatic chlorocarbonyls was further exemplified on **3b–d** and **3b–d\*** based on the solvent optimized procedure for **3a** and **3a\***. As shown in Table 4.4, the corresponding aliphatic chloroformates **3b** and **3c** as well as the trichloromethyl carbonates **3b\*** and **3c\*** were obtained in 1:1 ratios equivalent to the chloroformylation reaction of **1a**.

In contrast, the reaction of **1d** and BTC in THF preferentially provided the aliphatic chloroformate **3d** versus the trichloromethyl carbonate **3d\*** in a ratio of 4 : 1, quantified by profile fitting using GSD (Supplementary information, Figure S7). This deviation in the reactivity observed for **1d** is in line with previous observations in Table 4.2. Here, the *ortho*-phenolic hydroxyl may activate the carbonyl **3d\*** for the decomposition into **3d** and phosgene, which further reacts to form **3d**.

Table 4.5: Substrate scope for for dialkyl carbonate diol



<sup>a</sup>By <sup>1</sup>H NMR and ESI-MS; <sup>b</sup>Purified Yield.

A synthetic method was developed for the chemoselective chloroformylation of (hydroxyalkyl)phenol at the aliphatic hydroxyl. Ultimately, it was intended to obtain dialkyl carbonate diols. It was reasoned that this goal may only be achieved, if auxiliaries such as pyridine are used to activate the chloroformate, which was otherwise stable under ambient conditions. In order to preserve the acidic reaction conditions pyridine was added slowly over the course of 20h to avoid the reactivity of the phenolate. Further, pyridine was added in excess to convert trichloromethyl carbonates into equivalents chloroformate and phosgene to maximize the conversion.

As shown in Table 4.5 the dialkyl carbonate diols **4a–c** were obtained at high chemoselectivity (> 91%) while the purified compounds were isolated at satisfying yields (> 50%). In turn only minor formation of aryl alkyl carbonate occurred (around 8%), which may potentially be reduced by further adjusting the conditions of pyridine addition. In contrast, **4d** was formed less selectively, since the intramolecular formation of a seven-membered cyclic carbonate occurs as a side reaction. Similarly strained cyclic carbonates were reported in previous studies (17).

In spite of the minor formation of side products, dialkyl carbonate diols **4a–c** can be

purified in a scalable process without the need to use column chromatography: Solubilization in heated aqueous base was followed by precipitation adding concentrated acid and cooling.

## 4.5 Conclusions

While the interfacial reaction of phosgene equivalents and diol under alkaline conditions is one of the most popular synthetic methods for polycarbonate synthesis, its potential for the chemoselective phosgenation of (hydroxyalkyl)phenols has not been previously explored. We have discovered that diaryl carbonate diols from (hydroxyalkyl)phenols are formed in a highly efficient and selective manner when NaOH is used as a base. Remarkably, the reactivity of the phenolate prevails over the alcoholic hydroxyl: Only residual aliphatic phosgenation products are formed impeding any polymerization to occur. Addition of organic base obstructs selectivity by promoting phosgenation of the aliphatic hydroxyl most likely by forming activated N-acyl ammonium adducts.

Conversely, selectivity for the alcoholic hydroxyl can be achieved in a polar aprotic solvent such as THF when acidic conditions are maintained. First, aliphatic chlorocarbonyls such as chloroformates and trichloromethyl carbonates are formed exclusively. Further, the dialkyl carbonate diol is obtained with an additional equivalent of (hydroxyalkyl)phenol under slow addition of pyridine.

This novel toolset for chemoselective phosgenations at the phenolic or alcoholic hydroxyl does not require the use of expensive protection groups or sophisticated catalytic auxiliaries. Therefore it may be of great utility for the synthetic community in natural product synthesis or prodrug development in medicinal chemistry.

In the framework of this thesis specifically, we will exploit the new obtained compounds as bifunctional monomers for the synthesis of biodegradable polycarbonates with controlled orientation of monomeric units. In this sense bifunctional carbonates

will serve as pre-programmed monomers to explore relationships between polymer primary structure and its functional behavior such as degradation and mechanical performance.

## Chapter 5

# Physicochemical Properties of Degradation Intermediates

### 5.1 Abstract

The resorption of a degradable biomedical device at the implant site is driven by the erosion of the polymeric material upon loss of  $M_w$ . In turn, the dissolution of the degradation products may limit the mass loss, which may occur long after the the loss of functional integrity of the device or never.

In this chapter, we characterized the physicochemical properties of degradation products of poly(tyrosol carbonate). Tyrosol and dialkyl carbonate diol (**4a**) from tyrosol were identified in the degradation supernatant by  $^1\text{H}$ -NMR. Then hydrolysis kinetics of **4a** and its counterpart, the diaryl carbonate diol **2a** were determined. The half-lives were 60 d for the slow degrading **4a** and 23 h for the fast degrading **2a** in buffered aqueous solution with  $\text{pH} = 7$  at  $37^\circ\text{C}$ . Both compounds leaned towards rapid, base catalyzed degradation as expressed in  $k_{OH} = 4.6 \cdot 10^{-2} [\text{M}^{-1}\text{s}^{-1}]$  and  $k_{OH} = 8.6 \cdot 10^{-1} [\text{M}^{-1}\text{s}^{-1}]$  for **4a** and **2a**, respectively. At  $37^\circ\text{C}$  and  $\text{pH} = 7$ , the solubility of tyrosol was two orders of magnitude higher than the solubility of **4a** with  $0.49 \pm 0.01 \text{ mg ml}^{-1}$  and **2a**  $0.60 \pm 0.02 \text{ mg ml}^{-1}$ . Further, QCM-D studies on the thin film erosion (thickness = 800 nm) showed the rapid formation of a transient, highly hydrated layer most likely comprised of **4a** and **2a**. This layer also existed during erosion of macroscopic polymer discs. SEM images showed microcompartments such as surface pits and cavities filled with dimers restricting dissolution into the bulk. The elucidation of the dynamics between the solubility and hydrolysis of intermediates

confronts the fundamental challenge to balance resorbability with the incorporation of diphenolic units desired for mechanical strength. Conversely, the use of diphenolic monomers that carry intrinsic degradability may entice a new generation of polycarbonates that is strong and easily resorbable.

## 5.2 Introduction

Within the context of degradable polymeric systems, polymer degradation is defined as a change in the chemical structure which may result in loss of  $M_w$ . Erosion is defined as the disappearance of the polymer which may be quantified by measuring the mass and thickness loss. Resorption refers to the assimilation of the biomaterial by the biological embodiment (97).

When the cleavage of polymer chains and dissolution of degradation products occurs faster than the uptake of water, surface erosion occurs. In turn, rapid water uptake with slower degradation rates results in bulk erosion (42). However, these two idealized scenarios leading to erosion as described in theory are rarely observed in experiment. For example, polyanhydrides are one of the few systems where surface erosion has been realized within practical device dimensions (104). In turn, polyesters show bulk erosion within a clinically relevant parameters (42). This phenomenon is explained on a fundamental level by dramatic differences in the hydrolysis kinetics of the two polymeric systems: the half-lives of the degradable bonds are  $t_{1/2} = 0.1$  h for polyanhydrides and  $t_{1/2} = 3.3$  yrs for polyesters (112).

The exploration of erosion phenomena is further complicated by the occurrence of transient degradation intermediates. The most prominent example is the formation of oligomeric lactic acid ester formed upon degradation of PLA leading to changes in the morphology of hollow erosion structures (77). In addition, solubility of the degradation products may be limiting the erosion process. A long term study on the erosion and degradation of poly(DTE carbonate) showed no mass loss *in vivo*,



while elevated, non-physiological temperatures where necessary to induce mass loss *in vitro* (126).

Here, we explored the degradation of poly(tyrosol carbonate) into dimeric compounds, namely carbonate diols which were merely water soluble. The hydrolysis kinetics of these dimers were characterized and related to the formation of a hydrated layer covering the polymer surface during erosion. Albeit the enzyme-mediated process, this model study provides general insight relating to the intricate interplay of erosion and resorption behavior of biomedical polycarbonates from diphenolic monomers.

### 5.3 Experimental

The **Chapter 2** generally described the herein used materials and procedures followed such as polymer characterization, compression molding and degradation experiments in lipase solution and PBS control, spin-coating of polymer thin films, SEM and QCM-D. It is noted that aromatic carbonate diol **2a** and aliphatic carbonate diol **4a** were synthesized as described in **Chapter 4** to conduct quantitative studies and characterize the physicochemical properties. The experimental procedures below are considered specific to this chapter.

#### 5.3.1 Qualitative Analysis of Erosion Products

Compression molded films of poly(tyrosol carbonate) approximate mass = 10 mg were incubated in lipase solution as described in Chapter 2. Here, the erosion supernatant was frozen in liquid N<sub>2</sub> and lyophilized for 48 h.

To analyze surface properties compression molded specimen's incubated in lipase solution for 10 weeks, were rinsed first with 2 ml H<sub>2</sub>O/ DI and then with 1 ml 70% (v/v) EtOH. The rinsates were collected and lyophilized separately. As a control, the procedures were performed on specimens incubated without lipase. After lyophilization, the solid was reconstituted in DMSO-*d*<sup>6</sup> and subjected to <sup>1</sup>H-NMR spectroscopic

analysis.

### 5.3.2 High Performance Liquid Chromatography with UV/Vis Detection

The HPLC system was comprised of an Alliance 2695 Separations Module equipped with 2487 Dual Absorbance UV/Vis detector (Waters Corporation, Milford, MA). As column for separation, a Synergi 4u polar RP80A (Phenomenex, Torrance CA), with a size of 250 x 4.60 mm set to a operating temperature of 25 °C . The analysis was operated using the manufacturers Empower Pro software. A gradient of ACN and H<sub>2</sub>O (both with 0.1% (v/v) of TFA) was used as a mobile phase at a flow rate of 1.0 ml min<sup>-1</sup>. The gradient changed composition from solvent ratios of 65: 35 to 5: 95 over a 14 minute period Samples were prepared by dissolving 3.0 mg of the analyte in 2.5 mL of ACN with 0.1% (v/v) TFA and then adding 7.5 mL of H<sub>2</sub>O with 0.1% (v/v) TFA. Approximately 2 mL of the prepared solution were filtered through a PTFE syringe filter (Whatman, Florham Park, NJ) with a poresize of 0.45 µm before injection.

### 5.3.3 Hydrolysis of Soluble Degradation Products

To follow the solution hydrolysis kinetics of carbonate diols from tyrosol (compounds **2a** and **4a**) the following procedure was conducted. Respective carbonate diol was pre-solubilized in ACN at  $c_w = 6.25 \text{ mg ml}^{-1}$ . Aqueous buffer solutions were prepared at with hydrochloric acid (pH = 3), sodium acetate (pH = 6), phosphate buffer (pH = 7), sodium carbonate (pH = 10), NaOH (pH = 12), respectively. Ionic strength was adjusted to 1 M with KCl. The buffer solutions contained 0.75 mg ml<sup>-1</sup> 3-(4-methoxyphenyl)propionic acid (MDAT) as internal standard. Carbonate diol was injected into buffer solutions at a start concentration of 0.25 mg ml<sup>-1</sup> at 37 °C. Solutions were acidified with HCl to pH= 1 at predetermined time points, immediately frozen and lyophilized for 48 h. The solid was reconstituted in ACN with 0.1% (v/v) TFA, to an approximate, total concentration (dimer and tyrosol) of  $c_{w,total} =$

0.25 mg ml<sup>-1</sup>. Then the mixture was analyzed by HPLC as described in the general methods section. The peak area under the curve was quantified for tyrosol, **2a** at  $\lambda = 220$  nm and **4a** at  $\lambda = 275$  nm

#### 5.3.4 Solubility of Carbonate Diols

To analyze solubility of tyrosol and the carbonate diols **2a** and **4a** in aqueous medium, excess solid of respective compound was dispersed in 2 ml PBS contained in a syringe. The heterogenous mixture was incubated at temperatures of 5 °C, 25 °C and 37 °C for 1 h and inverted frequently. Then, the mixture was filtered through a 0.45 PTFE filter. Immediately, 1 ml of the homogeneous filtrate was mixed with 1 ml ACN with 0.1% (v/v) TFA. Analysis of the aqueous concentration was conducted relative to a curve from standards of respective compounds with concentrations of standards of 1 mg ml<sup>-1</sup>, 0.5 mg ml<sup>-1</sup>, 0.25 mg ml<sup>-1</sup>, 0.1 mg ml<sup>-1</sup>, 0.05 mg ml<sup>-1</sup> in ACN with 0.1% (v/v) TFA. Injection volume of both, standard and solubility analyte was 20 ul with triplicate analysis.

### 5.4 Results and discussion

#### 5.4.1 Qualitative Analysis of Degradation Products

Films of poly(tyrosol carbonate) undergo enzyme-mediated erosion, when incubated in an aqueous solution of lipase from TLL. The erosion supernatant is comprised of tyrosol and carbonate diol **2a** and traces of **4a** as identified by <sup>1</sup>H NMR spectroscopy (Supplementary information).

#### 5.4.2 UV Absorption Spectroscopy

In order to follow the hydrolysis kinetics of the degradation intermediates the UV absorption of the diaryl carbonate diol **2a** and dialkyl carbonate diol **4a** of tyrosol

was characterized. Exemplary UV absorption spectra are shown in Figure 5.1.

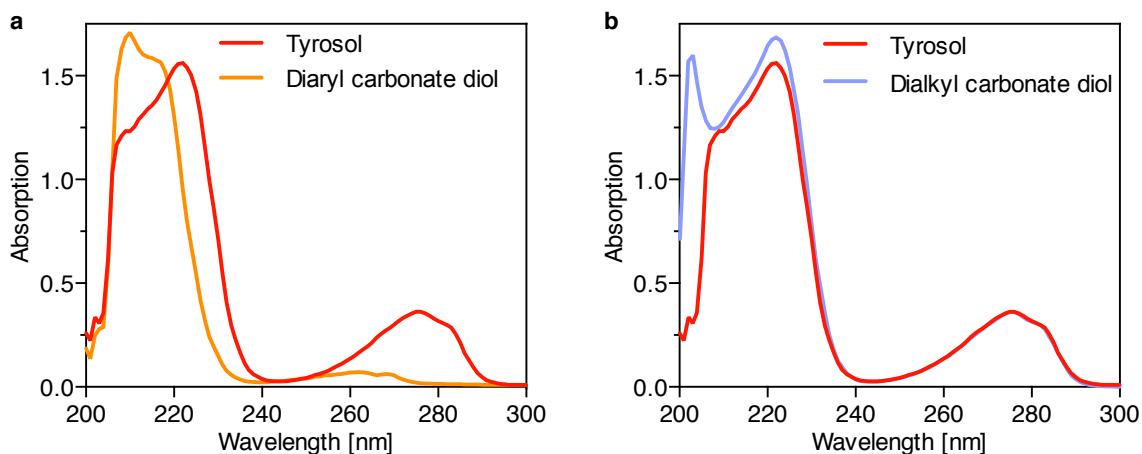


Figure 5.1: UV absorption spectra (200–300 nm, acetonitrile): (A) Diaryl carbonate diol **2a**, (B) dialkyl carbonate diol **4a**, tyrosol **1a**.

The absorption spectrum of the diaryl carbonate diol **2a** was distinguishable from tyrosol including local absorption maxima at  $\lambda_{max} = 262$  and  $\lambda_{max} = 275$ , respectively. In turn, the shape of the curve for the dialkyl carbonate diol **4a** appeared identical to tyrosol. Therefore it was necessary to perform chromatographic separation of the compounds (HPLC) prior to UV analysis and kinetic analysis

#### 5.4.3 Hydrolysis Kinetics and Solubility of Degradation Intermediates

Carbonate diols are degradation intermediates in the erosion of poly(tyrosol carbonate). In order to explore the possible impact of these intermediates on the polycarbonate resorption, the hydrolysis kinetics as well as the solubilities were characterized. In aqueous solution diphenolic carbonate diols were expected to undergo hydrolysis into the parent compound tyrosol and  $\text{CO}_2$  over time according to the reaction scheme in Figure 5.2. The overall observed rate constant of hydrolysis is  $k_{obs}$ .

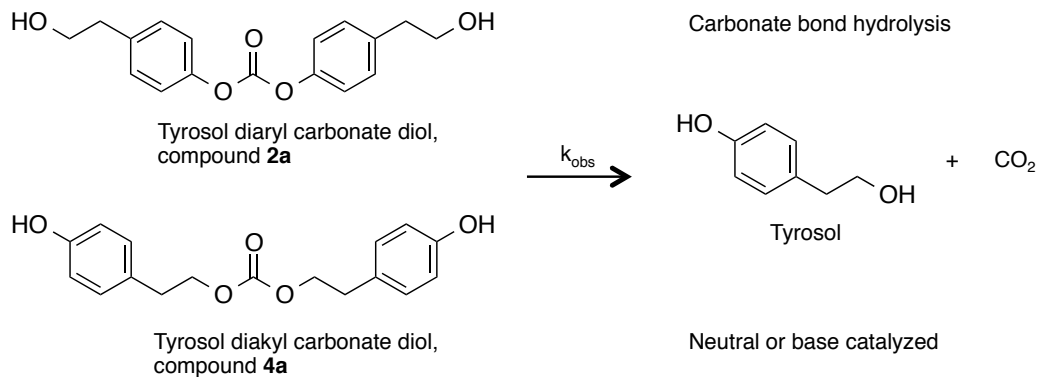


Figure 5.2: Reaction scheme for the hydrolytic degradation of carbonate diols **2a** and **4a** in aqueous solution with rate constant  $k_{obs}$ .

The rate of hydrolysis can be described as a differential equation of the change of concentration of the carbonate ( $[carbonate]$ ) as a function of the time ( $t$ ) and the product of the rate constant, observed ( $k_{obs}$ ) and the carbonate concentration in a pseudo-first order kinetic model.

$$Rate = -\frac{d[carbonate]}{dt} = k_{obs}[carbonate] \quad (5.1)$$

The contributions to  $k_{obs}$  are the rate constants from acidic and basic catalysis  $k_H$  and  $k_{OH}$ . In addition,  $\text{H}_2\text{O}$  contributes with  $k_N$ .

$$k_{obs} = k_H[H^+] + k_N + k_{OH}[OH^-] \quad (5.2)$$

The integrated rate equation allowed to quantify  $k_{obs}$  as the slope of the logarithmic ratio of the concentration at start  $t = 0$  and time point  $t$

$$\ln\left(\frac{[carbonate]_t}{[carbonate]_0}\right) = -k_{obs}t \quad (5.3)$$

Experimentally, we determined the  $k_{obs}$  from the relative peak areas in the chromatogram from HPLC with UV absorption detection.

$$\ln\left(\frac{[peak\ area]_t}{[peak\ area]_0}\right) = -k_{obs}t \quad (5.4)$$

From the decay curve, exemplified on the disappearance of compound **2a** at pH = 10 in Figure 5.3 A it was possible to follow hydrolysis of the carbonate over time. To quantify  $k_{obs}$  of this reaction, the logarithmic values were plotted according to equation 5.4. The slope from the linear regression on the logarithmic values in Figure 5.3 B directly provided  $k_{obs}$ .

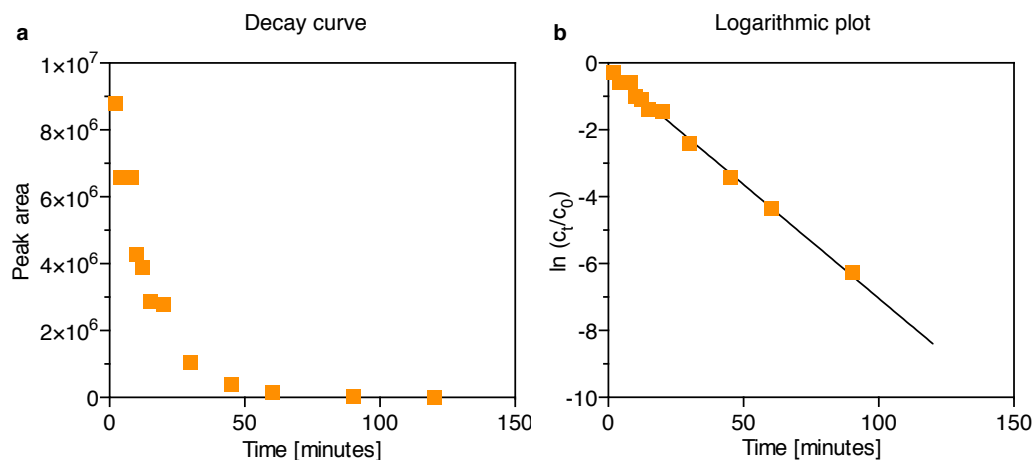


Figure 5.3: Kinetic plots for the hydrolysis of carbonate diols (**2a**, pH = 10): (A) Decay curve (area under peak from HPLC), (B) logarithmic concentration change over time.

The half-life of the carbonate in aqueous solution  $t_{1/2}$  can also be obtained from the integrated rate equation by a simple rearrangement.

$$t_{1/2} = -\frac{\ln 2}{k_{obs}} \quad (5.5)$$

The hydrolysis rate constants  $k_{obs}$  were quantified over a range of pH values. In Figure 5.4,  $k_{obs}$  for carbonate diols **2a** and **4a** is plotted in dependence of a pH = 3–12.

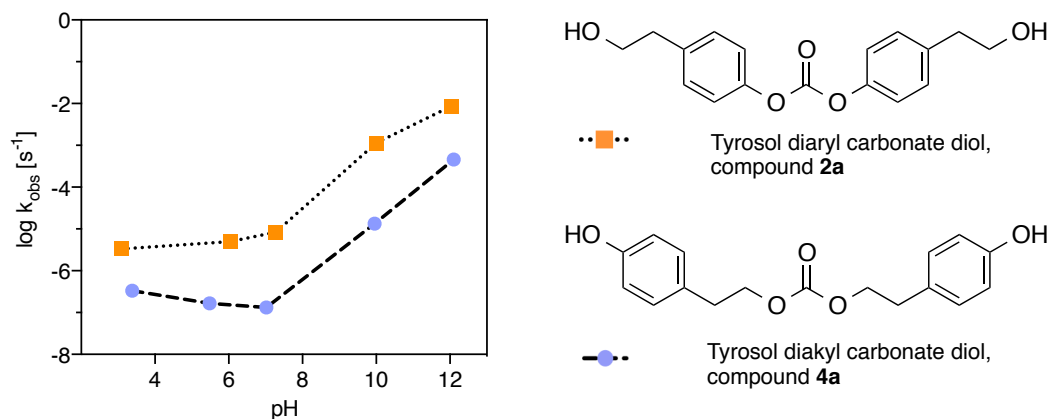


Figure 5.4: Logarithmic plots of hydrolysis rate constant ( $k_{obs}$ ) over the pH for carbonate diols **2a** and **4a**.

Both carbonate diols from tyrosol **2a** and **4a** were stable under acidic conditions and showed very slow hydrolysis. This was evident in low values for  $\log(k_{obs}) = -5.5$  for **2a** and  $-6.5$  for **4a** at  $\text{pH} = 3$ . Increasing the pH beyond  $\text{pH} = 7$  resulted in increasing values of  $k_{obs}$ . According to equation 5.2 this increase of  $k_{obs}$  is due to the contribution of the product  $k_{OH}[OH^-]$ . As the hydroxyl ion concentration was considered constant the pseudo-first order rate constant at given pH,  $k_{OH}$  was calculated.

The hydroxyl dependent rate constants  $k_{OH}$  and the pH dependent half-lives give more insights into the hydrolysis kinetics of **2a** and **4a**, as listed in Table 5.1. Striking differences in the hydrolysis kinetics of **2a** and **4a** appeared in dependence of the pH. While at neutral conditions  $\text{pH} = 7$  the half-life of **2a** in aqueous solution is 23 h, the half-life of **4a** is much longer with  $t_{1/2} = 60$  days. This finding may explain, why the degradation supernatant mostly contained tyrosol and **4a**, while only traces of **2a** and the aryl alkyl carbonate diol were found by  $^1\text{H-NMR}$  spectroscopy.

The values of  $k_{OH}$  for **2a** and **4a** were compared to those of important, structurally related organic carbonates. Strikingly, diethyl carbonates has very similar hydrolyses kinetics under basic conditions as compared to the dialkyl carbonate diol with rate constants,  $k_{OH} = 4.6 \times 10^{-2} [\text{M}^{-1}\text{s}^{-1}]$  and  $k_{OH} = 4.7 \times 10^{-2} [\text{M}^{-1}\text{s}^{-1}]$  (33), respectively.

In turn, diphenyl carbonate has a  $k_{OH} = 12.6 \text{ [M}^{-1}\text{s}^{-1}]$  (96), which is a magnitude higher than the corresponding **2a**  $8.6 \times 10^{-1} \text{ [M}^{-1}\text{s}^{-1}]$ . This result maybe explained by the relative differences between hydrophilicity of carbonate versus the hydrolysis product.

Table 5.1: Half-lives of pH-dependent hydrolysis and rate constants  $k_{OH}$  in aqueous solution for carbonate diols from tyrosol.

Compound	Diaryl carbonate diol <b>2a</b>	Dialkyl carbonate diol <b>4a</b>
pH	Half-live ( $t_{1/2}$ )	
3	2 days	24 days
6	1.5 days	48 days
7	23 hours	60 days
10	10 minutes	14 hours
12	1 minute	25 minutes
Rate constant, $k_{OH} \text{ [M}^{-1}\text{s}^{-1}]$		
	$8.6 \times 10^{-1}$	$4.6 \times 10^{-2}$

In addition to the hydrolysis kinetics, the aqueous solubilities of carbonate diols in PBS (pH = 7.4) were characterized and referenced to tyrosol (Table 5.2). Both carbonate diols, **2a** and **4a** were only slightly soluble, which is due to there diphenolic structure. The solubility of tyrosol was at least two orders of magnitude higher in comparison. Noteworthy, the obtained solubility for tyrosol is in good agreement with the literature record with  $S(\text{tyrosol}) = 107 \text{ mg ml}^{-1}$  at  $25^\circ\text{C}$  (108). In relation to other diphenolic structures related to polycarbonates, the solubilities of **2a** and **4a** are similar to BPA with  $S(\text{BPA}) = 0.381 \text{ mg ml}^{-1}$  at  $25^\circ\text{C}$  (76). In the design of degradable polycarbonates, diphenolic structures, featuring an internal amide bond, such as DTE and the carboxylic acid containing DT have slightly higher solubilities



with  $S(\text{DTE}) = 1.4 \text{ mg ml}^{-1}$  and  $S(\text{DT}) = 9.3 \text{ mg ml}^{-1}$  (126). However, the continued metabolization by cleavage of the peptide bond of DTE and DT into more soluble units remains elusive. This is may be due to steric hindrance caused by ester or carboxylic acid group.

Table 5.2: Temperature-dependent solubility of carbonate diols from tyrosol and tyrosol in PBS at  $\text{pH} = 7$

Compound	Diaryl carbonate diol <b>2a</b>	Dialkyl carbonate diol <b>4a</b>	Tyrosol <b>1a</b>
Temperature	Solubility $\text{mg ml}^{-1}$		
5 °C	$0.21 \pm 0.02$	$0.15 \pm 0.01$	$3 \pm 0.5$
25 °C	$0.27 \pm 0.01$	$0.24 \pm 0.01$	$102 \pm 20$
37 °C	$0.60 \pm 0.02$	$0.49 \pm 0.01$	$135 \pm 20$

#### 5.4.4 Hydrated Layers of Degradation Intermediates

The viscoelastic properties of thin films from poly(tyrosol carbonate) during enzymatic degradation were studied using QCM-D, respective to the effect of degradation intermediates. The QCM-D curves for experiments conducted under constant flow and stopped flow are shown in Figure 5.5 A and B, whereas an illustration of the interpretation of processes at the surface is provided in Figure 5.5 C.

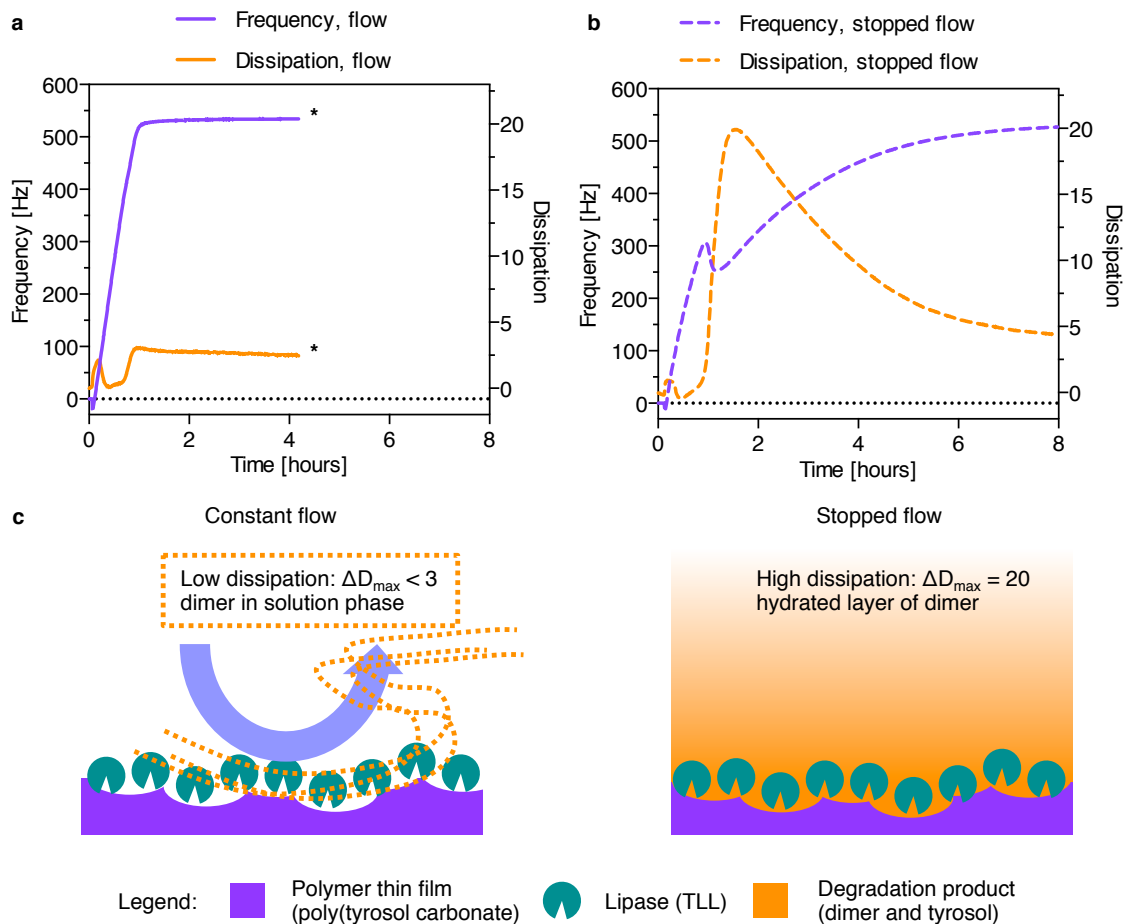


Figure 5.5: QCM-D comparison of lipase erosion of thin films from poly(tyrosol-carbonate): (A) Flow =  $24 \mu\text{l min}^{-1}$  (sink condition),\* indicates end of experiment, (B) stopped-flow at  $t = 1 \text{ h}$  (simulated compartmentalization) at  $37^\circ\text{C}$  in PBS, (C) illustration of thin film erosion by lipase. Constant flow: Removal of partially-soluble degradation products and erosion completed within 1.5 h. Stopped-flow: Formation of hydrated, dissipative layer. Erosion delayed, hydrolysis of dimeric degradation products within 8 h.

Under sink conditions, thin films from poly(tyrosol carbonate) were eroded by lipase at a flow rate of  $24 \mu\text{l min}^{-1}$  ( $T = 37^\circ\text{C}$ ). While an overall frequency change of  $\Delta f = 520 \text{ Hz}$  (film thickness =  $800 \text{ nm}$ ) was observed within 1.5 h, the dissipation values were low:  $\Delta D_{\max} < 3$ . This result indicated that the surface layer was minimally hydrated during erosion and degradation products such as tyrosol and dimeric intermediates **2a** and **4a** transitioned into the solution phase. The solubility limit of dimers was not reached due to the constant solution exchange under flow conditions.

In contrast, when the flow was purposefully stopped during erosion ( $t = 1$  h) (Figure 5.5 B), a massive increase of the dissipation of  $\Delta D_{max} = 20$  was recorded. The frequency curve also reached a local maximum of  $\Delta f = 300$  Hz ( $t = 1$  h) then continued to increase  $\Delta f = 520$  Hz, more slowly within 8h. This transition implied that the surface became highly hydrated due the formation of a layer of partially insoluble, degradation products. A simple approximation provides a hint to the composition of this hydrated layer: Complete erosion of the thin film resulted in  $m = 14$   $\mu$ g of material dissolved in a QCM-D volume of  $V = 40$   $\mu$ l. This means the highest possible concentration was  $c_w = 0.35$  mg ml<sup>-1</sup>. Solubility limits of the dimers **2a** and **4a** were shown to fall within this order magnitude, whereas highly soluble tyrosol remained in solution. The slow disappearance of the hydrated, dimeric layer can be explained by the subsequent hydrolysis of the intermediates into the fully soluble tyrosol.

During the *in vitro* enzymatic erosion of macroscopic, compression molded discs from poly(tyrosol carbonate) the formation of a surface layer was also observed under sink conditions. The surface morphology of the eroded polymer films is shown as analyzed by SEM in Figure 5.6.

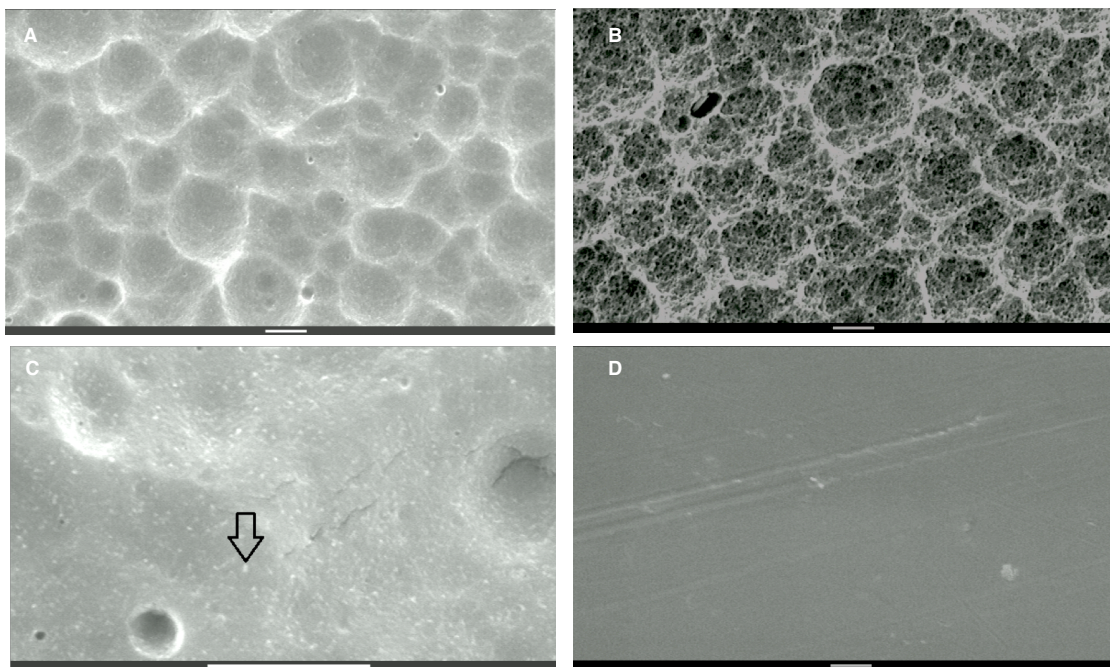


Figure 5.6: SEM images of surface layers of poly(tyrosol carbonate): (A) and (C) aqueous rinse, (B) rinse with 70% (w/v) ethanol, after lipase incubation, (D) PBS control, *in vitro* incubation for 10 weeks at 37 °C; scale bar = 10  $\mu$ m.

In Figure 5.6 A, the erosion morphology of poly(tyrosol carbonate) films after aqueous rinse featured a buckled structures. In turn, a rinse with 70% (w/v) ethanol was able to dissolve the surface layer giving rise to the pits and cavities in Figure 5.6 B. The removed layer was comprised of dialkyl carbonate diol **4a**, as identified by  $^1\text{H}$ -NMR spectroscopic analysis. As a control, the rinsate of pristine poly(tyrosol carbonate) films was analyzed. It did not contain dimer or tyrosol and the surface morphology of the film remained without noticeable features (Figure 5.6 D).

The existence of a transient layer of degradation intermediates can be explained with

creation of pits and cavities by the enzyme. This activity lead to compartmentalization and posed a diffusion barrier to the transport of slightly soluble degradation products into the bulk solution, where sink conditions prevailed. As a result precipitation of dimers occurred within the realm of the erosion structures. Apparently, this highly hydrated layer of dimers does not completely impair enzymatic degradation of the film as shown by QCM-D. This is the first time such intermediate layer was identified in polycarbonates. For example, erosion structures of PTMC only showed pits and cavities, but no additional surface layers were reported (8). This may be due to the water miscibility of the degradation product 1,3-propanediol (19). It may be worthwhile to characterize the phase behavior of such transient layer using XPS. For example, oligomers of PLA generated by hydrolysis transition from the amorphous into the crystalline phase adding additional complexity to the erosion process (78).

## 5.5 Conclusion

The characterization of diphenolic degradation intermediates relates to the challenge in degradable materials design achieving simultaneous polymer erosion alongside the degradation of  $M_w$ . While many degradable polymer systems show sometimes rapid, initial  $M_w$  degradation, the erosion of the partially degraded material is delayed due to low solubility. Under sink conditions, poly(tyrosol carbonate) has shown surface erosion mediated by lipase activity leading to complete dissolution of milligrams of polymer film within weeks. However, a close-up view into the nano scale behavior using QCM-D demonstrated: surface erosion behavior rapidly collapsed when non-sink conditions were instigated. The formation of a hydrated layer directly demonstrates how partially insoluble degradation products hamper the dissolution process. This phenomenon may generally apply to *in vivo* situations where degradation, but no resorption occurs independent if the mechanism is enzymatic or hydrolytic.

In turn, the insights from this chapter may be applied to adjust the design parameters for degradable polymer systems. Specifically, the diphenolic carbonate diols may find use replacing other structurally related units in advanced co-and terpolymer formulations for biomedical applications. Though the diphenolic unit is desired within the backbone to provide strong mechanical properties, their low solubility impairs erosion. Less soluble, hydrophobic monomers containing an internal carbonate bond may overcome this long-standing challenge as they will further hydrolyze into readily soluble (hydroxyalkyl)phenols such as tyrosol.

## Chapter 6

# Sequence Structure in Degradable, Aromatic–aliphatic Polycarbonates from Tyrosol Provides Control Over Phase Transitions and Bioerosion

### 6.1 Abstract

Synthetic degradable polymer systems are applied as surrogate materials for temporary biomedical applications requiring supportive functionality during loss of tissue integrity. Recent efforts inspired by the architecture of natural, structural materials such as silk and collagen featuring short, recurring sequence motifs are leading to a new generation of synthetic, sequence-controlled biomaterials. Here, we report on a new aromatic–aliphatic polycarbonate from tyrosol with a strictly alternating sequence (*alt*) of diaryl and dialkyl carbonates in comparison to a scrambled sequence (*scr*) of diaryl, dialkyl and aryl alkyl carbonates. The effects of polymer sequence on the phase behavior were studied in detail by DSC and Xray diffraction. For instance, oriented and semi-crystalline films of *alt* showed a 3-dimensional lamellar order (with  $d = 135 \text{ \AA}$ ) and a structural model for *alt* was fitted into a monoclinic unit cell. In contrast, *scr* led to a 1-dimensional quasi-crystalline order. Practical relevance was shown, as the mechanical performance such as the tensile moduli ( $E_T$ ) in the wet state of oriented, semi-crystalline films from *alt* was significantly improved with  $E_T = 5.4 \pm 0.3 \text{ GPa}$  as compared to *scr* and poly(L-lactic acid) PLLA. Amorphous *alt* underwent rapid lipase mediated bioerosion *in vitro* at a rate of  $0.36 \pm 0.01 \text{ mg cm}^{-2} \text{ d}^{-1}$  while *scr* eroded at a slower rate of  $0.12 \pm 0.01 \text{ mg cm}^{-2} \text{ d}^{-1}$ . Qualitative differences

in the erosion behavior also appear after subcutaneous implantation, *in vivo*.

This interplay of sequence control in conjunction with polymer processing hints to exciting strategies to advance polycarbonate systems tailored for biomedical applications.

## 6.2 Introduction

Synthetic polymers are widely used in biomedical applications, including scaffolds for tissue engineering (111; 41; 71), drug delivery systems (130) and sutures (3). Synthetic polymers have significant advantages as compared to naturally derived polymers such as tunable mechanical and structural properties, controlled degradation and high batch-to-batch stability (93; 63). In contrast, natural polymers generally have low mechanical properties, inherent structure and degradation, and composition can be inconsistent depending on polymorphisms (86). Natural polymers such as extracellular matrix derived materials intrinsically carry bioactive cues whereas synthetic polymers are in blank state, yet bioactivity can be incorporated in a highly controlled manner (20).

In turn, the make-up of natural polymers inspires a new generation of tailor-made, synthetic materials. In a paradigm shift, design strategies are being developed to create synthetic polymers that resemble structure and function of biological macromolecules (80; 98). One such feature is found in structural biomacromolecules, specifically fibrillar proteins such as silk. Here, small repeating fragments of controlled sequences lead to supramolecular associations of these proteins (69).

A classic approach to artificially obtain well-defined sequences is the Merrifield peptide synthesis, but only limited amounts of synthetic peptide are obtained from the solid phase (88). Bulk synthesis of polymers offers a way to obtain higher yields of materials. However, sequence control in the bulk is more difficult and was even identified as a key challenge towards the advancement of the field (81). Recent reports



highlight radical polymerization as in the case of limonene analogues yielding periodically functionalized maleimide-base copolymers (85) and ATRA formation of vinyl based copolymers (128). An earlier study described the synthesis of sequence ordered poly(s-alkyl thioester) by backbone transformation of poly(s-aryl thioester) (56).

In direct relevance to polymers applied in the biomedical field, beautiful work has been performed on the sequence control of degradable polyester. The intricacies of sequence effects in complex poly(lactic-co-glycolic acid)s were characterized structurally and respective to the thermal behavior (121). Microparticles comprised of sequenced PLGA showed slower, linear degradation rates and a sustained release of Rhodamin-B, when used as a model drug (75). Further, the syndiotactic, alternating synthesis of poly( $\beta$ -hydroxyalkanoate) was achieved by employing Yttrium-derived catalysts (65).

In polycarbonates, another important class of polymers containing potentially degradable bonds only few examples of sequence specificity have been reported. Organometallic catalysis was used to preferentially incorporate the *trans*- versus the *cis*- isomer of (R)-limonene during the polymerization of respective epoxide and CO<sub>2</sub> (22). Similarly, atactic and isotactic poly(1,2-glycerol carbonate) with high head-to-tail selectivity was obtained (140). Further, sequence control in multiblock poly(cyclohexene carbonate)s was achieved by living copolymerization (60).

We have previously reported on aromatic-aliphatic polycarbonates from tyrosol containing diaryl, dialkyl and aryl alkyl carbonates as three distinctive backbone bonds arranged in a scrambled sequence (*scr*) (119). In this study, we present the facile synthesis of poly(tyrosol carbonate) with alternating diaryl and dialkyl carbonates (*alt*) from pre-programmed carbonate dimers without using expensive organo-metallic catalysts. Beyond synthesis, application of processing methods was conducted as a powerful tool emphasizing sequence-dependent differences, as previously shown for recombinant silk (69). In analogy, we explored the phase behavior of *alt* and *scr* in

detail: Upon heating, *alt* readily formed a 1-dimensional mesophase, and then a 3-dimensional crystalline phase, but *scr* showed slow transition into the 1-dimensional mesophase only. The fiber diffraction pattern on oriented, crystalline *alt* was used to solve the experimental aromatic polycarbonate structure. As practical implications for biomedical use, the oriented films of *alt* had superior stiffness as compared to PLLA, while amorphous *alt* showed rapid enzymatic erosion as compared to *scr*.

## 6.3 Experimental

The standard procedures were followed as described in **Chapter 2** for the evaluation of mechanical properties by the Instron set up as well as the degradation experiments in lipase solution and PBS control.

The experimental procedures below are considered specific to this chapter.

### 6.3.1 Polymer synthesis

The general synthesis method was followed for poly(tyrosol carbonate) to obtain *scr* and *alt* from **2a**. The methods described in **Chapter 4** were used to obtain compounds **3a** and **2a**. The oligomer *dir* was obtained by biphasic reaction of **3a** in DCM/ aqueous NaOH.

### 6.3.2 Polymer Characterization

The following polymer properties were analyzed as described in chapter 2 above: Relative molecular weight averages by GPC in DCM, Chemical structure and carbonate backbone composition by  $^1\text{H}$ -NMR and  $^{13}\text{C}$  NMR spectroscopy, thermal properties by DSC and TGA.

### 6.3.3 Compression Molding

Polymer films were compression molded at  $T = 220^\circ\text{C}$  using a Carver press (model 4122, Carver, Wabash, IN) using a shim with a thickness of  $250\ \mu\text{m}$ . To obtain amorphous, quenched films (q), the samples were immersed in a slush of ice and water immediately upon removal from heat. To obtain ambient cooled films (ac), the samples were removed from heat and cooled under ambient temperature. To anneal films (an), quenched film were subjected to an annealing temperature ( $T_{an}$ ) with  $T_{an} = T_{crys}$ . Film samples of unoriented films: p = polymer powder, q = quenched, ac = ambient cool, an = annealed.

### 6.3.4 Oriented Polymer Films

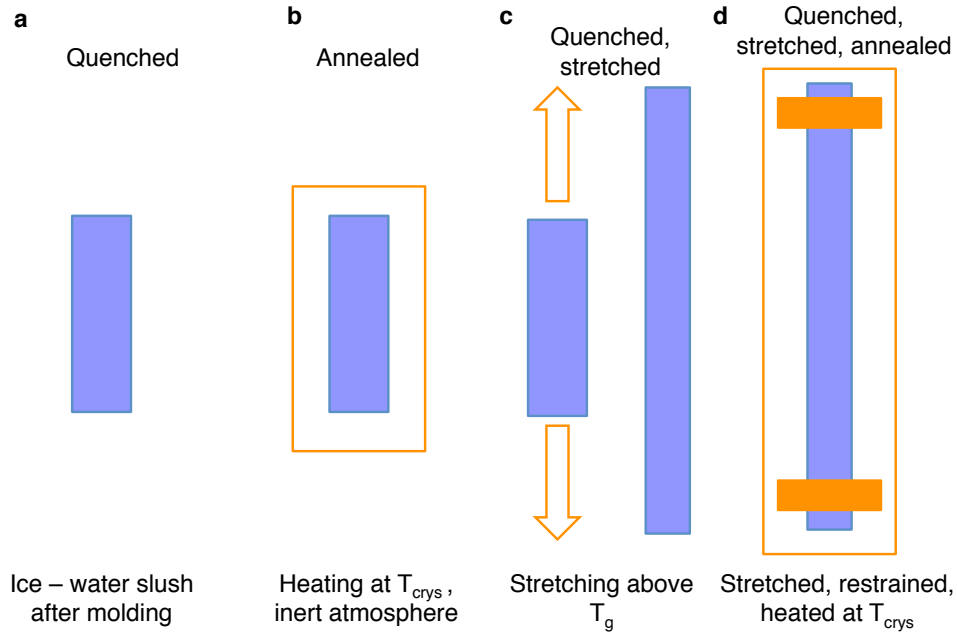


Figure 6.1: Fabrication of oriented polymer films: (A) Quenched from compression molding (q), (B) annealed after quenching (an), (C) stretched above  $T_g$  from quenched film (q, s), (D) stretched and further annealed (q, s, an).

The fabrication of oriented and semi-crystalline films of *scr*, *alt*, *PLLA* and oriented films of poly(DTE carbonate) is shown in Figure 6.1. Rectangular-shaped specimens were cut from compression molded films with an approximate thickness of  $250\ \mu\text{m}$

to a width of 6 mm and length of 4 cm. The samples were hydrated in H<sub>2</sub>O/ DI for 24 h at 37 °C. To orient the polymer chains the quenched specimens were stretched at a cross head speed of 500 mm min<sup>-1</sup> in a heating bath at a temperature of  $T_{stretch} > T_g$ . The specimens were removed from heat immediately after stretching was completed and dried *in vacuo*. Further, selected specimens were subject to annealing conditions: oriented films were place onto stain-less steel fixtures of 5 cm length to prevent shrinkage during annealing. The incubation temperature was  $T_{an} = T_{crys}$  in a furnace under inert atmosphere. Samples from *alt* and PLLA control were annealed for 2 h and *scr* was annealed for 20 h due to the slow progress of crystallization. In turn, poly(DTE carbonate) due to the lack of a crystallization point. Specimens: q = quenched (unoriented), an = annealed, q, s = quenched and stretched, q, s, an = quenched, stretched and annealed.

### 6.3.5 X-ray Diffraction

1D WAXD patterns from unoriented films were obtained in parafocus mode on a Xpert diffractometer (Philips, Netherlands). 2D WAXD patterns from oriented films were collected in transmission geometry using a AXSs Hi-Star multiwire area detector Bruker (Billerica, MA). Nickel filtered copper radiation (Cu K<sub>α</sub>,  $\lambda = 1.542 \text{ \AA}$ ) was used in both instances. The 2D patterns were processed using the manufacturer's GADDS software to obtain 1D radial and azimuthal scans. The radial scans were profile fitted using MDI software to obtain the crystallinity and crystallite size using the method describe in (91). Azimuthal scans were used to determine the degree of orientation (90). Crystal structure analysis was carried out by identifying the equatorial, meridional, and layer-line reflections in the diffraction patterns of the oriented films (annealed and stretched). Powder diffraction scans with crystalline reflections to  $2\Theta = 60^\circ$  was used to determine the crystal structure using Materials Studio. The diffraction pattern could be indexed on a monoclinic with the following unit cell of dimensions:  $a = 7.288 \text{ \AA}$ ,  $b = 8.120 \text{ \AA}$ ,  $c = 19.355 \text{ \AA}$ ,  $\beta = 45^\circ$ .

## 6.4 Results and Discussion

### 6.4.1 Polymer Synthesis and Sequence Analysis

Polycarbonates from the (hydroxyalkyl)phenol tyrosol contained three distinct carbonate sequence isomers in the backbone: diaryl (HH), dialkyl (TT) and aryl alkyl (HT) carbonates, respectively. The strategies applied to achieve an alternating (*alt*), scrambled (*scr*) and directional (*dir*) sequence in the carbonate backbone are illustrated in Figure 6.2.

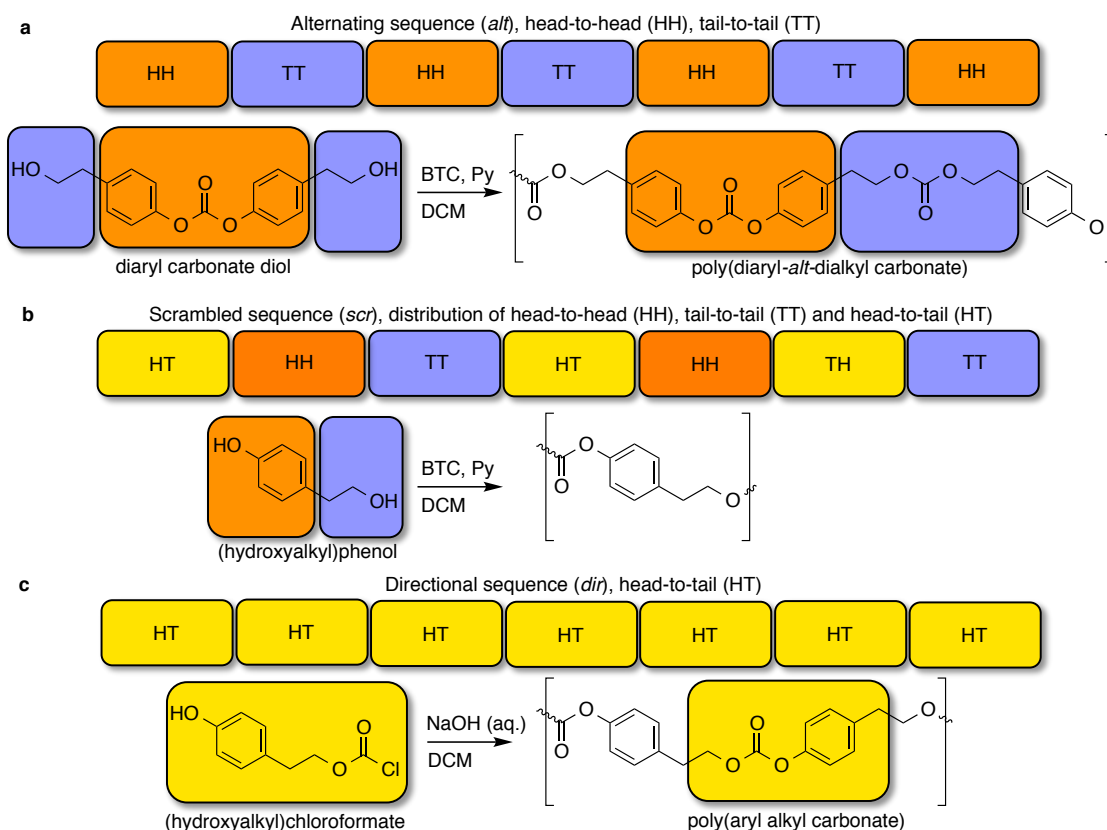


Figure 6.2: Synthesis and structure of polycarbonates from tyrosol with controlled carbonate isomer sequences: (A) Alternating sequence (*alt*), (B) scrambled sequence (*scr*), (C) directional sequence (*dir*); Respective to diaryl, dialkyl aryl alkyl carbonates.

A strictly alternating sequence of diaryl and dialkyl carbonate in poly(tyrosol carbonate) (*alt*) was obtained by polymerization of a preformed diaryl carbonate diol

using BTC and Py in DCM. Scrambled poly(tyrosol carbonate) (*scr*) featuring also aryl alkyl carbonates was obtained when tyrosol was used as the starting material as previously described in chapter 3. Further, a locally directional sequence of an aryl alkyl carbonate backbone was obtained by interfacial polymerization of (hydroxyalkyl)chloroformate and its equivalents in a biphasic DCM/ NaOH system.

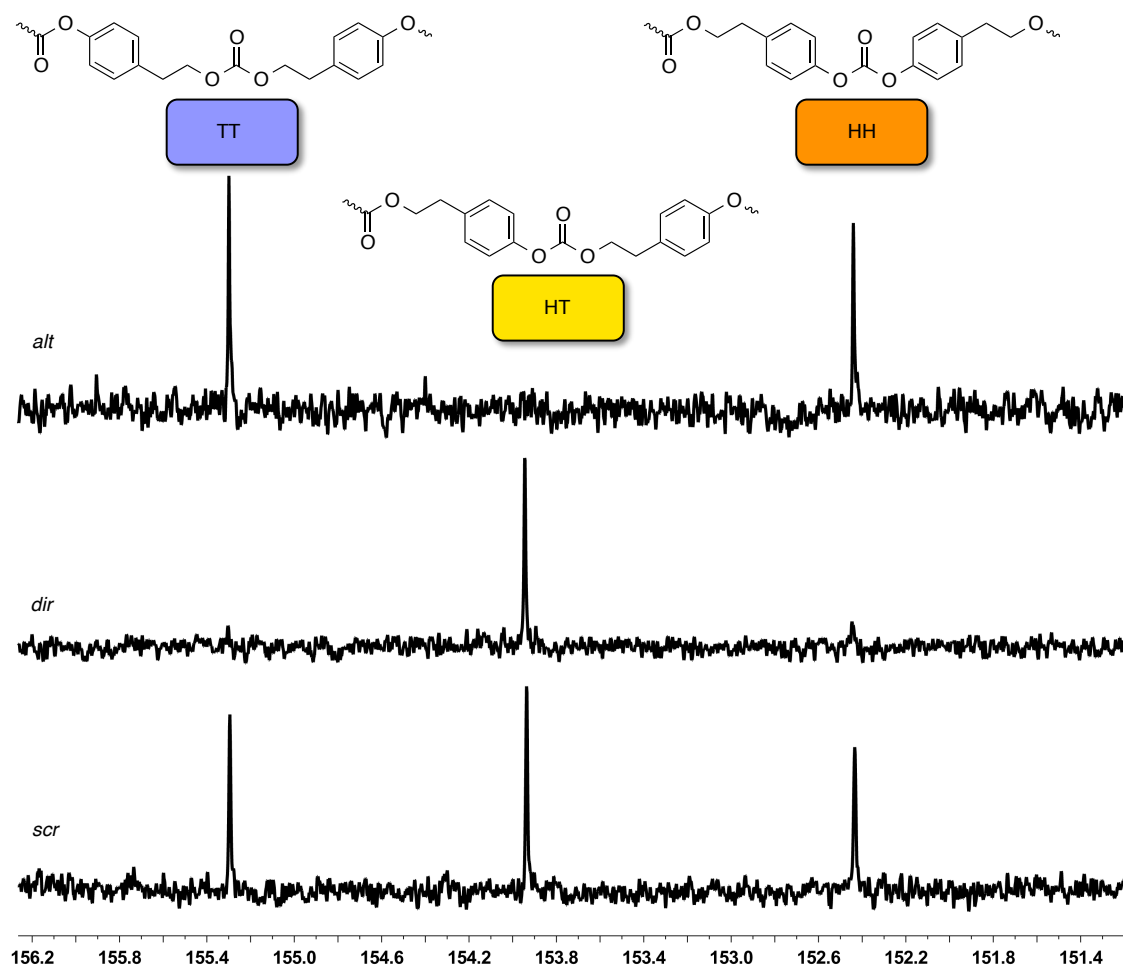


Figure 6.3:  $^{13}\text{C}$  NMR spectra (126 MHz,  $\text{CDCl}_3$ ), poly(tyrosol carbonate): (top) *alt*, (middle) *dir*, (bottom) *scr*, zoom into carbonate chemical shift ( $\delta$  151–156 ppm) with assignments of HH, TT, HT.

A comparative sequence analysis of *alt*, *dir* and *scr* allowed the identification of the carbonate sequence isomers in the overlay of the  $^{13}\text{C}$  NMR spectra (Figure 6.3). The overview spectra provide insights into the polymer structure in the supplementary section (Figure S16).

The dialkyl carbonate (TT) appeared at the most downfield chemical shift ( $\delta$  155.3 ppm), which is in good agreement with values observed for the dialkyl carbonate in poly(trimethylene carbonate) (PTMC) (68). Most upfield in the carbonate chemical shift ( $\delta$  152.4 ppm) was correlated to the diaryl carbonate which was subdued to the shielding effect of two neighboring aromatic rings. It corresponded to the chemical shift in aromatic polycarbonates (138). Lastly, the signal of the aryl alkyl carbonate was detected at an intermediate chemical shift ( $\delta$  153.9 ppm).

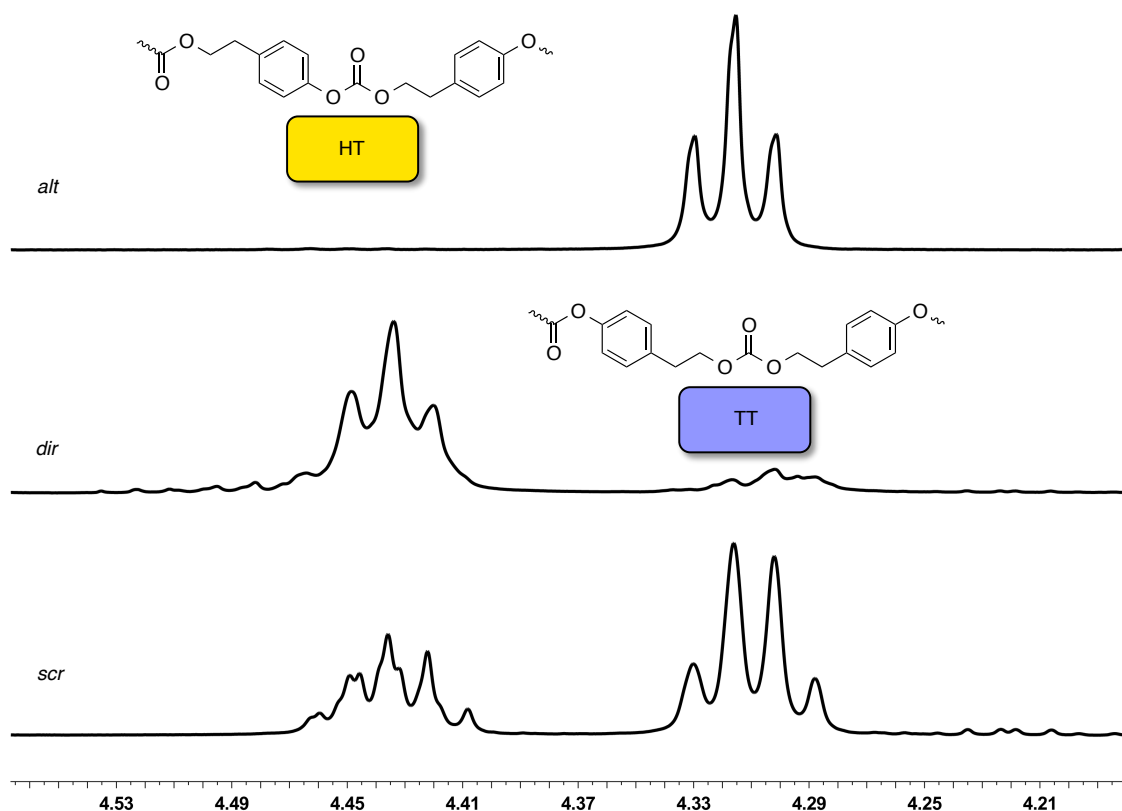


Figure 6.4:  $^1\text{H}$  NMR (500 MHz,  $\text{CDCl}_3$ ), poly(tyrosol carbonate): (top) *alt*, (middle) *dir*, (bottom) *scr*, zoom into  $\text{C}_\alpha\text{H}_2$  chemical shift ( $\delta$  4.2 – 4.5 ppm) with assignments of HH, TT, HT.

The  $^1\text{H}$  NMR spectra provide additional quantitative information (Figure 6.4). Expansion into the  $\text{C}_\alpha\text{H}_2$  chemical shift shows that *alt* was obtained with a sequence purity of around 99%.

### 6.4.2 Controlled Crystallinity of Isotropic Polycarbonates

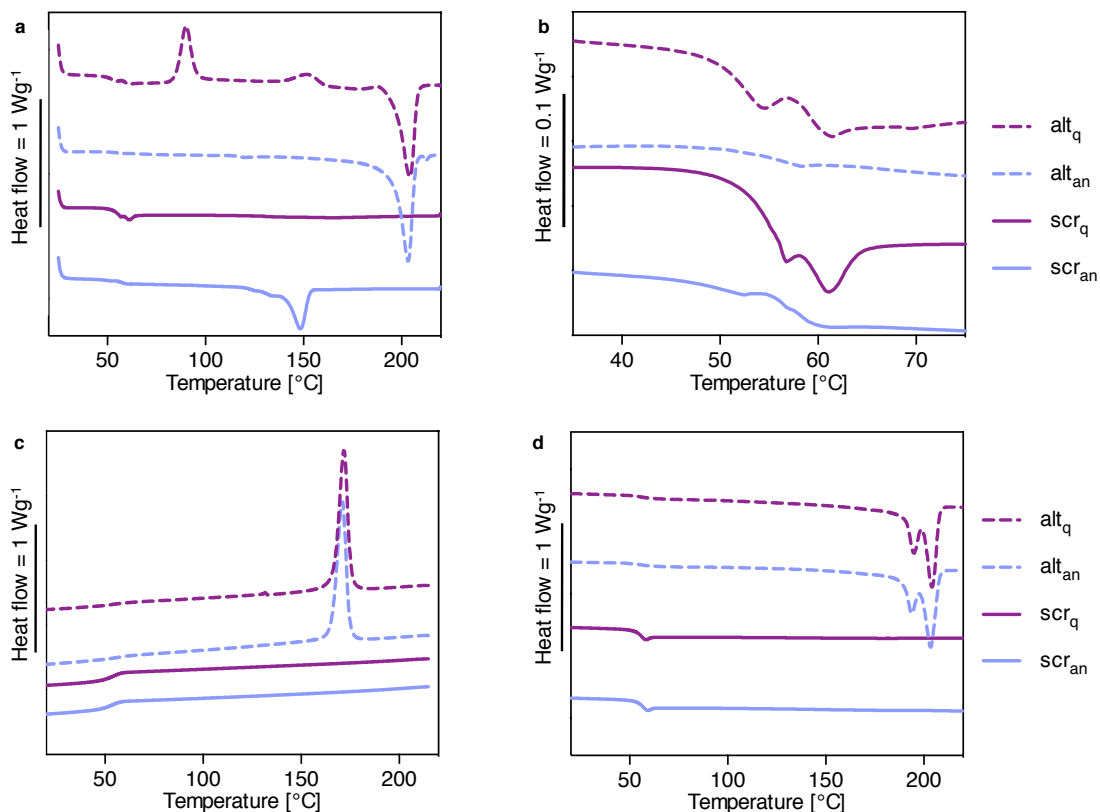


Figure 6.5: DSC scans of quenched and annealed polycarbonate films of *scr* and *alt*: (A) First heating, overview, (B) first heating, zoom into  $T_g$ , (C) cooling, (D) second heating. Rate =  $10\text{ }^{\circ}\text{C min}^{-1}$ , exotherm up.

The sequence order of the carbonate bond isomers in *alt* and *scr* dictated striking differences in the melting and crystallization behaviors of poly(tyrosol carbonate)s. Our results obtained from compression molded films by differential scanning calorimetry (Figure 6.5) and X-ray diffraction (Figure 6.6), demonstrated that *alt* readily underwent melt crystallization, whereas *scr* showed only poor crystallization behavior. For instance, the DSC curve of quenched films from *alt* featured two crystallization exotherms upon heating (rate =  $10\text{ }^{\circ}\text{C min}^{-1}$ ) at  $89\text{ }^{\circ}\text{C}$  and  $150\text{ }^{\circ}\text{C}$  (Figure 6.5 A). A strong melting endotherm appears at  $204\text{ }^{\circ}\text{C}$  which was also observed for *alt* after annealing for 4 h at  $160\text{ }^{\circ}\text{C}$ . Upon cooling, *alt* showed a crystallization exotherm at  $171\text{ }^{\circ}\text{C}$  after the thermal history of the samples was deleted at  $220\text{ }^{\circ}\text{C}$  (Figure 6.5 C).



Reheating of *alt* resulted in a double peak for melting at 194 °C and 204 °C (Figure 6.5 D). The melting peak at lower temperature represented the initial melting of small, defective crystals formed upon cooling. This premelting phenomenon was followed by recrystallization and ultimately complete transition into a polymer melt. In addition, ambient cooled films of *alt* and polymer power also showed the respective melting peak (Figure S17, supplementary information).

In contrast, for quenched films from *scr* no melting or crystallization was observed by DSC, even at a slower rate of 1 °C min<sup>-1</sup> (Figure S19, supplementary information). The crystallization of *scr* occurred at a much longer timescale than for *alt* indicated by a melting endotherm at 149 °C that appeared after annealing of films at 100 °C for 20 h.

While the thermal properties above  $T_g$  such as in the melt and in the rubbery state were distinguishable due to the sequence order, the behavior around  $T_g$  was not. Surprisingly, the glass transition was observed for both *alt* and *scr* around  $T_g = 58$  °C (Figure 6.5B). In addition, quenched specimens showed relaxation peaks characteristic for the release of residual stresses in the glassy structure 60 °C. The annealed samples were semicrystalline and showed a less pronounced  $T_g$ .

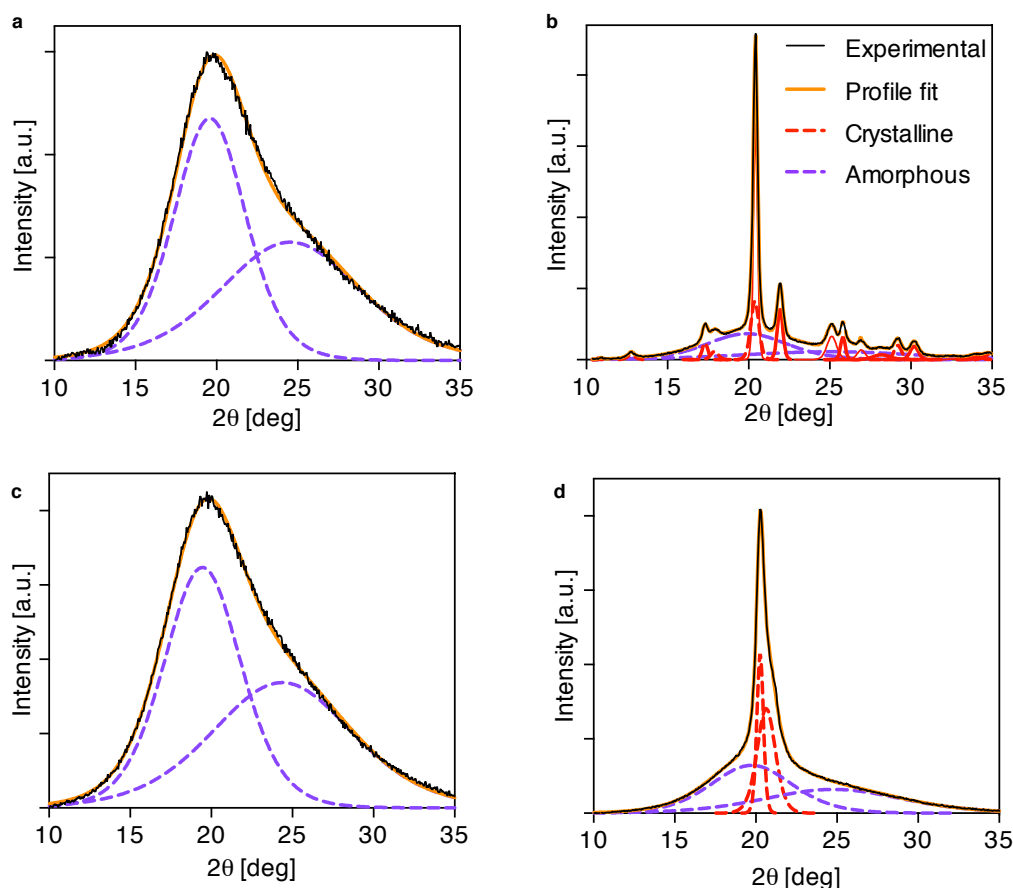


Figure 6.6: Powder X-ray diffraction patterns of films from poly(tyrosol carbonate): (Top) *alt*, (bottom) *scr*, (A) and (C) quenched, (B) and (D) annealed.

The X-ray patterns from powder diffraction confirmed that annealed films from *alt* were highly crystalline and to a lesser extent *scr<sub>an</sub>* was also semicrystalline (Figure 6.6). The crystallinity was 45% and 29% and the crystallite sizes were 227 Å and 111 Å, for *alt* and *scr*, respectively (Table 6.1, controls in Figure S20, supplementary information). This was determined by profile fit analysis of the experimental intensities. For *alt* a multitude of peaks was fitted whereas *scr* gave rise to only two crystalline peaks. Qualitatively, *alt<sub>ac</sub>* and *alt<sub>p</sub>* resembled the diffraction pattern of *alt<sub>ac</sub>*, but at lower crystallite sizes and crystallinity (Figure S20, supplementary information).

Remarkably, the amorphous structure in quenched films did not depend on the backbone sequence of poly(tyrosol carbonate). The reflections of *alt* and *scr* were indistinguishable by powder diffraction and could be fitted by two amorphous halos at  $2\theta = 19^\circ$  and  $24^\circ$  (Figure 6.6 A and C).

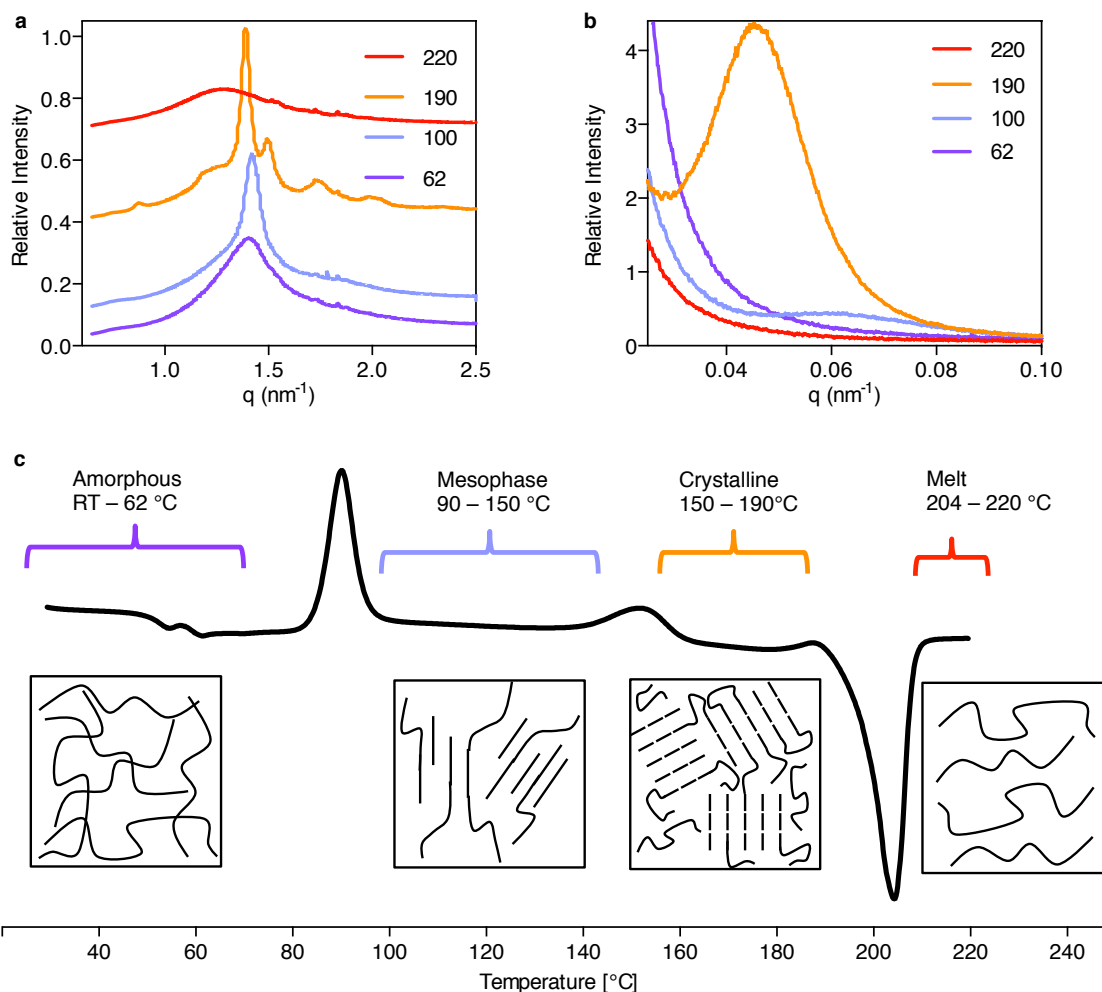


Figure 6.7: (A) SAXS and (B) WAXS scans of *alt<sub>q</sub>*, simultaneous experiment during heating. (C) Interpretation of phase behavior of *alt<sub>q</sub>* during heating in DSC, rate = 10 °C min<sup>-1</sup>, exotherm up.

Analysis of the phase behavior of poly(tyrosol carbonate) in regards to the thermal processing conditions provided insight on how the polycarbonate backbone sequence was able to effect bioerosion and mechanical performance. Simultaneous SAXS/ WAXS studies were performed on *alt*, which rapidly encountered various

phase transitions upon heating at  $10\text{ }^{\circ}\text{C min}^{-1}$  (Figure 6.7A and B). The observations from SAXS/ WAXS were matched with the enthalpic changes in the DSC curve and assigned to the physical states as shown in the schematic overlay (Figure 6.7C). In comparison to *alt*, *scr* did not readily undergo phase transitions beyond  $T_g$  unless annealed for an extended period of time. However, interpretation of phase behavior of *scr* in relation to *alt* was possible by the analysis of stand-alone Xray and DSC data.

The amorphous state existed for *alt* up until  $62\text{ }^{\circ}\text{C}$  evident in the broad signal of the WAXS pattern. When amorphous, the physical polymer properties of *alt* and *scr* were equivalent. In contrast, the backbone chemistry played out leading to a rapid bioerosion of *alt* in lipase solution as compared to a slower eroding *scr*.

At  $100\text{ }^{\circ}\text{C}$ , *alt* has transitioned into a quasi-crystalline mesophase featuring a 1-dimensional order. This is evident in the WAXS and SAXS patterns of *alt*, when crystalline peaks start to appear at  $90\text{ }^{\circ}\text{C}$  with  $q = 1.45\text{ nm}^{-1}$  and  $q = 0.065\text{ nm}^{-1}$ , respectively. This mesophase also pertained to *scr*, but was only formed after extensive annealing at  $100\text{ }^{\circ}\text{C}$  for 20h. Heating of *scr* beyond  $150\text{ }^{\circ}\text{C}$  resulted in the formation of a melt, that did not crystallize at all. In contrast, *alt* form a 3-dimensional crystalline phase at  $150\text{ }^{\circ}\text{C}$ . At  $190\text{ }^{\circ}\text{C}$ , folded chain lamellae have developed with spacings of  $140\text{ }\text{\AA}$ , which can be derived from the SAXS peak at  $q = 0.047\text{ nm}^{-1}$ . Interestingly, *scr* could not produce a 3-dimensional order, which in aligned polymer films resulted in an additional tensile properties. At  $220\text{ }^{\circ}\text{C}$ , the transition into the melt is fully achieved, when all crystalline peaks have disappeared.

Table 6.1: Summary of thermal and crystalline properties of *scr* and *alt*

Polymer	Condition	$T_g$ (°C)	$T_m$ (°C)	$\chi$	Crystallite
		dry	(°C)	(%)	Size (Å)
<i>alt</i>	Quenched	58	-	-	-
	Annealed	56	204	44.7	227
<i>scr</i>	Quenched	55	-	-	-
	Annealed	57	149	29.1	111

The quick melt-crystallization of aromatic-aliphatic polycarbonates from tyrosol such as *alt* was unique. Generally, polycarbonates do not show the tendency to readily transition into the crystalline phase as compared to other polymer systems such as polyesters. Only few examples showed crystallization in aromatic polycarbonate such as poly(BPA carbonate) which maybe kinetically unfavored due to bulky substituents. For poly(BPA carbonate), crystallization could be induced by solvent vapor (87) or supercritical CO<sub>2</sub> (11). Polycarbonates from tyrosol were less rotationally constraint then poly(BPA carbonate) and thus maybe resembled crystallization behavior of aliphatic polycarbonates such as PTMC. Low molecular weight PTMC of less than 12kDa was reported to spontaneously crystallize under ambient condition with a low melting point of  $T_m = 36^\circ\text{C}$ . Further, strain induced crystallization was also observed for high molecular weight PTMC (100). Albeit, stretched, semi-crystalline PTMC does not recoil and its low melting point prohibits a possible practical advantage under physiological conditions. In contrast, crystallites of *alt* showed melting at much higher temperatures. Most likely, the aromatic component or *alt* with diaryl carbonate moieties contributed to lock in crystallinity over a much wider temperature range that may be of practical relevance.

### 6.4.3 Oriented Polymer Films

Differences in the formation of crystalline phases between *alt* and *scr* were emphasized by the chain orientation in stretched and annealed polymer films.

Oriented films were obtained by stretching the samples above  $T_{g,wet}$ . In addition, stretched films were annealed under inert and mechanically constraint conditions at 160 °C and 100 °C, respectively for *alt* and *scr*. A 3-dimensional crystalline order is achieved for  $alt_{q,s,an}$  evident in the fiber diffraction pattern showing multiple off-equatorial crystalline reflections, symmetrically distributed around the draw axis (Figure 6.8). In contrast,  $scr_{q,s,an}$  obtained only the 1-dimensional order of a quasi-crystalline mesophase showing crystalline scattering at the equatorial axis. This 1-dimensional order was also obtained for  $scr_{q,s}$  by stretching alone. The diffraction patterns from stretched polycarbonates appeared equivalent featuring equatorial peak intensities for *alt* and *scr*. These reflections indicated that strain-induced crystallization occurred, which was supported by the strain-hardening phenomena observed in the MTS curves recorded during stretching (Figure S21 A, supplementary information). As expected quenched samples were isotropic showing azimuthal scattering and  $alt_{an}$  showed several distinct rings corresponding to the crystalline peaks observed in the powder diffraction patterns in Figure 6.6. It can be noted, that annealing of *alt* at 100 °C also lead to a 3-dimensional crystalline order, but less pronounced as the off-equatorial diffraction reflections appeared diffuse (Figure S21 B, supplementary information). In turn, annealing of *scr* at 160 °C for 3–20 h lead to melting of the 1-D crystals and upon cooling to an amorphous glassy structure at RT. The 2-D diffraction pattern from control samples such as films from PLLA and poly(DTE carbonate) are shown in Figure S22 (supporting information).

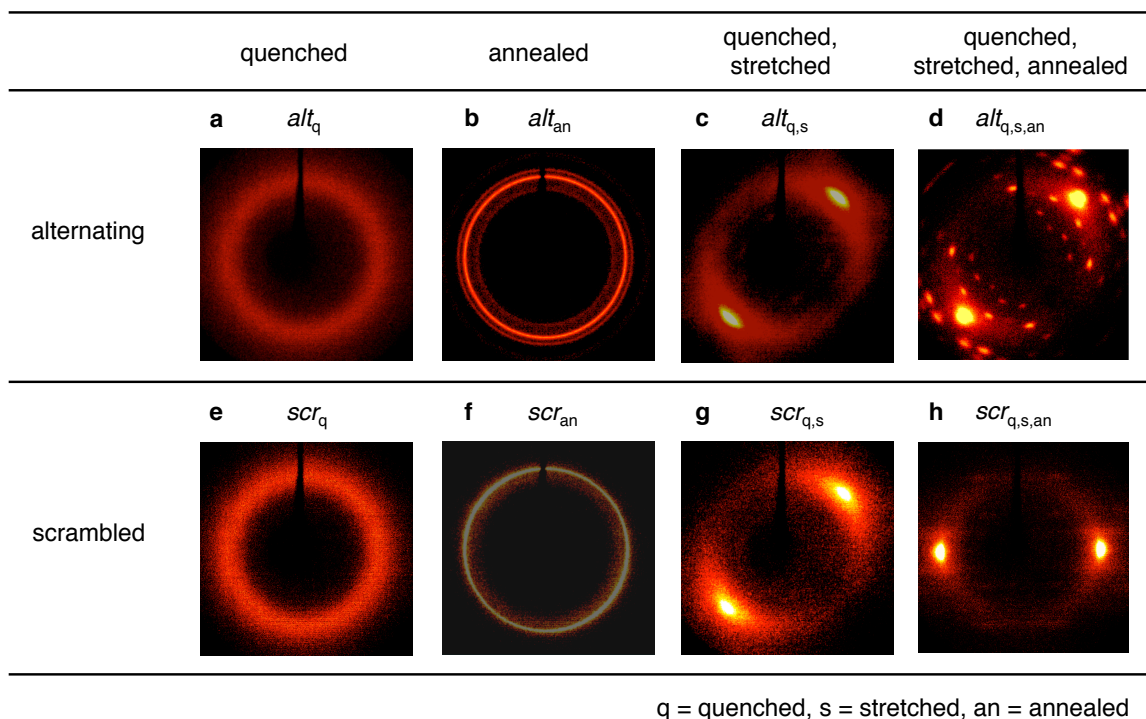


Figure 6.8: X-ray diffraction in 2-D of films from poly(tyrosol carbonate): (Top) *alt*, (bottom) *scr*, (A) and (E) quenched, (B) and (F) annealed, (C) and (G) quenched and stretched, (D) and (H) quenched, stretched and annealed.

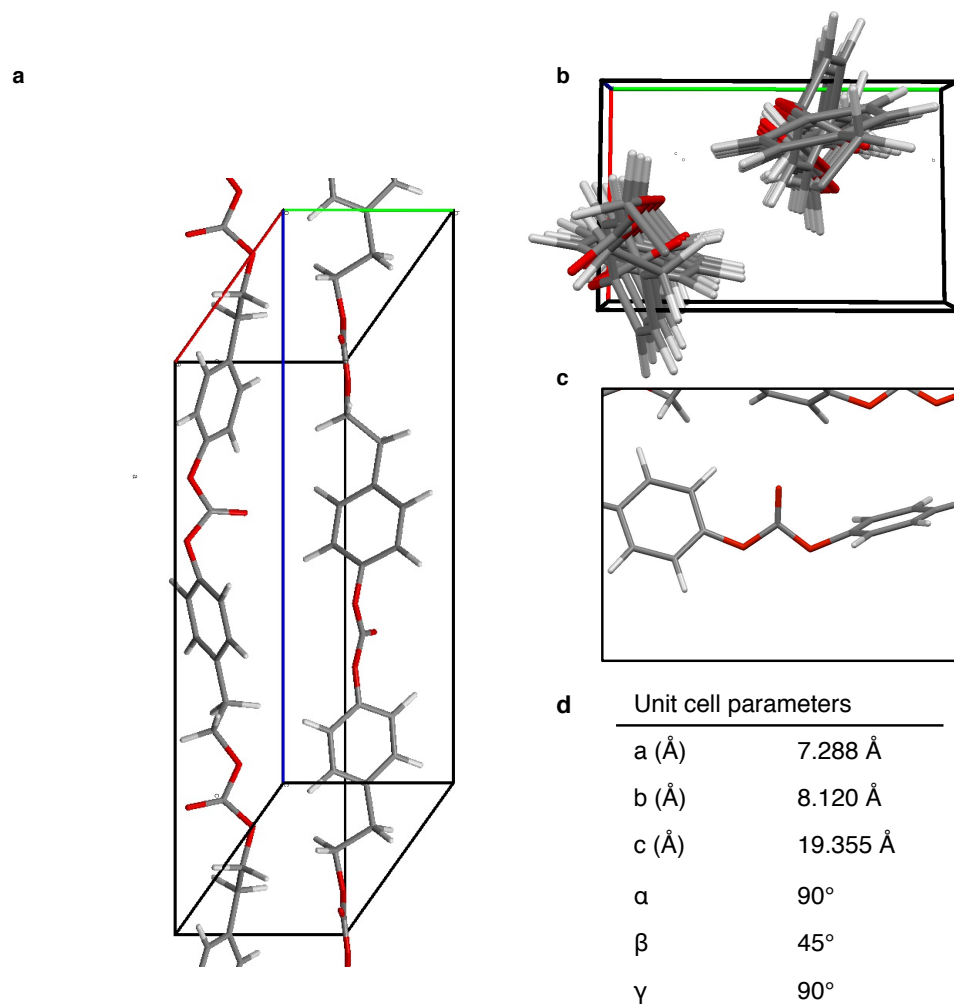


Figure 6.9: A 3-dimensional structural model for *alt* derived from the diffraction pattern of the highly oriented and crystalline film (quenched, stretched and annealed): (A) Side view of the unit cell, (B) top view, (C) zoom into the diaryl carbonate, (D) unit cell parameters (Structural model developed by Jim Kaduk).

At least 34 unique reflections were identified from the diffraction pattern of the highly crystalline and oriented film from *alt*<sub>q,s,an</sub> (quenched, stretched and annealed, Figure 6.8 D). Based on this diffraction pattern of *alt*<sub>q,s,an</sub> it was possible to derive a 3-dimensional structural model for the unit cell (Figure 6.9 A–C). First, a triclinic unit cell was assigned: (Space group P1) with the dimensions shown in Figure 6.9 D. With these unit cell parameters the positions of all the reflections could be reproduced. Next, the molecular structure was built and minimized using density functional theory



module (Crystal09 package, Italy). All of the bond distances fall within the normal ranges. Some of the torsion angles were located on the tails of the commonly observed distributions. This is a tentative structure that still needs to be refined by further analysis. Two important observations of the structure is that the aromatic groups on adjacent chains are staggered along the chain- axis, and that the carbonate bonds of one chain is found close to the aromatic ring of the adjacent chain. This is one of the few examples of a polycarbonate structure derived from crystallographic data, other than the structure of PTMC (123).

#### 6.4.4 Mechanical Performance

Stretched films of *scr* and *alt* showed improvement of the mechanical properties such as the modulus and the stress at yield. In particular, *alt<sub>q,s,an</sub>* stood out as the best performing species most likely due to the 3-dimensional order in oriented crystallites. These changes depending on the processing conditions were illustrated qualitatively in the stress-strain curves from mechanical tensile testing under dry conditions for *alt* and *scr* (Figure 6.10). It can be noted that quenched samples of *alt* and *scr* showed a very similar performance. Further, the effect of annealing of isotropic films leading to highly crystalline *alt<sub>q</sub>*, causes embrittlement indicated by failure upon yield. The annealing did not effect the performance of *scr*: no changes were observed for poorly crystalline *scr<sub>an</sub>* as compared to amorphous *scr<sub>q</sub>*.

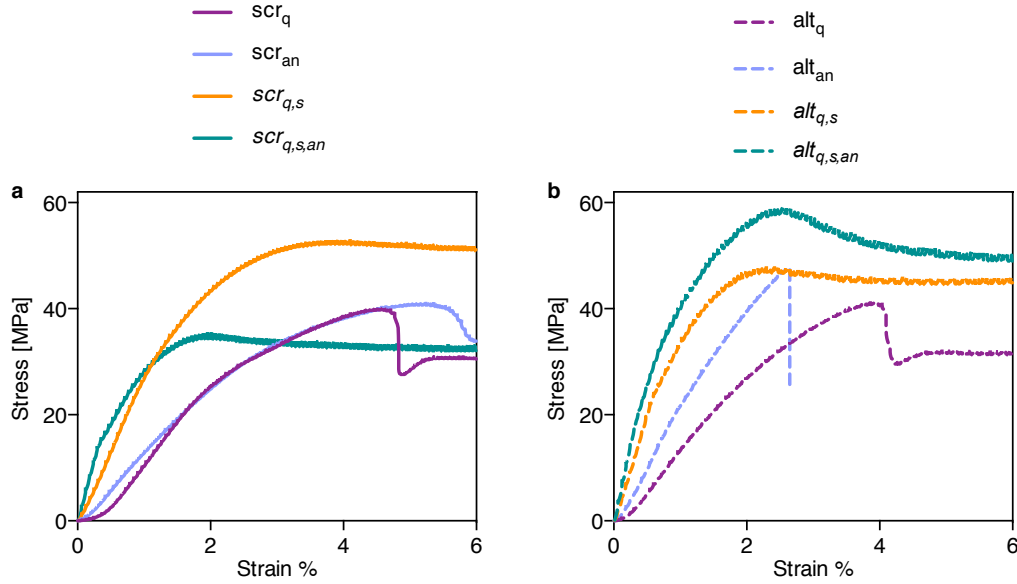


Figure 6.10: Stress-strain curves of films from poly(tyrosol carbonate) *alt* and *scr*: (A) Unoriented, (B) oriented. Quenched or annealed, tested in dry state at ambient temperature.

The high stiffness of  $alt_{q,s,an}$  persists with a tensile modulus of  $5.4 \pm 0.3$  GPa under simulated, wet conditions in PBS at  $37^\circ\text{C}$  as compared to  $5.6 \pm 0.2$  GPa under dry conditions at ambient temperature Figure 6.11. Interestingly, the stiffness of  $alt_{q,s,an}$  supersedes PLLA, the most common biodegradable polymer.  $PLLA_{q,s,an}$  that was stretched and annealed achieved a dry modulus of  $5.2 \pm 0.2$  GPa. However,  $PLLA_{q,s,an}$  lost stiffness under physiological conditions, the tensile modulus was reduced to  $3.8 \pm 0.3$  GPa. A similar loss of stiffness is observed for the stretched controls  $PLLA_{q,s}$  and  $DTE_{q,s}$ .

For the stretched samples,  $scr_{q,s}$  and  $alt_{q,s}$  the tensile modulus were also improved compared to the isotropic species with moduli ranging from 3.1–4.4 GPa and 3.1–4.1 GPa under dry and wet conditions, respectively. However, the 1-dimensional crystalline order observed could not improve stiffness as much as the 3-dimensional crystalline order. For all stretched samples, the  $\epsilon_{yield}$  showed a slight improvement with values around 50 MPa. Whereas,  $\epsilon_{yield}$  of  $scr_{q,s,an}$  was reduced to the value of the isotropic, amorphous sample.

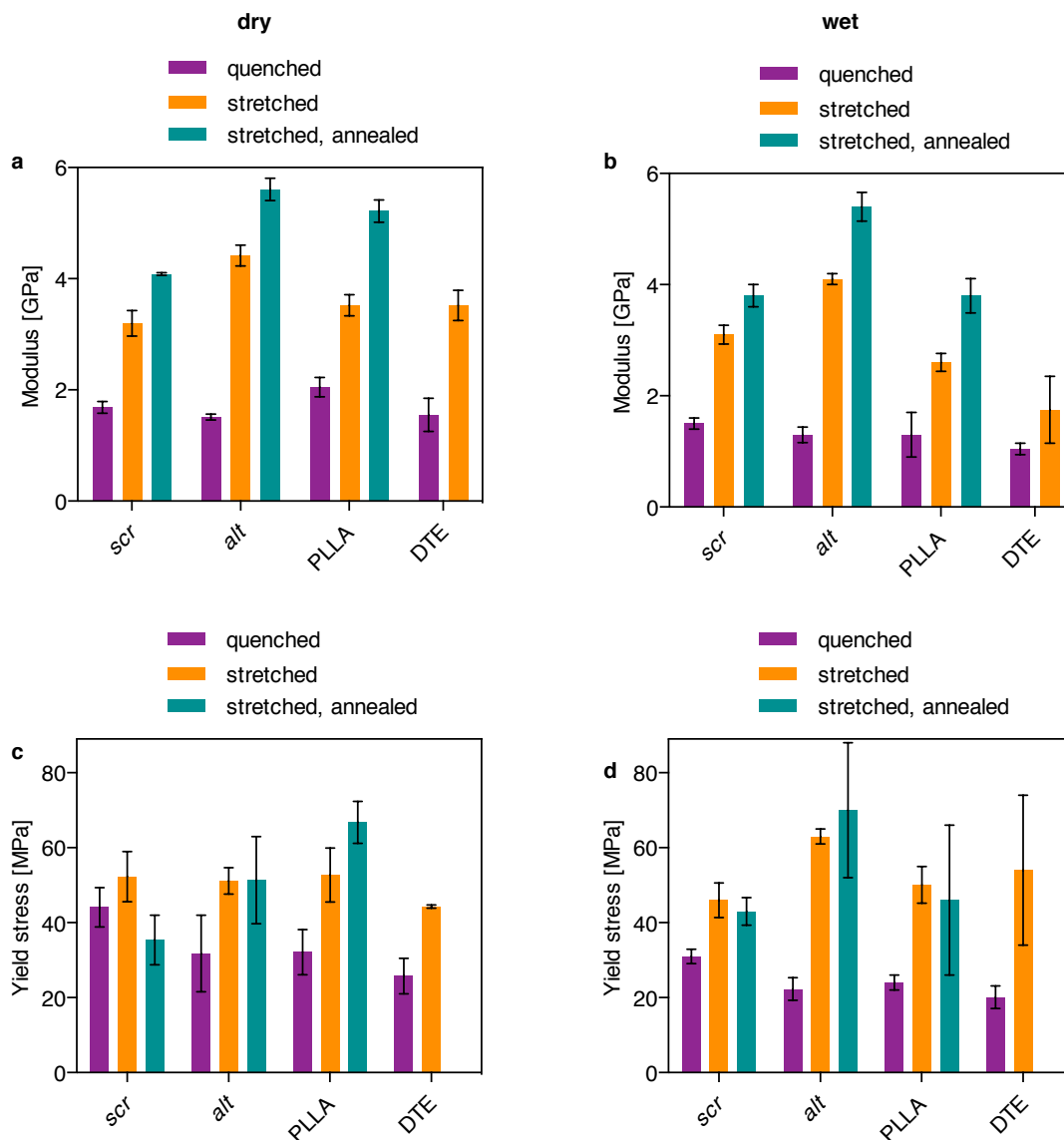


Figure 6.11: Mechanical properties of films from poly(tyrosol carbonate) *alt* and *scr* in comparison to PLLA and poly(DTE carbonate): (A) and (B) Tensile Modulus, (C) and (D) stress at yield.

In perspective, the poly(tyrosol carbonate) of either *scr* and *alt* sequence is a viable alternative for biomedical applications respective to mechanical performance, when high stiffness is required. Our results show that in comparison oriented and semi-crystalline *alt* has a higher modulus than PLLA, the most commonly applied degradable, biomedical polymer. Previous studies have reported moduli in a range from 3.6–5.4 GPa for melt drawn, oriented PLLA fibers (139), matching our results

on molded films. Noteworthy, the highest tensile modulus for a degradable polymer of 16 GPa was reported for hyper-branched polyester derived from the lignin component cinnamic acid (57).

Upon implantation of a biomedical device, polymeric materials were subjected to wet conditions and physiological temperatures. This may potentially cause loss of mechanical properties from the dry state as well as device shrinkage. Therefore, it is beneficial that *scr* and *alt* preserve most of their mechanical properties. Stretched films of *scr* and *alt* had high dimensional stability showing no significant shrinkage within a 8 week timeframe of immersion in PBS at 37 °C (Figure S27, supplementary information). In contrast, stretched PLLA and poly(DTE carbonate) lost stiffness and also significant shrinkage occurred upon exposure to physiological conditions. Shrinkage did not occur for semi-crystalline  $PLLA_{q,s,an}$  confirming previous studies that reported high dimensional stability for semi-crystalline PLLA (4). In turn, the crystallinity well as the low water uptake of stretched *scr* and *alt* samples were key contributor to the dimensional stability.

### 6.4.5 Sequence-Dependence of Bioerosion

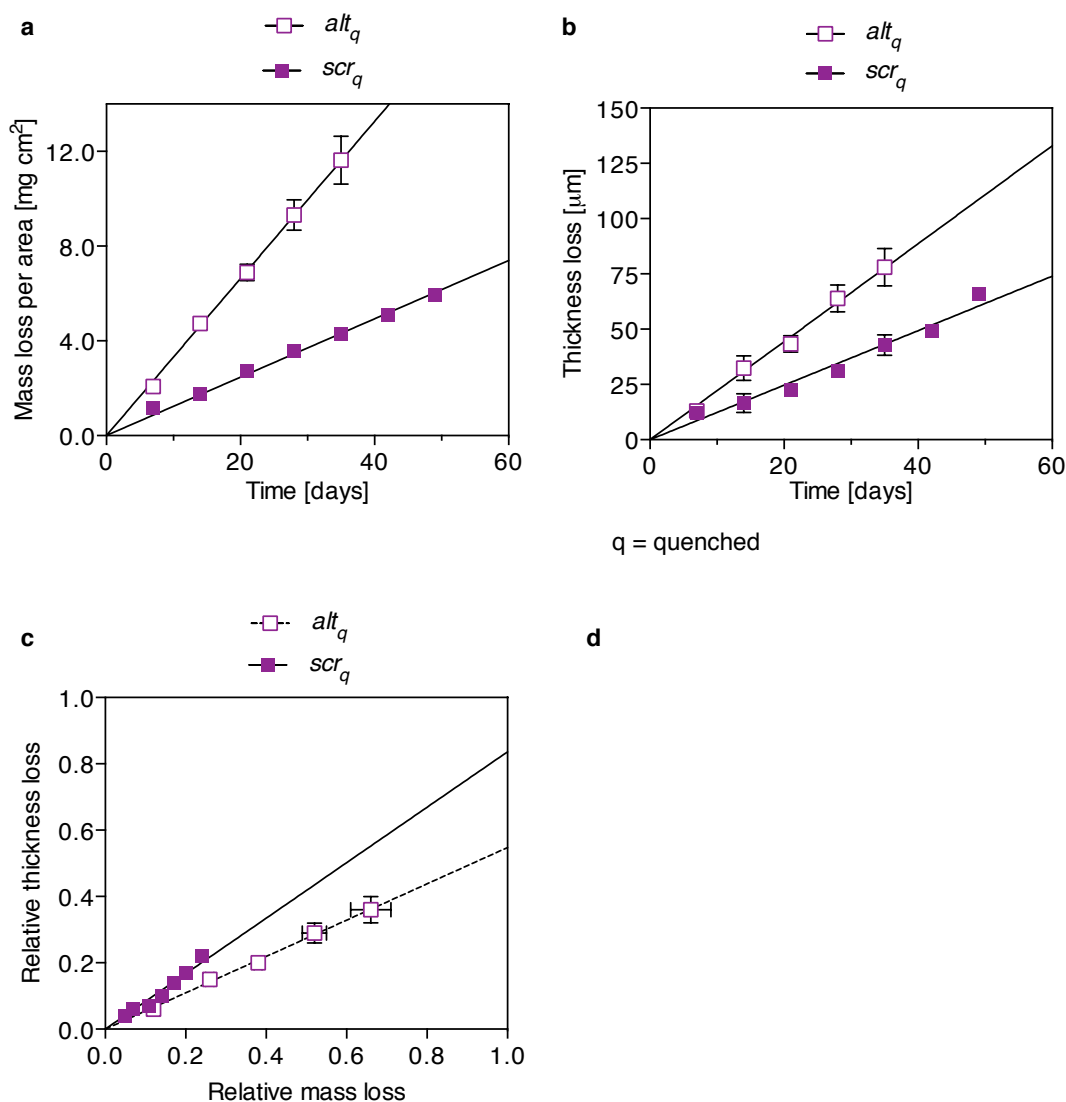


Figure 6.12: Bioerosion of poly(tyrosol carbonate) *alt* and *scr*: (A) Mass loss per area, (B) thickness loss, (C) correlation between relative mass and thickness loss. Disc shaped specimens incubated in lipase solution at 37 °C, (mean  $\pm$  SD, n = 3). The linear regression lines were plotted.

The bioerosion behavior of compression molded films from *alt* and *scr* was compared respective to effects of the physical polymer states such as amorphous, semi-crystalline, oriented and isotropic. The evaluation was conducted using TLL as model

enzyme previously shown to simulate the *in vivo* bioerosion in aliphatic polycarbonates such as PTMC (106; 141). Remarkably, *alt* showed rapid mass and thickness loss over time as compared to a slower eroding *scr* for quenched films in the amorphous state, (Figure 6.12 ). No erosion was observed in PBS (Figure S24 , supplementary information) and the  $M_n$  in the bulk remained unchanged over time (data not shown). In addition it can be noted, that quenched films of *alt* and *scr* did not crystallize during incubation for 8 weeks at 37 °C (Figure S23, supporting information).

The relative thickness loss was plotted in dependence of the relative mass loss to evaluated whether surface erosion occurs for *alt* in comparison to *scr* (Figure 6.12 C). The slope of the regression curve in the plot represented the ratio of thickness to mass erosion ( $r_{\Delta d/\Delta m}$ ). For ideal surface erosion behavior, the slope would obtain the value  $r_{\Delta d/\Delta m} = 1$ . While *scr* approximated the ideal surface erosion behavior as previously described (119), the mass erosion in *alt* occurred preferentially as compared to the thickness erosion with ratios of  $r_{\Delta d/\Delta m} = 0.84$  and  $0.55$  for *scr* and *alt*, respectively. Phenomenological, it can be reasoned that the rapid erosion of *alt* causes uneven structures on the eroded structures such as pits and cavities that translated into artificially higher film thickness as compared to functional bulk thickness. The mechanism by which eroded structures were temporarily conserved maybe crystallization induced by degradation confined to the surface layer. Future studies using XPS may elucidate the exact mechanism.

The physical states such as crystallinity and orientation of the polymer films appear as overlaying factors influencing the erosion rates. Stretched, oriented *scr* underwent enzymatic bioerosion, while equivalent specimens from *alt* did not (Table 6.2). This difference can be explained with the higher crystallinity in *alt* as compared to *scr* decreasing the susceptibility to enzymatic erosion. A similar effect was previously studied on semi-crystalline PLLA as an example (110). The scenario most likely pertains to biodegradable polycarbonates from *scr* and *alt*. However, it is not possible to separately analyze the effects of orientation and crystallinity on the erosion, because strain-induced crystallization occurred.

The rates of mass loss and thickness loss determined by linear regression on the erosion curves are summarized in Table 6.2. Noteworthy, no erosion is observed for specimens that were stretched and annealed due to the further increased crystallinity. While *alt* crystallizes upon cooling under ambient conditions and is non-erodible, ambient cooled *scr* is amorphous and eroded similar to the quenched species (Figure S25, supplementary information).

Table 6.2: Bioerosion rates of *scr* and *alt*

Polymer	Physical state	Mass <sup>a</sup> loss	Thickness <sup>a</sup>	Ratio <sup>a</sup> of	=
		per area ( $\Delta m$ )	loss ( $\Delta d$ )	$r_{\Delta d/\Delta m}$ $\frac{\Delta m_{rel}}{\Delta d_{rel}}$	
		( $\text{mg cm}^{-2} \text{d}^{-1}$ )	( $\mu\text{m d}^{-1}$ )		
<i>alt<sub>q</sub></i> (143 kDa)	Amorphous,	$0.33 \pm 0.01$	$2.2 \pm 0.05$	$0.55 \pm 0.01$	
	isotropic				
<i>alt<sub>an</sub></i>	Semi-crys.,	No erosion	-	-	
	isotropic				
<i>alt<sub>q,s</sub></i>	Semi-crys.,	No erosion	-	-	
	oriented				
<i>alt<sub>q,s,an</sub></i>	Semi-crys.,	No erosion	-	-	
	oriented				
<i>scr<sub>q</sub></i> (167 kDa)	Amorphous,	$0.12 \pm 0.01$	$1.2 \pm 0.01$	$0.84 \pm 0.03$	
	isotropic				
<i>scr<sub>ac</sub></i>	Amorphous,	$0.13 \pm 0.01$	$1.4 \pm 0.04$	$0.9 \pm 0.07$	
	isotropic				
<i>scr<sub>an</sub></i>	Semi-crys.,	No erosion	-	-	
	isotropic				
<i>scr<sub>q,s</sub></i>	Oriented	$0.14 \pm 0.01$	$1.9 \pm 0.1$	$0.76 \pm 0.07$	
<i>scr<sub>q,s,an</sub></i>	Semi-crys.,	No erosion	-	-	
	oriented				

<sup>a</sup>Values determined by linear regression on erosion curves.

The putative *in vivo* relevance of the *in vitro* bioerosion of *alt* as compared to *scr* was qualitatively evaluated after subcutaneous implantation of specimens in the back of rats. The location for implantation was selected because of lipase expression in the subcutaneous, fatty tissue as well as previous studies demonstrating surface erosion of



rubbery, aliphatic polycarbonates. The erosion of glassy, poly(tyrosol carbonate) of either *scr* and *alt* sequence appeared to be slower than under simulated conditions in lipase solutions. After the 3 months, the explant from *scr* showed 2% mass loss, while thickness loss was negligible. For *alt* 2.5% mass loss and a measured thickness loss  $4\mu m$  (radius = 3.5 mm). In SEM images, the surface morphology of the *invivo* explant from *scr* was strikingly similar to the structures observed after *in vitro* incubation in lipase solution (Figure 6.13 A, C, E). Erosion structures comprised of pits and cavities of similar dimensions with approximately 1–10  $\mu m$  in diameter appeared on the surfaces. In contrast, the morphology of *in vivo* explants from *alt* appears more irregular in shape: remnants of pits appear to transition in to erosion structures caused by layers sheets of material leaving the surface (Figure 6.13 B and D). In this interpretation, the morphology observed for *alt* may represent a later stage in the *in vivo* surface erosion when thickness loss becomes measurable. After 3 weeks, the *in vitro* appearance of *alt* matches what is expected from a more rapid progression of erosion (Figure 6.13 F).

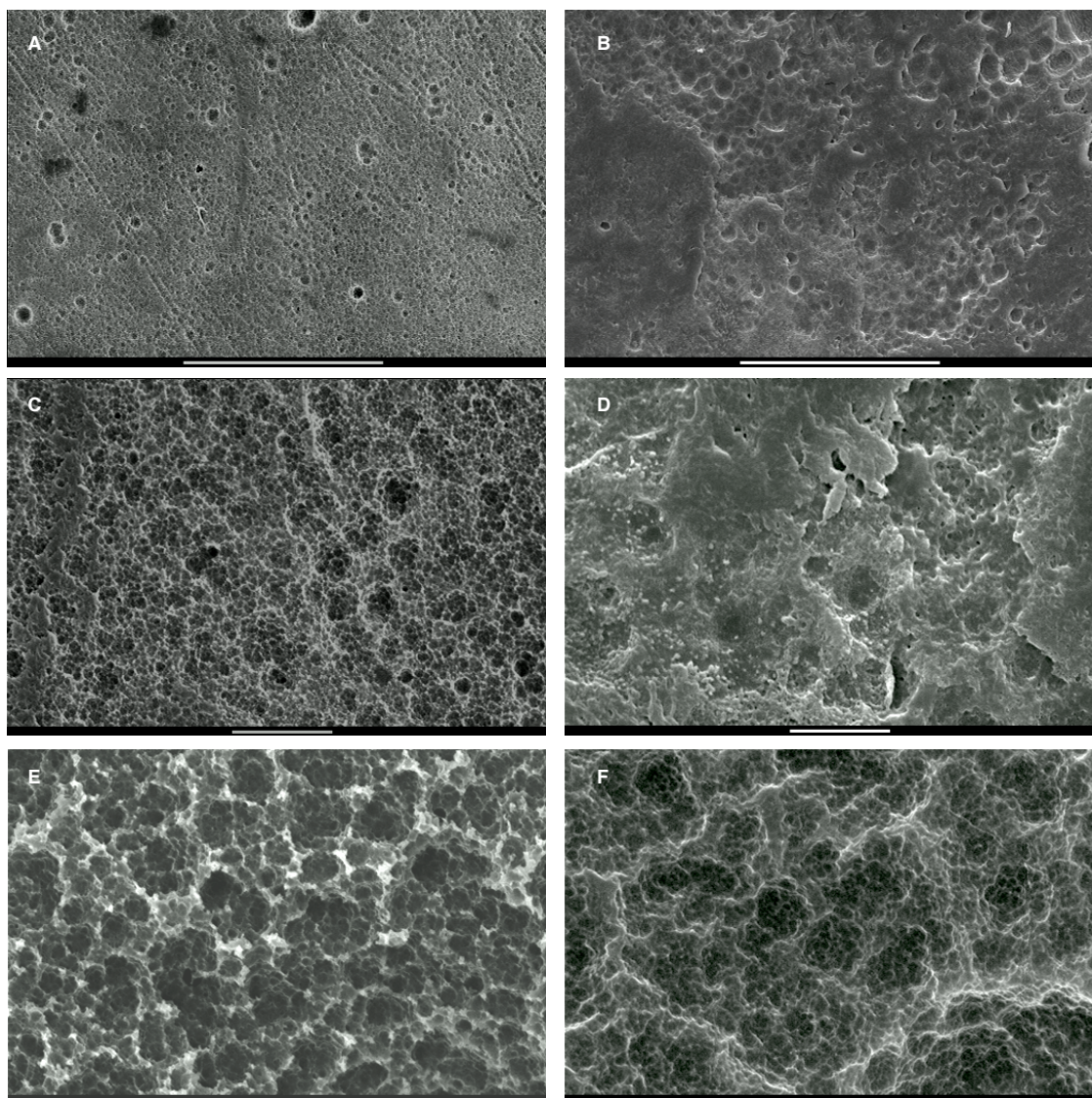


Figure 6.13: SEM morphology of surfaces of compression molded discs of poly(tyrosol-carbonate): (Left) *scr*, (right) *alt*, (A) and (B) 3 months *in vivo*, scale bar = 100  $\mu\text{m}$ , (C) and (D) 3 month *in vivo*, scale bar = 10  $\mu\text{m}$ , (E) and (F) 3 weeks *in vitro*, incubation in lipase solution at 37 °C, scale bar = 10  $\mu\text{m}$ .

SEM morphology of surfaces of compression molded discs of poly(tyrosol carbonate) after incubation in lipase solution: (A) 0 weeks, (B) 1 week, (C) 4 weeks, (D) 6 weeks, (E) 9 weeks, (F) 9 weeks, PBS control, after rinse with 70% (v/v) ethanol. Scale bar = 10  $\mu\text{m}$ .

In addition to *in vivo* implantations, we evaluated the cytotoxicity of *alt* and *scr* in comparison to controls PLLA, poly(DTE carbonate) respective to putative leachables at a 5 day timepoint (Figure S28).

## 6.5 Conclusion

In summary, the interplay of polymer sequence control and phase behavior in aromatic–aliphatic polycarbonates from tyrosol adds a dimension tailoring synthetic polymers systems to specific biomedical applications. In the amorphous state, different backbone sequences do not translate into differences in the physical characteristics. The polymer properties such as the mechanical performance are equivalent. Remarkably, the erosion rates are increased for the alternating sequence. Here, the backbone chemistry directly dictates enzymatic erosion rates likely by ease of access to the active site.

In turn, thermal polymer processing can exploit the differences in phase behavior arising from the polymer backbone chemistry. 3-dimensional, oriented films of alternating polycarbonate provide superior stiffness as compared to oriented films of the scrambled sequence. Here, the chemistry plays out in the background as phase transitions during processing may manifest devices that carry physical characteristics such as orientation and crystallinity. Future studies will investigate the mechanism of sequence dependence of the erosion rate in detail and elucidate the role of the carbonate bonds for the crystallization behavior.

## Chapter 7

### The *In Vivo* Behavior of Polycarbonates from Tyrosol and 1,3-propanediol

#### 7.1 Abstract

In this chapter, the *in vivo* behavior of mechanically strong and stiff poly(tyrosol carbonate) was evaluated respective to *in vitro* results and compared to softer copolymer compositions with 1,3-propanediol (PD).

Copolymers with 100, 85 and 76 mol % of Ty as compared to PD were synthesized with values of  $M_w$  between 96 and 138 kDa. Similar to poly(tyrosol carbonate), copolymers with 15 and 24 mol % of PD were also strong and stiff in the dry state. However, the copolymers became softer under physiological conditions due to the lower  $T_{g(wet)}$ . For example, the modulus was  $E_T = 0.5 \pm 0.1$  GPa for the copolymer with 76 mol % of Ty and  $T_{g(wet)} = 39^\circ\text{C}$ . *In vitro*, compression molded discs showed rapid surface erosion mediated by lipase. The erosion proceeded faster for softer copolymers with increasing PD content. The rates of mass loss were  $0.15 \pm 0.01 \text{ mg cm}^{-2} \text{ d}^{-1}$ ,  $0.23 \pm 0.01 \text{ mg cm}^{-2} \text{ d}^{-1}$  and  $0.29 \pm 0.01 \text{ mg cm}^{-2} \text{ d}^{-1}$  for 0, 15 and 24 mol % of PD, respectively.

*In vivo* experiments were conducted by subcutaneous implantation in the back of rats. Explants were harvested after periods of 3 weeks and 3 months. All explants were enclosed by a fibrous capsule. The mass loss *in vivo* proceeded slower than *in vitro* with only about 2 % (w/w) for all compositions. In turn, the morphology of explant surfaces as characterized by SEM showed striking similarities to the erosion structures observed *in vitro*. After 3 weeks, the surfaces featured pits and cavities.

The size of these erosion structures ranged between 1  $\mu\text{m}$  and 10  $\mu\text{m}$  and increased along with the softness of the compositions. After 3 months the cavities in the softer compositions appeared constricted, while only poly(tyrosol carbonate) maintained regular erosion structures. This finding may be explained by mechanical stresses acting on the polymer discs at the implant site, thus influencing the microscopic surface structure.

In perspective, polycarbonates from tyrosol and 1,3-propanediol are surface eroding *in vivo*, but clinically relevant, faster erosion may be observed by adjusting parameters such as the surface to volume ratios of the specimens. Implant locations entailing high enzymatic activity in surrounding solution such as the gastrointestinal tract or the synovial fluid may be considered in future investigations respective to clinical applications.

## 7.2 Introduction

Degradable, polymeric systems that undergo surface erosion mediated by biological activity are used in the clinic for applications such as hernia repair, adhesion barriers or drug-delivery complementing the technologies based on hydrolytically degradable polymers (9). *In vivo*, soft and flexible polymers based on poly(trimethylene carbonate) (PTMC), the polycarbonates from 1,3-propanediol (PD), are prone rather to erosion by biological factors than by abiotic hydrolysis. Early studies suggested the involvement of enzymes in the erosion of PTMC. At the same time no significant molecular weight degradation caused by hydrolysis was reported (106).

The biotic aging and erosion of polymeric devices may be strongly related to the foreign body response evoked at the implant site. When a biomaterial is exposed to the tissue environment upon implantation protein adsorption initiates a cascade of events leading to the acute inflammatory response. During the initial acute inflammatory response the release of cytokines instigates the recruitment of cells of the immune

system such as monocytes. The later occurring macrophages may further differentiate into foreign body giant cells during the chronic inflammatory state. By then, the implant is surrounded by a fibrous capsule of a specific thickness, depending on the severeness of the chronic inflammatory state (2).

Specifically, the cells of the immune system such as macrophages and foreign body giant cell may induce morphological changes as shown for polyurethanes (144). For long term devices from polyurethanes these changes are considered as adverse effects, since surface cracking negatively impacts implant stability (142). If in turn, the biological erosion was considered as a design parameter for temporary biomedical devices, the activity of macrophages is able to mediate the complete resorption of the implant as reported for PTMC networks (7). Further, copolymers of PD and D,L-lactide or  $\epsilon$ -caprolactone showed resorption *in vivo* as a result from overlaying biotic and abiotic contributions (102).

The immune cells associated with biomaterial surfaces release factors such as enzymes and reactive oxygen species that are the direct mediators of the biological degradation processes (48; 47; 70). Interestingly, the *in vivo* degradation behavior of high-molecular weight PTMC is recapitulated *in vitro* by incubation in an aqueous solution of a model lipase from *Thermomyces lanuginosus* pointing to enzymes as the main contributor to the erosion process (141). A role for reactive oxygen species in the degradation of polycarbonates was specifically suggested for poly(ethylene carbonate) (PEC) (31). For the degradation by ROS, a reaction mechanism was suggested that involves polymer chain unzipping and cyclic reaction intermediates (29). However, these studies did not directly prove the presence of free oxygen radicals in degradation of polycarbonates. Non-physiological conditions using organic solvents were required to show ROS degradation of PTMC elastomers *in vitro* (24).

In this chapter, a comparison of the *in vivo* and *in vitro* behavior of poly(tyrosol carbonate) and copolymers of tyrosol and PD is reported. The enzyme mediated erosion of strong and stiff aromatic-aliphatic polycarbonates was explored previously *in vitro*

(119). Therefore, the purpose of this study was to determine the design space for polymers susceptible to biotic surface erosion respective to materials that have superior mechanical properties as compared to PTMC. Due to the wealth of available literature respect was given to the environment posed to the classical subcutaneous implant.

## 7.3 Experimental

The experimental procedures from **Chapter 2** were followed, except noted otherwise. The mechanical properties were characterized using the tensile testing instrument from MTS systems. For polycarbonate synthesis, the general synthesis procedure was followed using tyrosol and 1,3-propanediol as the monomers.

### 7.3.1 Polycarbonate Synthesis

#### **Poly(4-(2-hydroxyethyl)phenol-co-15% 1,3-propanediol carbonate)**

$^1\text{H}$  NMR (500 MHz, DMSO- $d^6$ )  $\delta$  7.36 – 7.22 (m, 2H), 7.22 – 7.16 (m, 2H), 4.42 (s, 2H), 4.27 (s, 2H), 4.17 (s, 2H), 4.09 (s, 2H), 3.01 (s, 2H), 2.91 (s, 2H), 2.09 (s, 2H), 2.00 (s, 2H), 1.91 (s, 6H), 1.12 – 0.94 (m, 54H).  $^{13}\text{C}$ -NMR (126 MHz, DMSO- $d^6$ )  $\delta$  154.44 (s), 153.20 (s), 152.05 – 151.89 (m), 149.58 (s), 130.17 (s), 68.94 – 68.78 (m), 67.92 (s), 33.73 (s). Molar ratio 4-(2-hydroxyethyl)phenol : 1,3-propanediol carbonate, feed 83 : 17, found (by  $^1\text{H}$  NMR) 85 : 15.

#### **Poly(4-(2-hydroxyethyl)phenol-co-24% 1,3-propanediol carbonate)**

$^1\text{H}$  NMR (500 MHz, DMSO- $d^6$ )  $\delta$  7.36 – 7.21 (m, 2H), 7.21 – 7.03 (m, 2H), 4.42 (s, 2H), 4.27 (s, 2H), 4.16 (s, 2H), 4.09 (s, 2H), 3.01 (s, 2H), 2.91 (s, 2H), 2.78 (s, 2H), 2.09 (s, 2H), 2.00 (s, 2H), 1.91 (s, 2H).  $^{13}\text{C}$ -NMR (126 MHz, DMSO- $d^6$ )  $\delta$  154.34 (s), 152.96 (s), 151.71 (s), 149.30 (m), 135.91 (s), 135.51 (s), 130.00 (m), 121.12 (m), 68.62

(s), 67.65 (s), 65.29 – 64.01 (m), 33.53 (s). Molar ratio 4-(2-hydroxyethyl)phenol : 1,3-propanediol carbonate, feed 69 : 31, found (by  $^1\text{H}$  NMR) 76 : 24.

### 7.3.2 Subcutaneous Implantation in *Rattus norvegicus*

Compression molded discs of 7 mm diameter were weighed and the thickness was measured. Then they were sterilized by UV radiation for 2 h on each side. The discs were implanted subcutaneously in the back of rats with a maximum number of 4 specimens per animal. Then the rats were sacrificed at 3 weeks and 3 months time points. A set of samples was subjected to analysis of erosion and degradation, while a second set was fixated in formalin for histological analysis. National Institute of Health laboratory guidelines for good animal practice were observed.

## 7.4 Results and Discussion

### 7.4.1 Polymer Synthesis and Characterization

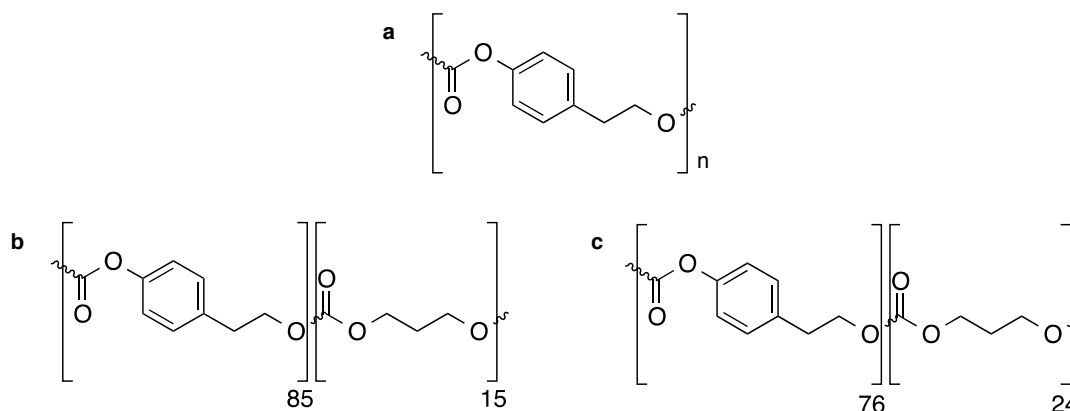


Figure 7.1: Chemical structures of (A) poly(tyrosol carbonate), (B) 85/15, (C) 76/24 molar ratios of Ty/PD in poly(tyrosol-*co*-1,3-propanediol carbonate).

Chemical structures of (A) tyrosol, (B) homovanillyl alcohol, (C) poly(tyrosol-*co*-1,3-propanediol carbonate).

The chemical structures of the polycarbonates synthesized from Ty and PD are



shown in Figure 7.1 and the physical properties are listed in Table 7.1. The polymer feed contained 0, 17 and 31 mol % of PD, resulting in the homopolymer from tyrosol (100/0) and copolymers with molar ratios of Ty/PD of 85/15 and 76/24 as determined by  $^1\text{H}$  NMR spectroscopy. The discrepancy of the reaction feed and polymer composition for PD content may be explained by formation of oligomers rich in PD. These oligomers were soluble in IPA and removed during the purification steps.

Table 7.1: Physical properties of polycarbonates from Ty and PD

Feed	Found	$M_w$	( $10^3$	PDI	$T_g$ ( $^{\circ}\text{C}$ )		Water
Ty/PD	Ty/PD	g/mol)					uptake
(mol %)	(mol %)				dry	wet	% (w/w)
100/0	100/0	138		1.7	60	50	< 1
83/17	85/15	111		1.7	50	41	< 1
69/31	76/24	96		1.7	44	39	< 1

All compositions reached high molecular weight averages around 100 kDa and  $T_{g,dry}$  was above ambient temperature rendering all compositions in the glassy state. Under physiological conditions, the copolymers were close to the rubbery transition with  $T_{g,wet} = 41^{\circ}\text{C}$  and  $T_{g,wet} = 39^{\circ}\text{C}$ , for 85/15 and 76/24, respectively. In comparison, PTMC has a much lower glass transition temperature with  $T_g = -20^{\circ}\text{C}$  (100).

The mechanical properties as characterized by mechanical tensile testing using strips from compression molded films under dry and wet conditions are shown in Table 7.2.

Table 7.2: Mechanical properties of polycarbonates from Ty and PD

Ty/PD (mol %)	Modulus [GPa]		Yield Stress [MPa]		Break Stress [MPa]		Elongation [%]	
	Dry <sup>a</sup>	Wet <sup>b</sup>	Dry <sup>a</sup>	Wet <sup>a</sup>	Dry <sup>a</sup>	Wet <sup>a</sup>	Dry <sup>a</sup>	Wet <sup>a</sup>
100/0	1.6 <sup>c</sup>	1.5 <sup>c</sup>	44 ± 5	31 ± 2	44 <sup>d</sup>	32 <sup>d</sup>	245 <sup>d</sup>	231 <sup>d</sup>
85/15	1.6 <sup>c</sup>	0.5 <sup>c</sup>	39 ± 7	4 ± 0.1	36 <sup>d</sup>	25 <sup>d</sup>	200 <sup>d</sup>	381 <sup>d</sup>
76/14	1.6 <sup>c</sup>	0.6 <sup>c</sup>	37 ± 4	3 ± 0.3	36 <sup>d</sup>	39 <sup>d</sup>	194 <sup>d</sup>	454 <sup>d</sup>

<sup>a</sup>Tested at RT; <sup>b</sup>Preconditioned 24 h & tested in PBS at 37 °C; <sup>c</sup>SD < 10%; <sup>d</sup>SD < 20%.

The copolymers 85/15 and 76/24 showed similar mechanical performance as compared to 100/0 under dry, ambients conditions. All composition were strong and stiff. However, under physiological conditions, 85/15 and 76/24 were softened with wet moduli  $E_T = 0.6 \pm 0.05$  GPa and  $E_T = 0.5 \pm 0.05$  GPa, respectively. This was due to the higher testing temperature very close to  $T_{g,wet}$ . In comparison, high  $M_w$  PTMC and copolymers of PD and  $\epsilon$ -caprolactone were reported with maximum tensile moduli of around  $E_T = 7$  MPa and poly( $\epsilon$ -caprolactone) with a modulus around  $E_T = 0.5$  GPa (8). Interestingly, copolymers of Ty and PD behaved comparable to a copolymer system of D,L-lactide (DLLA) and PD: At 80 mol % DLLA higher moduli of around  $E_T = 1.1$  GPa with  $T_{g,wet} = 33$  °C were reported. However, at 50 mol % DLLA (101) the modulus dropped to  $E_T = 13$  MPa with  $T_{g,wet} = 11$  °C (101). In addition, the copolymers from Ty and PD showed strain-hardening, which was evident in the increased break stress. As expected, flexibility increased with PD with the ultimate elongation values of around 380% and 450% for 85/15 and 76/24 as compared to 230% for 100/0.

#### 7.4.2 Subcutaneous Implantation *In Vivo*

Disc shaped specimen's from 100/0 as well as copolymers 85/15 and 76/24 were implanted subcutaneously. The explants retrieved after 3 weeks and 3 months are shown in Figure 7.2.

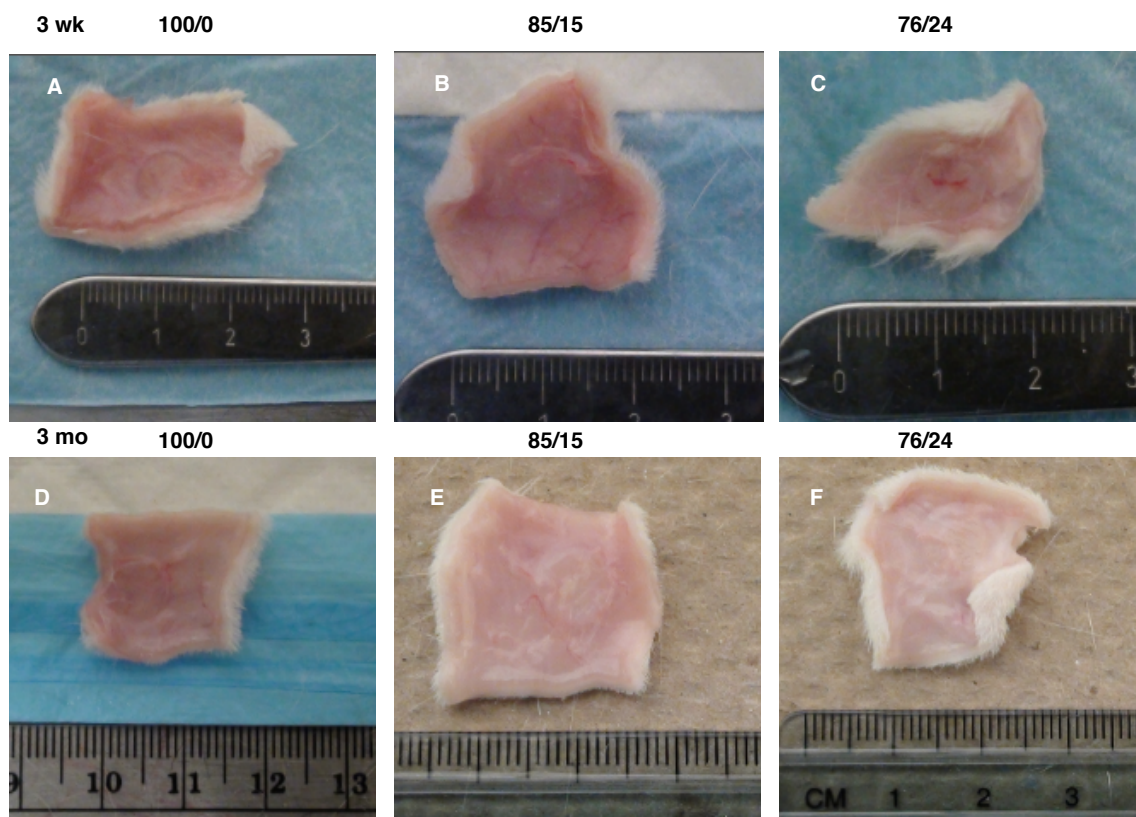


Figure 7.2: Explant overview images: (Top) 3 weeks, (bottom) 3 months, (A) and (D) 100/0, copolymers with molar ratios of Ty/PD of (B) and (E) 85/15, (C) and (F) 76/24. Disc shaped specimens retrieved embedded in tissue after subcutaneous implantation.

Visual inspection of the explants revealed that the specimens are contained within a fibrous capsule. After 3 weeks, a few red blood vessels around the location of the capsule and light redness were observed, that may indicate a mild initial inflammatory response to the materials. After 3 months, the area around the polymer discs appeared less vascularized and redness had disappeared. Most likely, the polymeric discs were all well tolerated by the host tissue.

For the purpose of polymer analysis, some of the discs were removed from the fibrous capsule. In the process, 100/0 was more easily removed from the surrounding tissue, than copolymers 85/15, right 76/24. This observation may have implications for the course of the *in vivo* erosion, as the progress of erosion is associated with the tissue adhesion.

### 7.4.3 Surface Morphology After *In Vivo* Erosion

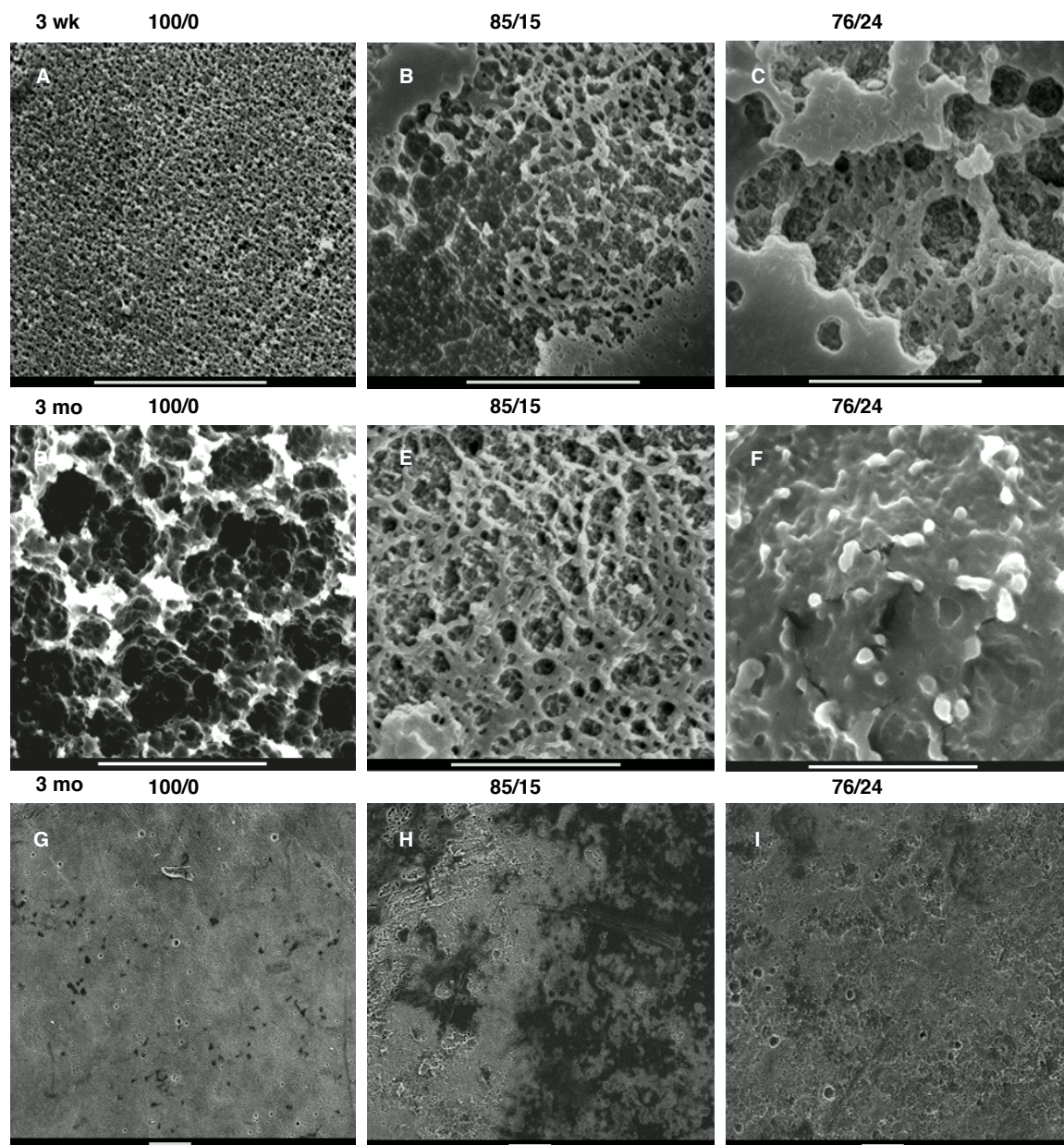


Figure 7.3: SEM morphology of explant surfaces of polycarbonates from Ty/PD of (left) 100/0, (middle) 85/15, (right) 76/24 molar ratios, (A), (B), (C) 3 weeks detail, scale bars = 10  $\mu\text{m}$ , (D), (E), (F) 3 months detail, scale bars = 10  $\mu\text{m}$ , (G), (H), (I) 3 months overview, scale bars = 100  $\mu\text{m}$ . Disc shaped specimens retrieved from separated from tissue after subcutaneous implantation and rinse with 70% (v/v) ethanol.

The SEM images in Figure 7.3 show the surface morphology of explanted polycarbonate specimens from poly(tyrosol carbonate) (100/0) and copolymers with molar ratios of Ty/PD of 85/15 and 76/24. After 3 weeks, all surfaces developed eroded structures of pits and cavities (Figure 7.3 A–C). Striking differences were visible comparing the stiffer 100/0 with the softer copolymers.

For 100/0, a regular pattern was apparent throughout the surface. This pattern featured small pits less than 1  $\mu\text{m}$  in size. The softer copolymers showed larger sized features craters. For 85/15 smaller pits had larger craters of approximately 1–2  $\mu\text{m}$  size and for 76/24 cavities of diameters around 2–5  $\mu\text{m}$  were visible.

Over time, the surface morphology underwent dramatic changes (Figure 7.3 D–F). After 3 months, explants from 100/0 resembled the morphology of specimen's eroded in lipase solution (119). A surface structure with a bimodal hierarchy had emerged: Relatively smaller sized pits with diameters around 10  $\mu\text{m}$  were embedded in larger craters of 50–100  $\mu\text{m}$  in size. This hierarchical structure may be explained with the progression of the biotic surface erosion: Initially, smaller sized pits were created. Later on, these pits unified into larger sized superstructures such as the craters, which in turn were textured with smaller pits.

In contrast, the softer copolymers 85/15, right 76/24 showed contracted erosion structures. The surfaces of these softer materials may have changed shape due mechanical stress within the implant side. The appearance of these irregular structures resembled the erosion surfaces of soft and rubbery PTMC (62).

Low magnification SEM images provide overview of specimen's surface area as shown in Figure 7.3 G–I. It is apparent that surface erosion *in vivo* did not proceed uniformly. Large areas featuring the erosion structures were intertwined with small patches of pristine polymer surfaces. Further, the periphery of the discs seemed to have more extensively eroded than the center for the disc. These findings can be related to previous studies on the biostability of polyurethanes (142). Anderson et al. showed that cells of the immune system mediated changes on polymer surfaces and supposed

that a microenvironment for the release of enzymes and reactive oxygen species was created. In turn, areas without these adherent immune cells remained non-eroded.

#### 7.4.4 Progress of Erosion *In Vitro* and *In Vivo*

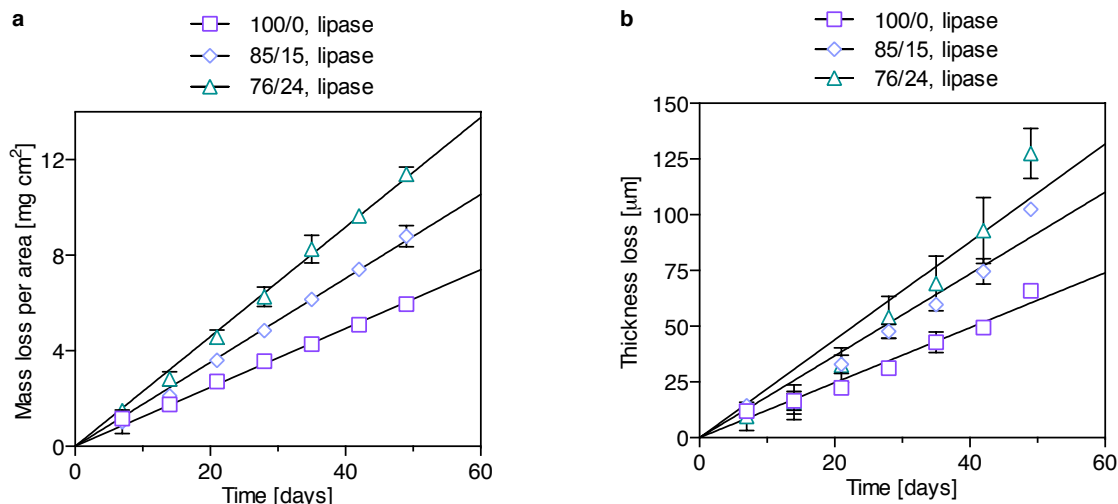


Figure 7.4: *In vitro* erosion: (A) Mass loss per area, (B) thickness loss of polycarbonates from Ty/PD with molar ratios of 100/0, 85/15 and 76/24 incubated in lipase solution at 37 °C.

In Figure 7.4 the *in vitro* erosion behavior of Ty/PD with molar ratios of 100/0, 85/15 and 76/24 is shown as the mass loss and thickness loss in lipase solution (Controls without lipase, supplementary information, Figure S32). The erosion rates were calculated respective to the slope from linear regression. The quantitative and qualitative data summarizing the progress of erosion *in vitro* and *in vivo* is shown in Table 7.3.

The erosion rates *in vitro* were tunable by the composition increasing with the content of PD and thus the softness of the polymer. The copolycarbonate of Ty/PD with a molar ratio of 76/24 showed a rate of thickness loss of  $2.2 \pm 0.1 \mu\text{m d}^{-1}$ , while 100/0 eroded at a rate of  $1.2 \pm 0.1 \mu\text{m d}^{-1}$ . This result for an increasing rate along with the PD content described a trend. Noteworthy, the rate for the thickness loss of high



molecular weight PTMC of  $6.7 \mu\text{m d}^{-1}$  also aligns with these results (141). *In vivo* the erosion appeared to occur at a slower pace. The erosion rates were not quantified using the two timepoints *in vivo*. Instead, the relative mass loss for the specimens was within 2% (w/w) after three months. This slow relative mass loss aligned with the progress of erosion in copolymers of PD and  $\epsilon$ -caprolactone, which was reported with a mass loss of 4% (w/w) after one year (102).

In part, the differences between *in vitro* and *in vivo* erosion may be explained by the dependence on the location of the implant site. Classically, a foreign body response is provoked upon subcutaneous implantation. Macrophages mediate the erosion phenomena by enzymes localized to the area of cell attachment to the substrate (2). In turn, *in vitro* bioerosion occurs by lipase that is adsorbed to the surface from the solution phase. In addition to the limitations posed by the microenvironment of the macrophages, the erosion activity of the macrophages itself may be regulated by the substrate. For example, a study suggested the dependence of macrophage activation on the substrate stiffness (53). It is suggested, a polymer that undergoes enzymatic erosion *in vitro*, is subject to a slower *in vivo* erosion in dependence to the subcutaneous tissue response.

Table 7.3: Comparison of *in vivo* and *in vitro* erosion

Ty/ PD (mol %)	Mass loss, <i>in vitro</i> <sup>a</sup> ( $\text{mg cm}^{-2} \text{d}^{-1}$ )	Thickness loss, <i>in vitro</i> <sup>a</sup> ( $\mu\text{m d}^{-1}$ )	Mass loss, <i>in vivo</i> (relative)	Morphology, <i>in vivo</i>
100/0	$1.5 \pm 0.01$	$1.2 \pm 0.1$	2 %	pits, cavities
85/15	$2.3 \pm 0.01$	$1.8 \pm 0.1$	2 %	deformed pits
76/24	$2.9 \pm 0.01$	$2.2 \pm 0.1$	2 %	constricted

<sup>a</sup>Values determined by linear regression on erosion curves.



### 7.4.5 Histological Overview

A light microscopic overview of histological slides prepared from samples at the implant site show the polymer discs embedded in the surrounding tissue (Figure 7.5).

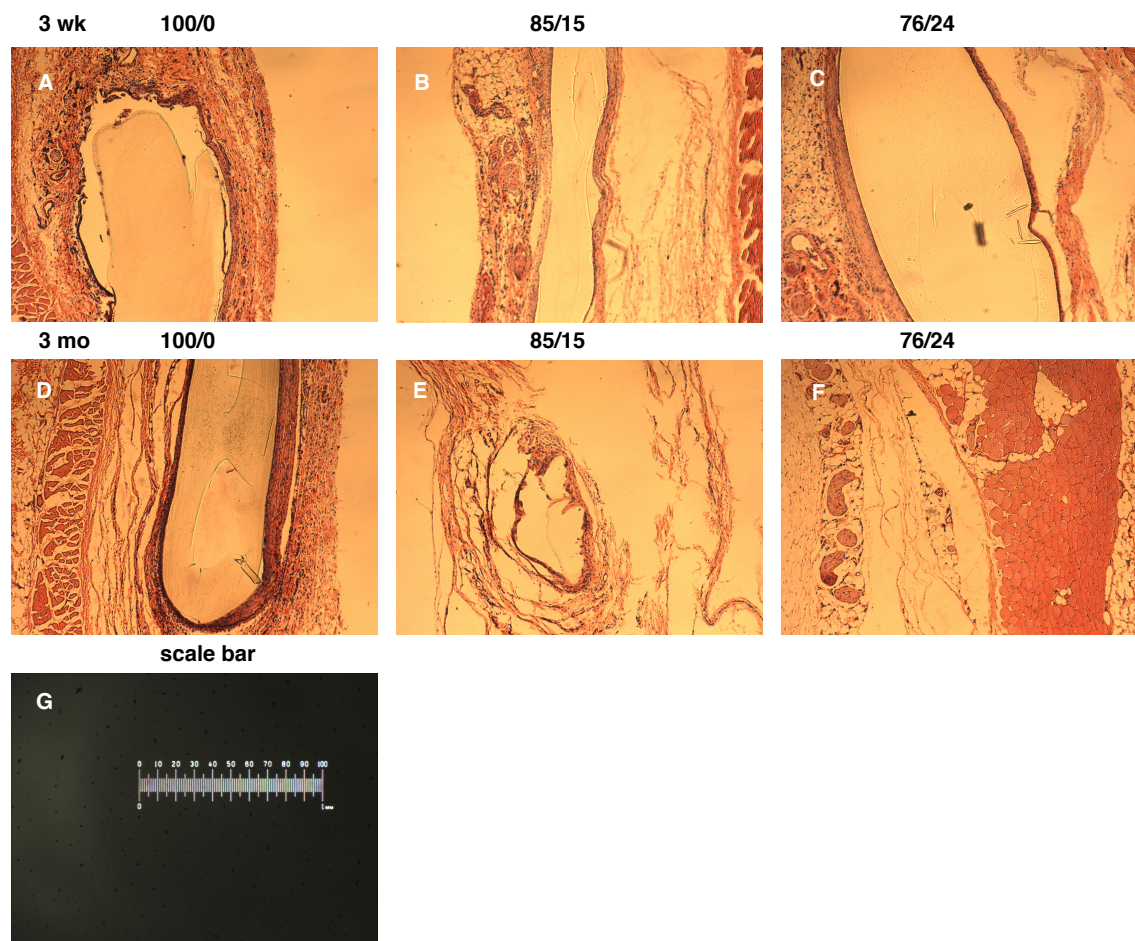


Figure 7.5: Microscopic images from histological slides of polycarbonates from Ty/PD with molar ratios of (left) 100/0, (middle) 85/15, (right) 76/24, (A), (B), (C) 3 weeks, (D), (E), (F) 3 months, (G) scale bar.

In this histological overview, all compositions of polycarbonates from Ty/PD with molar ratios of 100/0, 85/15 and 76/24 were encompassed by a fibrous capsule confirming the visual inspection of the explants. Future studies will evaluate the severeness of the foreign body response in terms of the thickness of the fibrous capsule as well as the cell count for the macrophages and foreign body giant cells. Finally, the inflammatory response will be related to the progress of *in vivo* erosion.

## 7.5 Conclusion

Only few degradable polymer compositions are known that undergo surface erosion mediated by biological contributions. In particular, soft and rubbery, aliphatic polycarbonates were reported to be erodible by enzymes *in vitro* and *in vivo*. Our previous *in vitro* studies added aromatic-aliphatic polycarbonates from tyrosol and homovanillyl alcohol to the design space for surface eroding materials. These polymers were relatively stiff and in the glassy state under physiological conditions. The erosion rates increased along with a decrease in  $T_{g,wet}$ . Here, we expanded on this trend: Increased erosion rates *in vitro* correlated with increasing softness and lower  $T_{g,wet}$  in copolymers from tyrosol and 1,3-propanediol.

Upon subcutaneous implantation *in vivo*, the erosion of relatively stiff and glassy polycarbonates appeared slower, which may be due to the mediation or erosion by adherent macrophages. Future studies will evaluate the foreign body response to aromatic-aliphatic polycarbonates to shed light onto the differences between *in vitro* and *in vivo* erosion. The surface morphology of *in vivo* explants featured similar erosion structure observed *in vitro*. Thus the surface erosion of strong and stiff materials occurred in principle.

Respective to potential biomedical applications it may be worthwhile to adjust the design parameters. For example, devices with high surface to volume ratios such as microspheres for drug delivery or highly-porous scaffolds for tissue engineering may show relevant erosion rates. In addition, the location of the implant site may be crucial: interstitial fluids or the gastrointestinal tract carry enzymatic activity and could be more conducive to surface erosion *in vivo*, than a subcutaneous location.

## Bibliography

- [1] Ann-Christine Albertsson and Indra K Varma. Aliphatic polyesters: synthesis, properties and applications. In *Degradable aliphatic polyesters*, pages 1–40. Springer, 2002.
- [2] James M Anderson, Analiz Rodriguez, and David T Chang. Foreign body reaction to biomaterials. In *Seminars in immunology*, volume 20, pages 86–100. Elsevier, 2008.
- [3] AR Anscombe, N Hira, and B Hunt. The use of a new absorbable suture material (polyglycolic acid) in general surgery. *British Journal of Surgery*, 57(12):917–920, 1970.
- [4] Kaoru Aou, Shuhui Kang, and Shaw Ling Hsu. Morphological study on thermal shrinkage and dimensional stability associated with oriented poly(lactic acid). *Macromolecules*, 38(18):7730–7735, 2005.
- [5] Harry Babad and Andrew G Zeiler. Chemistry of phosgene. *Chemical Reviews*, 73(1):75–91, 1973.
- [6] Erhan Bat, Martin C Harmsen, Josée A Plantinga, Marja JA van Luyn, Jan Feijen, and Dirk W Grijpma. Flexible scaffolds based on poly(trimethylene carbonate) networks for cardiac tissue engineering. *Journal of Controlled Release*, 148(1):e74–e76, 2010.
- [7] Erhan Bat, Josee A Plantinga, Martin C Harmsen, Marja JA Van Luyn, Jan Feijen, and Dirk W Grijpma. *in vivo* behavior of trimethylene carbonate and

- $\epsilon$ -caprolactone-based (co)polymer networks: Degradation and tissue response. *Journal of Biomedical Materials Research Part A*, 95(3):940–949, 2010.
- [8] Erhan Bat, Theo G van Kooten, Martin C Harmsen, Josée A Plantinga, Marja JA van Luyn, Jan Feijen, and Dirk W Grijpma. Physical properties and erosion behavior of poly(trimethylene carbonate-co- $\epsilon$ -caprolactone) networks. *Macromolecular Bioscience*, 13(5):573–583, 2013.
- [9] Erhan Bat, Zheng Zhang, Jan Feijen, Dirk W Grijpma, and André A Poot. Biodegradable elastomers for biomedical applications and regenerative medicine. *Regenerative Medicine*, 9(3):385–398, 2014.
- [10] Gary K Beauchamp, Russell SJ Keast, Diane Morel, Jianming Lin, Jana Pika, Qiang Han, Chi-Ho Lee, Amos B Smith, and Paul AS Breslin. Phytochemistry: ibuprofen-like activity in extra-virgin olive oil. *Nature*, 437(7055):45–46, 2005.
- [11] Eric Beckman and Roger S Porter. Crystallization of bisphenol a polycarbonate induced by supercritical carbon dioxide. *Journal of Polymer Science Part B: Polymer Physics*, 25(7):1511–1517, 1987.
- [12] F Bedoui, Leonardus Kresna Widjaja, A Luk, D Bolikal, NS Murthy, and J Kohn. Anomalous increase in modulus upon hydration in random copolymers with hydrophobic segments and hydrophilic blocks. *Soft Matter*, 8(7):2230–2236, 2012.
- [13] Roberta Bernini, Enrico Mincione, Maurizio Barontini, and Fernanda Crisante. Convenient synthesis of hydroxytyrosol and its lipophilic derivatives from tyrosol or homovanillyl alcohol. *Journal of Agricultural and Food Chemistry*, 56(19):8897–8904, 2008.
- [14] GC Berry and TG Fox. *The viscosity of polymers and their concentrated solutions*. Springer, 1968.

- [15] Durgadas Bolikal, George L Brode, Sylvie I Ertel, Shuiyun Guan, John E Kemnitzer, and Joachim B Kohn. Biodegradable, anionic polymers derived from the amino acid l-tyrosine, September 19 2000. US Patent 6,120,491.
- [16] Henry Brem, Rafael J Tamargo, Alessandro Olivi, Michael Pinn, Jon D Weingart, Moody Wharam, and Jonathan I Epstein. Biodegradable polymers for controlled delivery of chemotherapy with and without radiation therapy in the monkey brain. *Journal of Neurosurgery*, 80(2):283–290, 1994.
- [17] Pierre Brignou, Marcelo Priebe Gil, Osvaldo Casagrande, Jean-François Carpentier, and Sophie M Guillaume. Polycarbonates derived from green acids: ring-opening polymerization of seven-membered cyclic carbonates. *Macromolecules*, 43(19):8007–8017, 2010.
- [18] Daniel J Brunelle and Thomas G Shannon. Preparation and polymerization of bisphenol a cyclic oligomeric carbonates. *Macromolecules*, 24(11):3035–3044, 1991.
- [19] S Budavar, MJ O’Neil, A Smith, and PE Heckelman. The merck index 11th edition. merck & co. *Inc., Rahway, New Jersey*, 1989.
- [20] Jason A Burdick and Kristi S Anseth. Photoencapsulation of osteoblasts in injectable rgd-modified peg hydrogels for bone tissue engineering. *Biomaterials*, 23(22):4315–4323, 2002.
- [21] Friederike von Burkersroda, Luise Schedl, and Achim Göpferich. Why degradable polymers undergo surface erosion or bulk erosion. *Biomaterials*, 23(21):4221–4231, 2002.
- [22] Christopher M Byrne, Scott D Allen, Emil B Lobkovsky, and Geoffrey W Coates. Alternating copolymerization of limonene oxide and carbon dioxide. *Journal of the American Chemical Society*, 126(37):11404–11405, 2004.

- [23] Wallace H Carothers and FJ Van Natta. Studies on polymerization and ring formation. iii. glycol esters of carbonic acid. *Journal of the American Chemical Society*, 52(1):314–326, 1930.
- [24] Rafi Chapanian, M Yat Tse, Stephen C Pang, and Brian G Amsden. The role of oxidation and enzymatic hydrolysis on the *in vivo* degradation of trimethylene carbonate based photocrosslinkable elastomers. *Biomaterials*, 30(3):295–306, 2009.
- [25] Saber Chatti, Gert Schwarz, and Hans R Kricheldorf. Cyclic and noncyclic polycarbonates of isosorbide. *Macromolecules*, 39(26):9064–9070, 2006.
- [26] Liang Chen and Byoung In Suh. Bisphenol a in dental materials: A review. *JSM*, 1(1004), 2013.
- [27] Elizabeth M Christenson, James M Anderson, and Anne Hiltner. Oxidative mechanisms of poly(carbonate urethane) and poly(ether urethane) biodegradation: *in vivo* and *in vitro* correlations. *Journal of Biomedical Materials Research Part A*, 70(2):245–255, 2004.
- [28] Geoffrey W Coates and David R Moore. Discrete metal-based catalysts for the copolymerization of co<sub>2</sub> and epoxides: Discovery, reactivity, optimization, and mechanism. *Angewandte Chemie International Edition*, 43(48):6618–6639, 2004.
- [29] LA Cornacchione, B Qi, J Bianco, Z Zhou, and BG Amsden. Photo-cross-linked poly(ethylene carbonate) elastomers: Synthesis, *in vivo* degradation, and determination of *in vivo* degradation mechanism. *Biomacromolecules*, 13(10):3099–3107, 2012.
- [30] C Counciler. Kohlensaures methyl. *Berichte der deutschen chemischen Gesellschaft*, 13(2):1697–1699, 1880.

- [31] M Dadsetan, EM Christenson, F Unger, M Ausborn, T Kissel, A Hiltner, and JM Anderson. In vivo biocompatibility and biodegradation of poly(ethylene carbonate). *Journal of Controlled Release*, 93(3):259–270, 2003.
- [32] Bronwin L Dargaville, Cdryck Vaquette, Hui Peng, Firas Rasoul, Yu Qian Chau, Justin J Cooper-White, Julie H Campbell, and Andrew K Whittaker. Cross-linked poly (trimethylene carbonate-co-l-lactide) as a biodegradable, elastomeric scaffold for vascular engineering applications. *Biomacromolecules*, 12(11):3856–3869, 2011.
- [33] Lewis W Dittert and Takeru Higuchi. Rates of hydrolysis of carbamate and carbonate esters in alkaline solution. *Journal of Pharmaceutical Sciences*, 52(9):852–857, 1963.
- [34] EC Dodds and Wilfrid Lawson. Synthetic estrogenic agents without the phenanthrene nucleus. *Nature*, 137(3476):996, 1936.
- [35] G Malcolm Dyson. Phosgene. *Chemical Reviews*, 4(1):109–165, 1927.
- [36] Heiner Eckert and Barbara Forster. Triphosgene, a crystalline phosgene substitute. *Angewandte Chemie International Edition in English*, 26(9):894–895, 1987.
- [37] Christopher J Ellison and John M Torkelson. The distribution of glass-transition temperatures in nanoscopically confined glass formers. *Nature Materials*, 2(10):695–700, 2003.
- [38] Israel Engelberg and Joachim Kohn. Physico-mechanical properties of degradable polymers used in medical applications: a comparative study. *Biomaterials*, 12(3):292–304, 1991.
- [39] Sylvie I Ertel and Joachim Kohn. Evaluation of a series of tyrosine-derived

- polycarbonates as degradable biomaterials. *Journal of Biomedical Materials Research*, 28(8):919–930, 1994.
- [40] T Fabre, M Schappacher, R Bareille, B Dupuy, A Soum, J Bertrand-Barat, and C Baquey. Study of a (trimethylenecarbonate-co- $\epsilon$ -caprolactone) polymerpart 2: in vitro cytocompatibility analysis and *in vivo* cell response of a new nerve guide. *Biomaterials*, 22(22):2951–2958, 2001.
- [41] Lisa E Freed, Gordana Vunjak-Novakovic, Robert J Biron, Dana B Eagles, Daniel C Lesnoy, Sandra K Barlow, and Robert Langer. Biodegradable polymer scaffolds for tissue engineering. *Nature Biotechnology*, 12(7):689–693, 1994.
- [42] Achim Göpferich. Mechanisms of polymer degradation and erosion. *Biomaterials*, 17(2):103–114, 1996.
- [43] Eliana Fortes Gris, Fulvio Mattivi, Eduardo Antonio Ferreira, Urska Vrhovsek, Danilo Wilhelm Filho, Rozangela Curi Pedrosa, and Marilde T Bordignon-Luiz. Stilbenes and tyrosol as target compounds in the assessment of antioxidant and hypolipidemic activity of vitis vinifera red wines from southern brazil. *Journal of Agricultural and Food Chemistry*, 59(14):7954–7961, 2011.
- [44] Lisoto Grizzi, H Garreau, S Li, and M Vert. Hydrolytic degradation of devices based on poly(dl-lactic acid) size-dependence. *Biomaterials*, 16(4):305–311, 1995.
- [45] Tiffany P Gustafson, Alexander T Lonneckker, Gyu Seong Heo, Shiyi Zhang, Andrew P Dove, and Karen L Wooley. Poly(d-glucose carbonate) block copolymers: A platform for natural product-based nanomaterials with solvothermotic characteristics. *Biomacromolecules*, 14(9):3346–3353, 2013.
- [46] J Heller. Controlled drug release from poly(ortho esters), a surface eroding polymer. *Journal of Controlled Release*, 2:167–177, 1985.



- [47] Peter M Henson. The immunologic release of constituents from neutrophil leukocytes i. the role of antibody and complement on nonphagocytosable surfaces or phagocytosable particles. *The Journal of Immunology*, 107(6):1535–1546, 1971.
- [48] Peter M Henson. The immunologic release of constituents from neutrophil leukocytes ii. mechanisms of release during phagocytosis, and adherence to nonphagocytosable surfaces. *The Journal of Immunology*, 107(6):1547–1557, 1971.
- [49] Kimberly A Hooper, Natalie D Macon, and Joachim Kohn. Comparative histological evaluation of new tyrosine-derived polymers and poly(l-lactic acid) as a function of polymer degradation. *Journal of Biomedical Materials Research*, 41(3):443–454, 1998.
- [50] Shohei Inoue. Copolymerization of carbon dioxide and epoxide: functionality of the copolymer. *Journal of Macromolecular Science–Chemistry*, 13(5):651–664, 1979.
- [51] Shohei Inoue, Hideomi Koinuma, and Teiji Tsuruta. Copolymerization of carbon dioxide and epoxide. *Journal of Polymer Science Part B: Polymer Letters*, 7(4):287–292, 1969.
- [52] Shohei Inoue, Hideomi Koinuma, and Teiji Tsuruta. Copolymerization of carbon dioxide and epoxide with organometallic compounds. *Die Makromolekulare Chemie*, 130(1):210–220, 1969.
- [53] EF Irwin, K Saha, M Rosenbluth, LJ Gamble, DG Castner, and KE Healy. Modulus-dependent macrophage adhesion and behavior. *Journal of Biomaterials Science, Polymer Edition*, 19(10):1363–1382, 2008.
- [54] Kenneth James, Howard Levene, J Russell Parsons, and Joachim Kohn. Small changes in polymer chemistry have a large effect on the bone–implant interface::

- evaluation of a series of degradable tyrosine-derived polycarbonates in bone defects. *Biomaterials*, 20(23):2203–2212, 1999.
- [55] Tina Jerman Klen and Branka Mozeti-Vodopivec. Ultrasonic extraction of phenols from olive mill wastewater: comparison with conventional methods. *Journal of Agricultural and Food Chemistry*, 59(24):12725–12731, 2011.
- [56] Atsushi Kameyama, Yasuharu Murakami, and Tadatomi Nishikubo. Novel sequence-ordered polymers by transformation of polymer backbone: quantitative and regioselective insertion of thiiranes into poly(s-aryl thioester). *Macromolecules*, 32(5):1407–1412, 1999.
- [57] Tatsuo Kaneko, Tran Hang Thi, Dong Jian Shi, and Mitsuru Akashi. Environmentally degradable, high-performance thermoplastics from phenolic phytonomers. *Nature Materials*, 5(12):966–970, 2006.
- [58] JL Keddie, RAL Jones, and RA Cory. Size-dependent depression of the glass transition temperature in polymer films. *EPL (Europhysics Letters)*, 27(1):59, 1994.
- [59] Brian E Kilfoyle, Larisa Sheihet, Zheng Zhang, Marissa Laohoo, Joachim Kohn, and Bozena B Michniak-Kohn. Development of paclitaxel-tyrospheres for topical skin treatment. *Journal of Controlled Release*, 163(1):18–24, 2012.
- [60] Jeung Gon Kim, Christina D Cowman, Anne M LaPointe, Ulrich Wiesner, and Geoffrey W Coates. Tailored living block copolymerization: multiblock poly(cyclohexene carbonate)s with sequence control. *Macromolecules*, 44(5):1110–1113, 2011.
- [61] Won Bae Kim and Jae Sung Lee. A new process for the synthesis of diphenyl carbonate from dimethyl carbonate and phenol over heterogeneous catalysts. *Catalysis Letters*, 59(1):83–88, 1999.

- [62] Otto S Kluin, Henny C van der Mei, Henk J Busscher, and Daniëlle Neut. A surface-eroding antibiotic delivery system based on poly(trimethylene carbonate). *Biomaterials*, 30(27):4738–4742, 2009.
- [63] Joachim Kohn. New approaches to biomaterials design. *Nature Materials*, 3(11):745–747, 2004.
- [64] Philip G Kosky, James M Silva, and Elizabeth A Guggenheim. The aqueous phase in the interfacial synthesis of polycarbonates. part 1. ionic equilibria and experimental solubilities in the bpa-sodium hydroxide-water system. *Industrial & Engineering Chemistry Research*, 30(3):462–467, 1991.
- [65] John W Kramer, Daniel S Treitler, Erin W Dunn, Pascal M Castro, Thierry Roisnel, Christophe M Thomas, and Geoffrey W Coates. Polymerization of enantiopure monomers using syndiospecific catalysts: a new approach to sequence control in polymer synthesis. *Journal of the American Chemical Society*, 131(44):16042–16044, 2009.
- [66] Hans R Kricheldorf, Sigrid Böhme, and Gert Schwarz. Polycondensations of bisphenol-a with diphosgene or triphosgene in water-free organic solvents. *Macromolecular Chemistry and Physics*, 206(4):432–438, 2005.
- [67] Hans R Kricheldorf and Dierk Lübbers. Polymers of carbonic acid, 1. synthesis of thermotropic aromatic polycarbonates by means of bis(trichloromethyl) carbonate. *Die Makromolekulare Chemie, Rapid Communications*, 10(8):383–386, 1989.
- [68] Hans R Kricheldorf and Andrea Stricker. Polymers of carbonic acid, 28. snoct2-initiated polymerizations of trimethylene carbonate (tmc, 1,3-dioxanone-2). *Macromolecular Chemistry and Physics*, 201(17):2557–2565, 2000.
- [69] Sreevidhya Tarakkad Krishnaji, Graham Bratzel, Michelle E Kinahan, Jonathan A Kluge, Cristian Staii, Joyce Y Wong, Markus J Buehler, and

- David L Kaplan. Sequence–structure–property relationships of recombinant spider silk proteins: Integration of biopolymer design, processing, and modeling. *Advanced Functional Materials*, 23(2):241–253, 2013.
- [70] Rosalind S Labow, Erin Meek, Loren A Matheson, and J Paul Santerre. Human macrophage-mediated biodegradation of polyurethanes: assessment of candidate enzyme activities. *Biomaterials*, 23(19):3969–3975, 2002.
- [71] Robert Lanza, Robert Langer, and Joseph P Vacanti. *Principles of tissue engineering*. Academic press, 2011.
- [72] Dan Lewitus, Karen L Smith, William Shain, and Joachim Kohn. Ultrafast resorbing polymers for use as carriers for cortical neural probes. *Acta Biomaterialia*, 7(6):2483–2491, 2011.
- [73] Dan Y Lewitus, Karen L Smith, William Shain, Durgadas Bolikal, and Joachim Kohn. The fate of ultrafast degrading polymeric implants in the brain. *Biomaterials*, 32(24):5543–5550, 2011.
- [74] Chun Li and Joachim Kohn. Synthesis of poly(iminocarbonates): Degradable polymers with potential applications as disposable plastics and as biomaterials. *Macromolecules*, 22(5):2029–2036, 1989.
- [75] Jian Li, Sam N Rothstein, Steven R Little, Harry M Edenborn, and Tara Y Meyer. The effect of monomer order on the hydrolysis of biodegradable poly(lactic-co-glycolic acid) repeating sequence copolymers. *Journal of the American Chemical Society*, 134(39):16352–16359, 2012.
- [76] Jin-Hua Li, Bao-Xue Zhou, and Wei-Min Cai. The solubility behavior of bisphenol a in the presence of surfactants. *Journal of Chemical & Engineering Data*, 52(6):2511–2513, 2007.

- [77] SM Li and Michel Vert. Morphological changes resulting from the hydrolytic degradation of stereocopolymers derived from l-and dl-lactides. *Macromolecules*, 27(11):3107–3110, 1994.
- [78] Suming Li and Michel Vert. Crystalline oligomeric stereocomplex as an intermediate compound in racemic poly(dl-lactic acid) degradation. *Polymer International*, 33(1):37–41, 1994.
- [79] Natalia Loscos, Purificacion Hernandez-Orte, Juan Cacho, and Vicente Ferreira. Release and formation of varietal aroma compounds during alcoholic fermentation from nonfloral grape odorless flavor precursors fractions. *Journal of Agricultural and Food Chemistry*, 55(16):6674–6684, 2007.
- [80] Jean-François Lutz. Polymer chemistry: a controlled sequence of events. *Nature Chemistry*, 2(2):84–85, 2010.
- [81] Jean-François Lutz. Sequence-controlled polymerizations: the next holy grail in polymer science? *Polymer Chemistry*, 1(1):55–62, 2010.
- [82] Maria Hanshella R Magno, Jinku Kim, Abiraman Srinivasan, Sean McBride, Durgadas Bolikal, Aniq Darr, Jeffrey O Hollinger, and Joachim Kohn. Synthesis, degradation and biocompatibility of tyrosine-derived polycarbonate scaffolds. *Journal of Materials Chemistry*, 20(40):8885–8893, 2010.
- [83] James E Mark. *Physical properties of polymers handbook*. Springer, 2007.
- [84] Raquel Mateos, Mariana Trujillo, Gema Pereira-Caro, Andres Madrona, Arturo Cert, and Jose Luis Espartero. New lipophilic tyrosyl esters. comparative antioxidant evaluation with hydroxytyrosyl esters. *Journal of Agricultural and Food Chemistry*, 56(22):10960–10966, 2008.

- [85] Masaru Matsuda, Kotaro Satoh, and Masami Kamigaito. Periodically functionalized and grafted copolymers via 1: 2-sequence-regulated radical copolymerization of naturally occurring functional limonene and maleimide derivatives. *Macromolecules*, 46(14):5473–5482, 2013.
- [86] Joseph Megerman, Esphiran Reddy, Gilbert J L’Italien, David F Warnock, and William M Abbott. A laboratory model to quantitate the resistance of collagen vascular grafts to biodegradation. *Journal of Biomedical Materials Research*, 25(3):295–313, 1991.
- [87] JP Mercier, G Groeninckx, and M Lesne. Some aspects of vapor-induced crystallization of polycarbonate of bisphenol a. In *Journal of Polymer Science Part C: Polymer Symposia*, volume 16, pages 2059–2067. Wiley Online Library, 1967.
- [88] Robert B Merrifield. Solid phase peptide synthesis. i. the synthesis of a tetrapeptide. *Journal of the American Chemical Society*, 85(14):2149–2154, 1963.
- [89] Koichiro Mikami, Alexander T Lonnecker, Tiffany P Gustafson, Nathanael F Zinnel, Pei-Jing Pai, David H Russell, and Karen L Wooley. Polycarbonates derived from glucose via an organocatalytic approach. *Journal of the American Chemical Society*, 135(18):6826–6829, 2013.
- [90] N Sanjeeva Murthy. *Scattering techniques fro structural analysis of biomaterials*. Woodhead Publishing, 2012.
- [91] NS Murthy and H Minor. General procedure for evaluating amorphous scattering and crystallinity from x-ray diffraction scans of semicrystalline polymers. *Polymer*, 31(6):996–1002, 1990.
- [92] Moshe Nahmany and Artem Melman. Chemoselectivity in reactions of esterification. *Organic & Biomolecular Chemistry*, 2(11):1563–1572, 2004.

- [93] Lakshmi S Nair and Cato T Laurencin. Biodegradable polymers as biomaterials. *Progress in Polymer Science*, 32(8):762–798, 2007.
- [94] Fredrik Nederberg, Ying Zhang, Jeremy PK Tan, Kaijin Xu, Huaying Wang, Chuan Yang, Shujun Gao, Xin Dong Guo, Kazuki Fukushima, Lanjuan Li, et al. Biodegradable nanostructures with selective lysis of microbial membranes. *Nature Chemistry*, 3(5):409–414, 2011.
- [95] Amandine Noel, Yannick P Borguet, Jeffery E Raymond, and Karen L Wooley. Poly(carbonate–amide)s derived from bio-based resources: Poly(ferulic acid-co-tyrosine). *Macromolecules*, 2014.
- [96] Jesper Ostergaard and Claus Larsen. Bioreversible derivatives of phenol. 2. reactivity of carbonate esters with fatty acid-like structures towards hydrolysis in aqueous solutions. *Molecules*, 12(10):2396–2412, 2007.
- [97] RM Ottenbrite, AC Albertsson, and G Scott. Discussion on degradation terminology. *Biodegradable Polymers and Plastics. The Royal Society of Chemistry. Cambridge, RU*, pages 73–92, 1992.
- [98] Makoto Ouchi, Nezha Badi, Jean-François Lutz, and Mitsuo Sawamoto. Single-chain technology using discrete synthetic macromolecules. *Nature Chemistry*, 3(12):917–924, 2011.
- [99] Lucia Pasquato, Giorgio Modena, Livius Cotarca, Pietro Delogu, and Silvia Mantovani. Conversion of bis(trichloromethyl) carbonate to phosgene and reactivity of triphosgene, diphosgene, and phosgene with methanol. *The Journal of Organic Chemistry*, 65(24):8224–8228, 2000.
- [100] Ana Paula Pêgo, Dirk W Grijpma, and Jan Feijen. Enhanced mechanical properties of 1,3-trimethylene carbonate polymers and networks. *Polymer*, 44(21):6495–6504, 2003.

- [101] Ana Paula Pêgo, André A Poot, Dirk W Grijpma, and Jan Feijen. Physical properties of high molecular weight 1,3-trimethylene carbonate and d,l-lactide copolymers. *Journal of Materials Science: Materials in Medicine*, 14(9):767–773, 2003.
- [102] AP Pego, MJA Van Luyn, LA Brouwer, PB Van Wachem, AA Poot, DW Grijpma, and J Feijen. *in vivo* behavior of poly(1,3-trimethylene carbonate) and copolymers of 1,3-trimethylene carbonate with d,l-lactide or  $\epsilon$ -caprolactone: Degradation and tissue response. *Journal of Biomedical Materials Research Part A*, 67(3):1044–1054, 2003.
- [103] Sebastian Pfeifer and Jean-François Lutz. A facile procedure for controlling monomer sequence distribution in radical chain polymerizations. *Journal of the American Chemical Society*, 129(31):9542–9543, 2007.
- [104] Thomas St Pierre and Emo Chiellini. Review: Biodegradability of synthetic polymers used for medical and pharmaceutical applications: Part 1—principles of hydrolysis mechanisms. *Journal of Bioactive and Compatible Polymers*, 1(4):467–497, 1986.
- [105] Giovanni Piersanti, Michele Retini, Jose Espartero, Andres Madrona, Giovanni Zappia, et al. An efficient, economical synthesis of hydroxytyrosol and its protected forms via baeyer-villiger oxidation. *Tetrahedron Letters*, 52(38):4938–4940, 2011.
- [106] Colin G Pitt, R Wayne Hendren, Anton Schindler, and Stephen C Woodward. The enzymatic surface erosion of aliphatic polyesters. *Journal of Controlled Release*, 1(1):3–14, 1984.
- [107] Satish Pulapura and Joachim Kohn. Tyrosine-derived polycarbonates: Backbone-modified pseudo-poly(amino acids) designed for biomedical applications. *Biopolymers*, 32(4):411–417, 1992.



- [108] António J Queimada, Fátima L Mota, Simao P Pinho, and Eugénia A Macedo. Solubilities of biologically active phenolic compounds: measurements and modeling. *The Journal of Physical Chemistry B*, 113(11):3469–3476, 2009.
- [109] William C Ray and Mark W Grinstaff. Polycarbonate and poly(carbonate-ester)s synthesized from biocompatible building blocks of glycerol and lactic acid. *Macromolecules*, 36(10):3557–3562, 2003.
- [110] Michael S Reeve, Stephen P McCarthy, Milton J Downey, and Richard A Gross. Polylactide stereochemistry: effect on enzymic degradability. *Macromolecules*, 27(3):825–831, 1994.
- [111] Langer Robert and Joseph P Vacanti. Tissue engineering. *Science*, 260(2):920–941, 1993.
- [112] Howard B Rosen, J Chang, GE Wnek, RJ Linhardt, and R Langer. Bioerodible polyanhydrides for controlled drug delivery. *Biomaterials*, 4(2):131–133, 1983.
- [113] GZ Sauerbrey. Use of quartz vibration for weighing thin films on a microbalance. *J. Physik*, 155:206–212, 1959.
- [114] M Schappacher, T Fabre, AF Mingotaud, and A Soum. Study of a (trimethylenecarbonate-co- $\epsilon$ -caprolactone) polymer—part 1: preparation of a new nerve guide through controlled random copolymerization using rare earth catalysts. *Biomaterials*, 22(21):2849–2855, 2001.
- [115] H Schnell. Polycarbonate, eine gruppe neuartiger thermoplastischer kunststoffe. herstellung und eigenschaften aromatischer polyester der kohlensäure. *Angewandte Chemie*, 68(20):633–640, 1956.
- [116] Michael Sefkow and Helvi Kaatz. Selective protection of either the phenol or the hydroxy group in hydroxyalkyl phenols. *Tetrahedron Letters*, 40(36):6561–6562, 1999.

- [117] Larisa Sheihet, Robert A Dubin, David Devore, and Joachim Kohn. Hydrophobic drug delivery by self-assembling triblock copolymer-derived nanospheres. *Biomacromolecules*, 6(5):2726–2731, 2005.
- [118] Larisa Sheihet, Karolina Piotrowska, Robert A Dubin, Joachim Kohn, and David Devore. Effect of tyrosine-derived triblock copolymer compositions on nanosphere self-assembly and drug delivery. *Biomacromolecules*, 8(3):998–1003, 2007.
- [119] Sven D Sommerfeld, Zheng Zhang, Marius C Costache, Sebastián L Vega, and Joachim Kohn. Enzymatic surface erosion of high tensile strength polycarbonates based on natural phenols. *Biomacromolecules*, 15(3):830–836, 2014.
- [120] Y Song, MMJ Kamphuis, Z Zhang, LM Sterk, I Vermes, AA Poot, J Feijen, and DW Grijpma. Flexible and elastic porous poly (trimethylene carbonate) structures for use in vascular tissue engineering. *Acta Biomaterialia*, 6(4):1269–1277, 2010.
- [121] Ryan M Stayshich and Tara Y Meyer. New insights into poly (lactic-co-glycolic acid) microstructure: using repeating sequence copolymers to decipher complex nmr and thermal behavior. *Journal of the American Chemical Society*, 132(31):10920–10934, 2010.
- [122] Tetsushi Suyama and Yutaka Tokiwa. Enzymatic degradation of an aliphatic polycarbonate, poly(tetramethylene carbonate). *Enzyme and Microbial Technology*, 20(2):122–126, 1997.
- [123] Yasuhiro Takahashi and Ryoji Kojima. Crystal structure of poly(trimethylene carbonate). *Macromolecules*, 36(14):5139–5143, 2003.
- [124] JA Tamada and R Langer. Erosion kinetics of hydrolytically degradable polymers. *Proceedings of the National Academy of Sciences*, 90(2):552–556, 1993.

- [125] Varawut Tangpasuthadol, Sanyog M Pendharkar, and Joachim Kohn. Hydrolytic degradation of tyrosine-derived polycarbonates, a class of new biomaterials. part i: Study of model compounds. *Biomaterials*, 21(23):2371–2378, 2000.
- [126] Varawut Tangpasuthadol, Sanyog M Pendharkar, Richard C Peterson, and Joachim Kohn. Hydrolytic degradation of tyrosine-derived polycarbonates, a class of new biomaterials. part ii: 3-yr study of polymeric devices. *Biomaterials*, 21(23):2379–2387, 2000.
- [127] Sarah Tempelaar, Laetitia Mespouille, Philippe Dubois, and Andrew P Dove. Organocatalytic synthesis and postpolymerization functionalization of allyl-functional poly(carbonate)s. *Macromolecules*, 44(7):2084–2091, 2011.
- [128] Xinming Tong, Bao-hua Guo, and Yanbin Huang. Toward the synthesis of sequence-controlled vinyl copolymers. *Chemical Communications*, 47(5):1455–1457, 2011.
- [129] Pietro Tundo and Maurizio Selva. The chemistry of dimethyl carbonate. *Accounts of Chemical Research*, 35(9):706–716, 2002.
- [130] Kathryn E Uhrich, Scott M Cannizzaro, Robert S Langer, and Kevin M Shakesheff. Polymeric systems for controlled drug release. *Chemical Reviews*, 99(11):3181–3198, 1999.
- [131] Tadao Uyehara, Naoki Chiba, Ichiro Suzuki, and Yoshinori Yamamoto. Diastereoselective intramolecular diels-alder reaction of n-alkoxycarbonyl-1-aza-1,3-butadienes and a total synthesis of the piperidine alkaloid,(±)-sedridine. *Tetrahedron Letters*, 32(34):4371–4374, 1991.
- [132] Selim Uzunoglu, Burcak Karaca, Harika Atmaca, Asli Kisim, Canfeza Sezgin, Bulent Karabulut, and Ruchan Uslu. Comparison of xtt and alamar blue assays

- in the assessment of the viability of various human cancer cell lines by at-101 (-/-gossypol). *Toxicology Mechanisms and Methods*, 20(8):482–486, 2010.
- [133] Andres Villalpando, Caitlan E Ayala, Christopher B Watson, and Rendy Kartika. Triphosgene–amine base promoted chlorination of unactivated aliphatic alcohols. *The Journal of Organic Chemistry*, 78(8):3989–3996, 2013.
- [134] Patrick Vlieghe, Frédéric Bihel, Thierry Clerc, Christophe Pannecouque, Myriam Witvrouw, Erik De Clercq, Jean-Pierre Salles, Jean-Claude Chermann, and Jean-Louis Kraus. New 3'-azido-3'-deoxythymidin-5'-yl o-( $\omega$ -hydroxyalkyl) carbonate prodrugs: synthesis and anti-hiv evaluation. *Journal of Medicinal Chemistry*, 44(5):777–786, 2001.
- [135] DF Williams. Enzymic hydrolysis of polylactic acid. *Engineering in Medicine*, 10(1):5–7, 1981.
- [136] Koichi Yamashita, Yoshihiro Kikkawa, Kenji Kurokawa, and Yoshiharu Doi. Enzymatic degradation of poly (l-lactide) film by proteinase k: quartz crystal microbalance and atomic force microscopy study. *Biomacromolecules*, 6(2):850–857, 2005.
- [137] Yusuke Yamazaki, Kasumi Kakuma, Ya Du, and Susumu Saito. Synthesis of carbonates directly from 1 atm co<sub>2</sub> and alcohols using ch<sub>2</sub>cl<sub>2</sub>. *Tetrahedron*, 66(51):9675–9680, 2010.
- [138] Chun Yu and Joachim Kohn. Tyrosine–peg-derived poly (ether carbonate) s as new biomaterials: part i: synthesis and evaluation. *Biomaterials*, 20(3):253–264, 1999.
- [139] Xiaoyan Yuan, Arthur FT Mak, KW Kwok, Brian KO Yung, and Kangde Yao. Characterization of poly (l-lactic acid) fibers produced by melt spinning. *Journal of Applied Polymer Science*, 81(1):251–260, 2001.

- [140] Heng Zhang and Mark W Grinstaff. Synthesis of atactic and isotactic poly(1,2-glycerol carbonate)s: Degradable polymers for biomedical and pharmaceutical applications. *Journal of the American Chemical Society*, 135(18):6806–6809, 2013.
- [141] Zheng Zhang, Roel Kuijer, Sjoerd K Bulstra, Dirk W Grijpma, and Jan Feijen. The *in vivo* and *in vitro* degradation behavior of poly(trimethylene carbonate). *Biomaterials*, 27(9):1741–1748, 2006.
- [142] Q Zhao, N Topham, JM Anderson, A Hiltner, G Lodoen, and CR Payet. Foreign-body giant cells and polyurethane biostability: In vivo correlation of cell adhesion and surface cracking. *Journal of Biomedical Materials Research*, 25(2):177–183, 1991.
- [143] KJ Zhu, RW Hendren, K Jensen, and CG Pitt. Synthesis, properties, and biodegradation of poly(1,3-trimethylene carbonate). *Macromolecules*, 24(8):1736–1740, 1991.
- [144] Nicholas P Ziats, Kathleen M Miller, and James M Anderson. *in vitro* and *in vivo* interactions of cells with biomaterials. *Biomaterials*, 9(1):5–13, 1988.

## Appendices

### Supporting Information Chapter 3

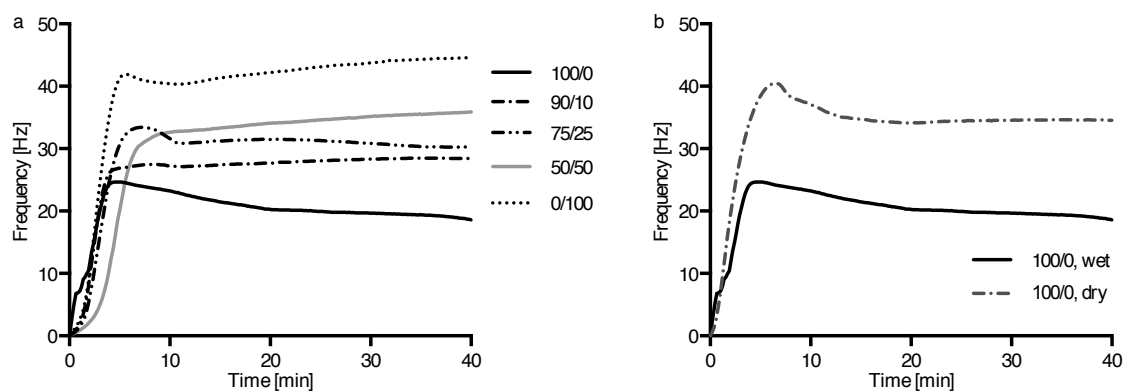
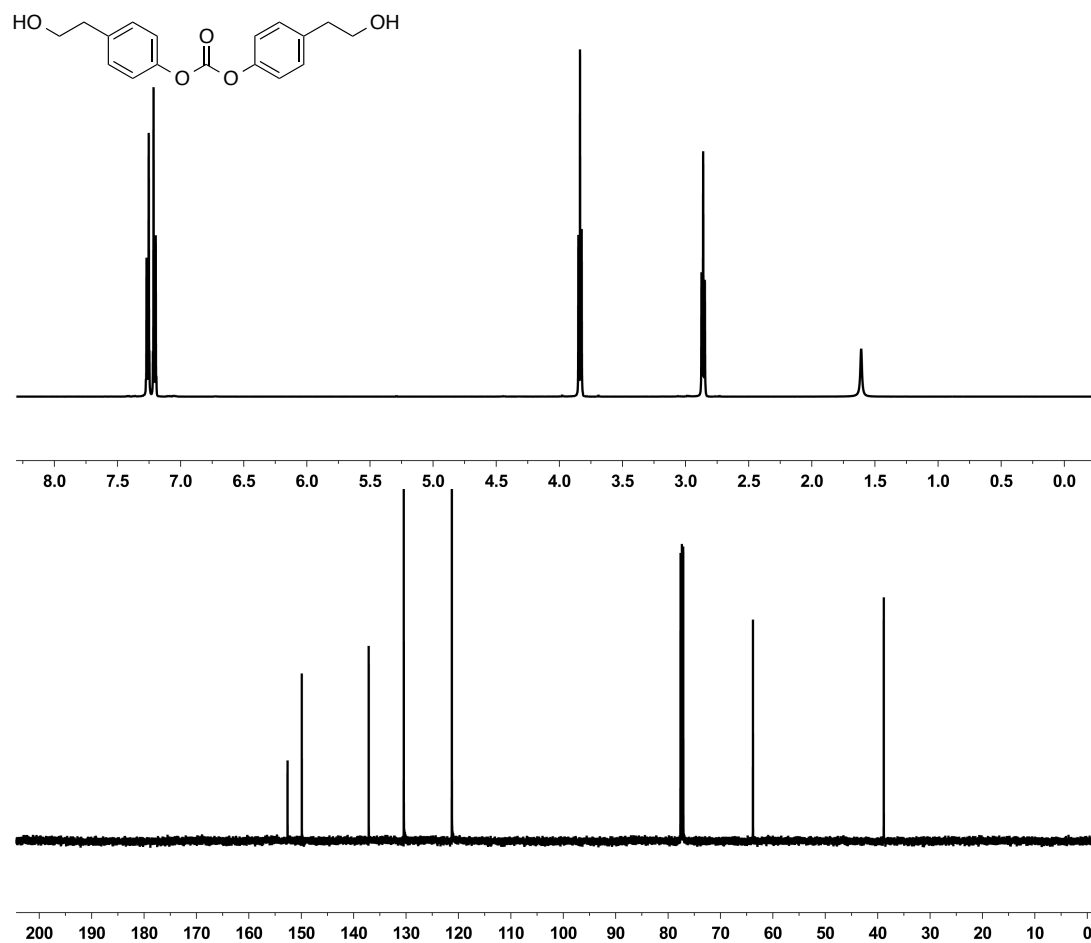


Figure S1: (A) Stress-strain curves of compositions of Ty/ Hva (mol %) 100/0, 90/10, 75/25, 50/50, 0/100 in the wet state, PBS at 37 °C, (B) Stress-strain curves for poly-(tyrosol carbonate) in the dry state at ambient temperature and wet state, PBS at 37 °C.

## Supporting Information Chapter 4

Figure S2: NMR spectra, bis(4-(2-hydroxyethyl)phenyl) carbonate **2a**.

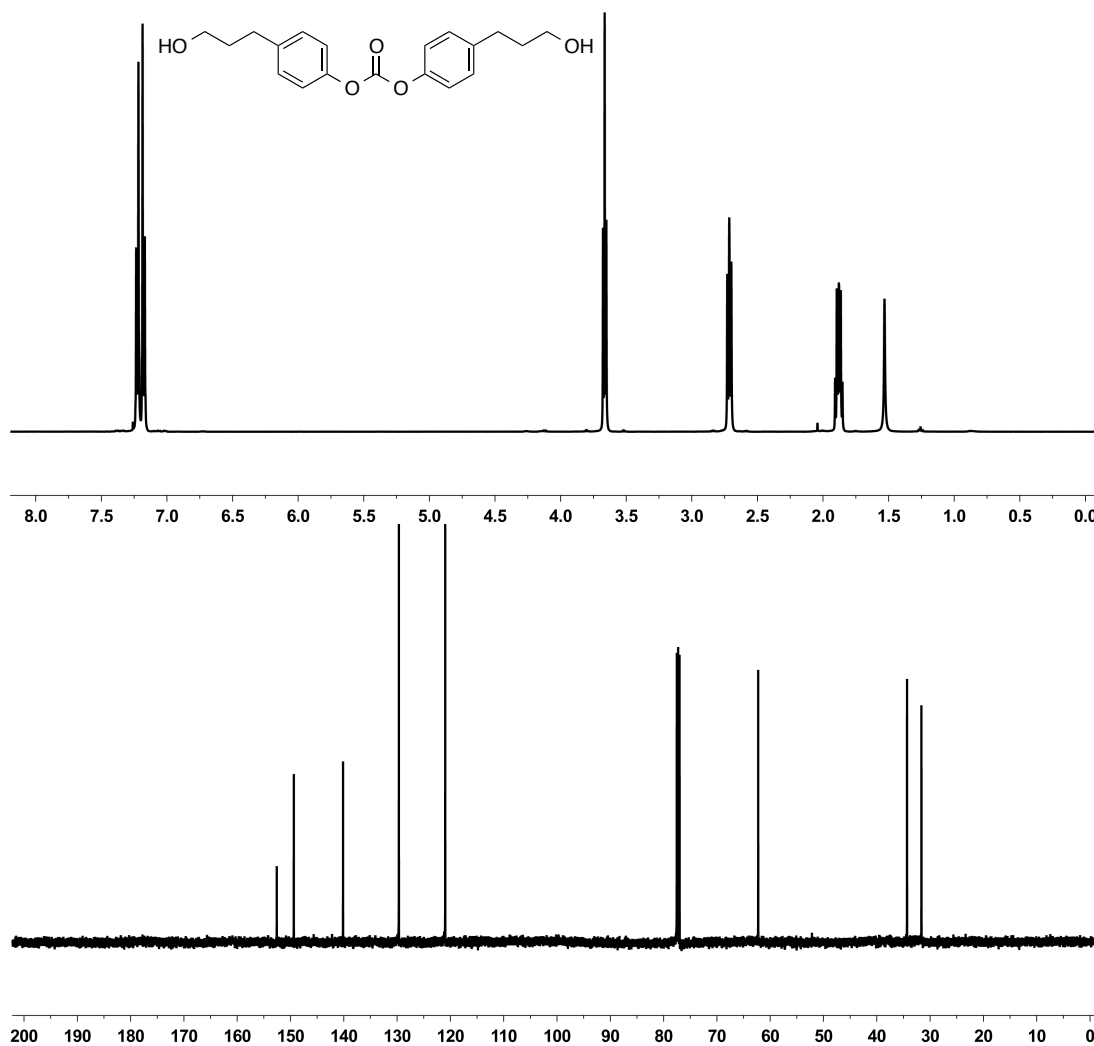


Figure S3: NMR spectra, bis(4-(3-hydroxypropyl)phenyl) carbonate **2b**.



Figure S4: NMR spectra, bis(4-(2-hydroxyethyl)-2-methoxyphenyl) carbonate **2c**.

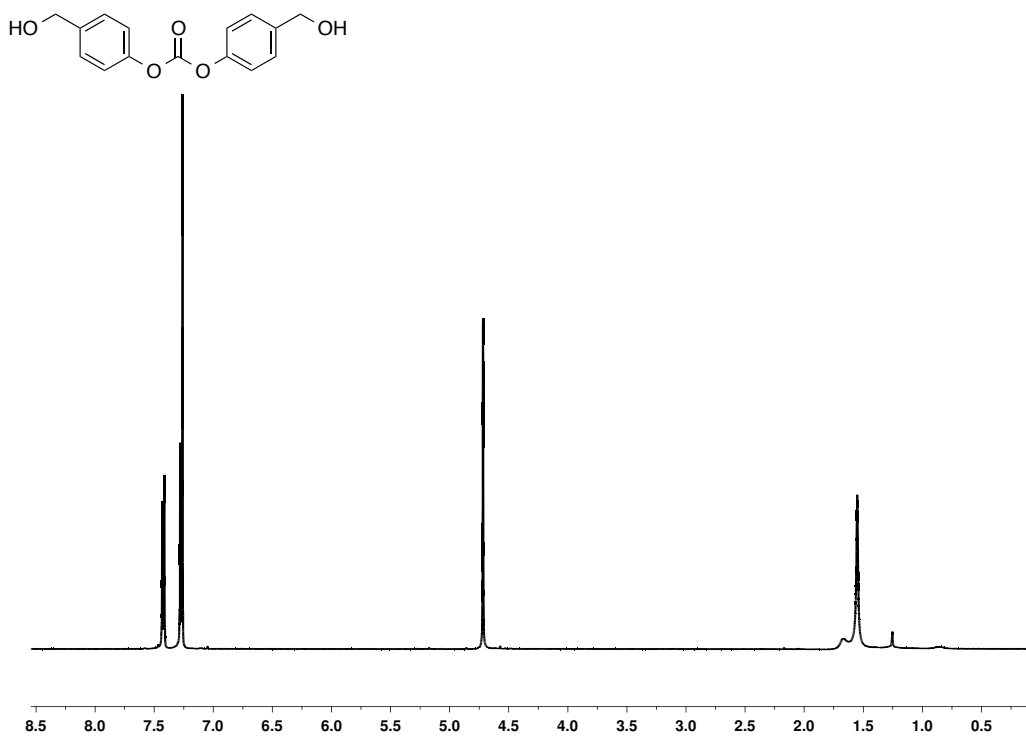


Figure S5: NMR spectra, bis(4-(2-hydroxymethyl)phenyl) carbonate **2e**.

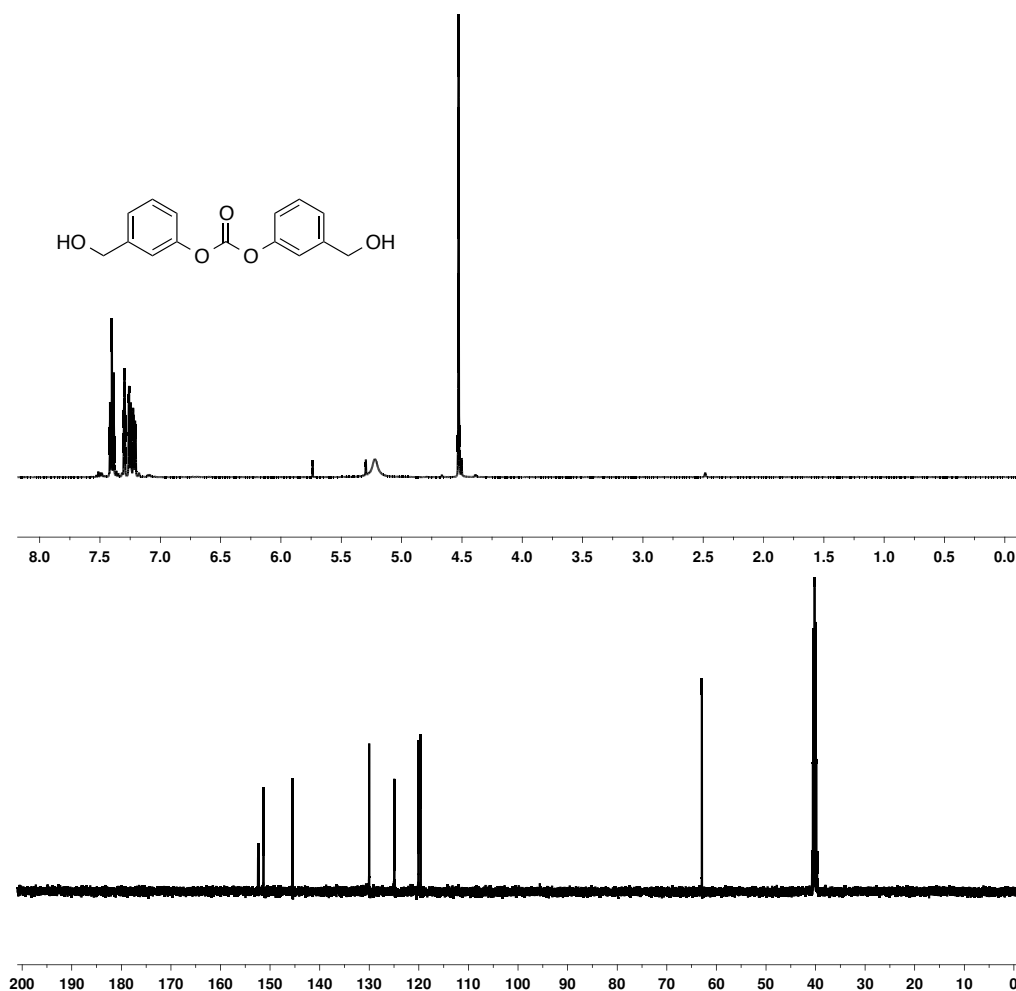


Figure S6: NMR spectra, bis(4-(3-hydroxymethyl)phenyl) carbonate **2f**.

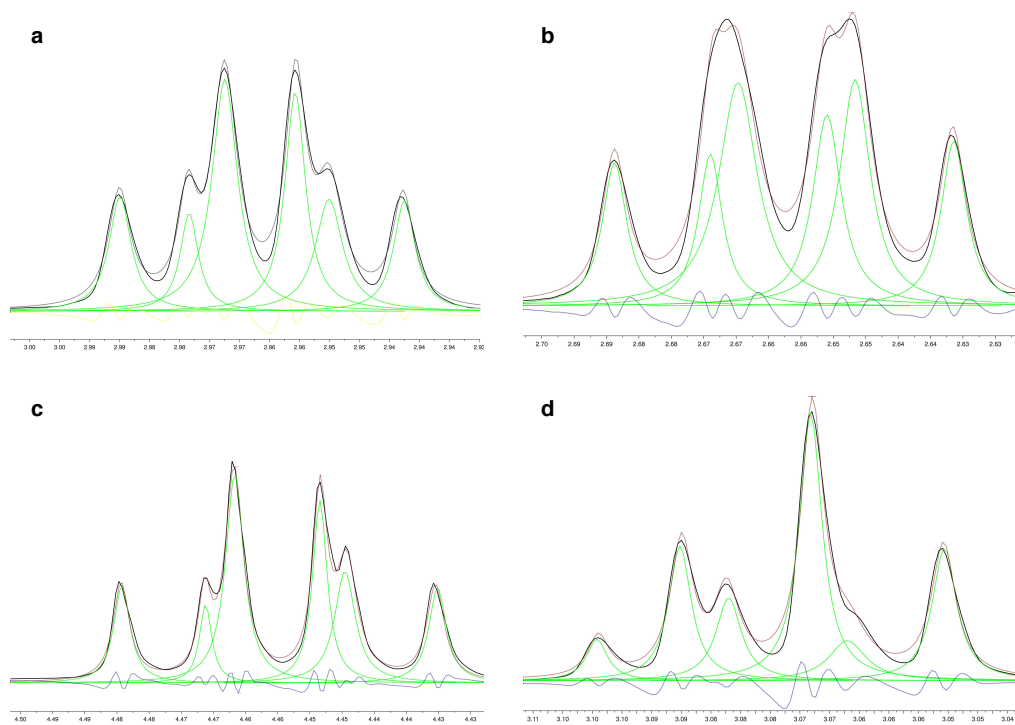


Figure S7:  $^1\text{H}$  NMR (400 MHz,  $\text{CDCl}_3$ ): Global spectral deconvolution of of chloroformate and trichloromethyl carbonate species formed *in situ*. Compounds (A) **3a** and **3a\***, (B) **3b** and **3b\***, (C) **3c** and **3c\***, (D) **3d** and **3d\***.

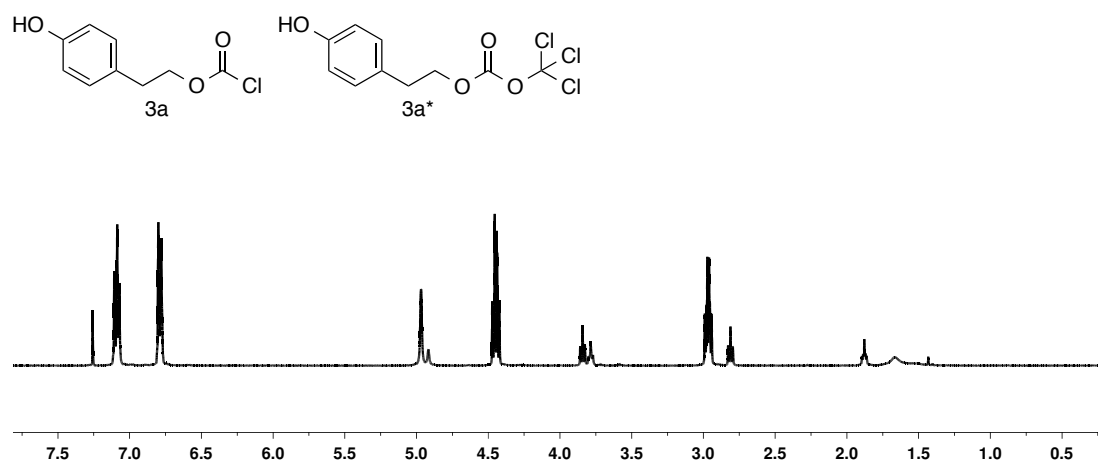


Figure S8: NMR spectra, 4-hydroxyphenethyl carbonochloridate **3a** and 4-hydroxyphenethyl(trichloromethyl)carbonate **3a\***.

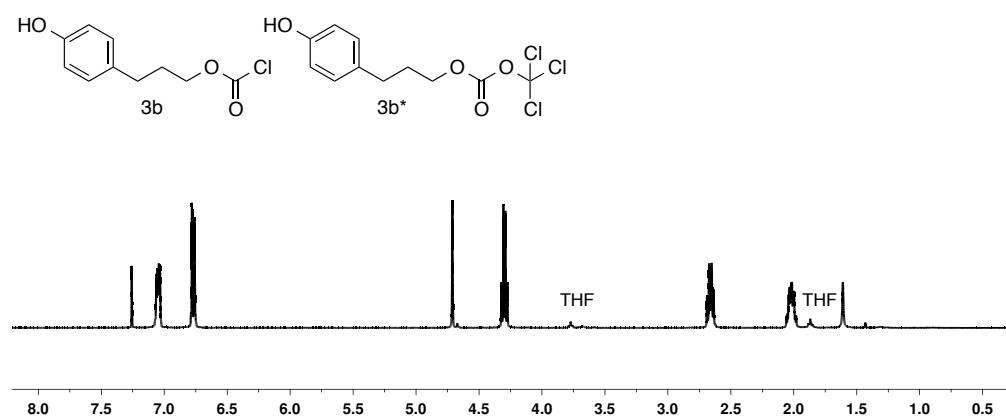


Figure S9: NMR spectra, 3-(4-hydroxyphenyl)propyl carbonochloridate **3b** and 3-(4-hydroxyphenyl)propyl(trichloromethyl)carbonate **3b\***.

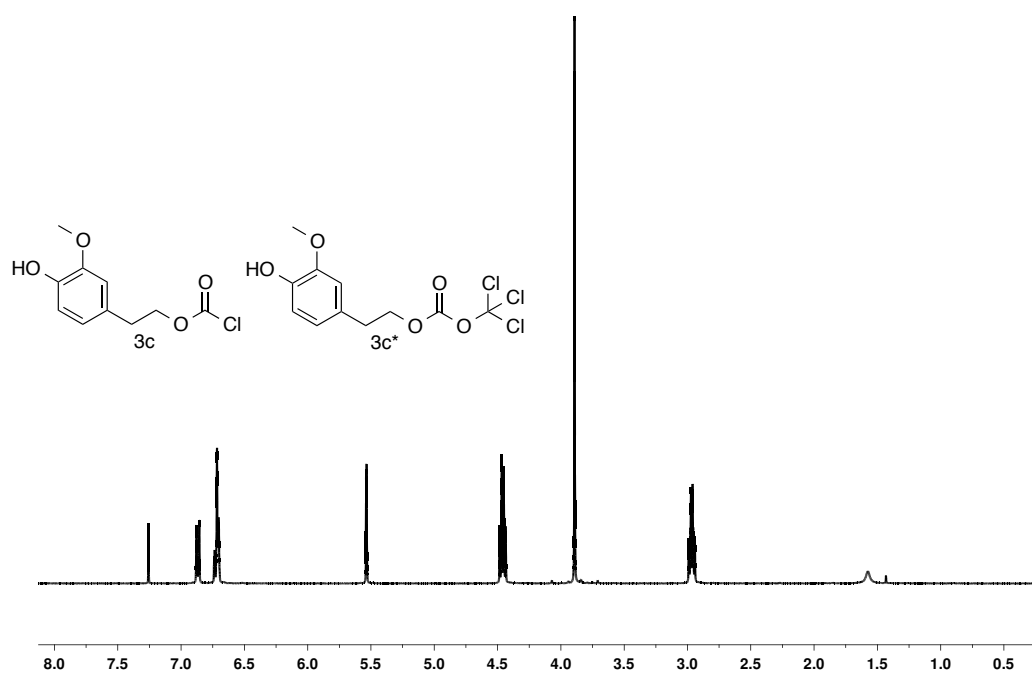


Figure S10: NMR spectra compounds, 4-hydroxy-3-methoxyphenethyl carbonochloridate **3c** and 4-hydroxy-3-methoxyphenethyl(trichloromethyl)carbonate **3c\***.

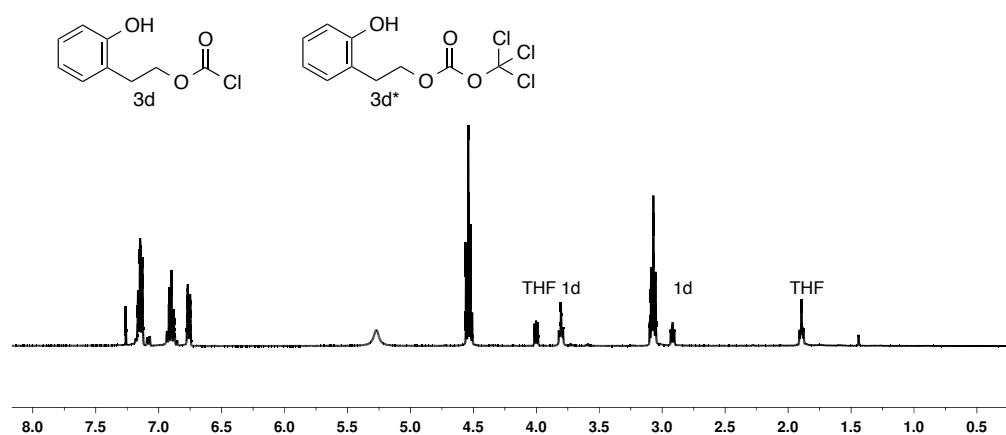


Figure S11: NMR spectra, 2-hydroxyphenethyl carbonochloridate **3d** and 2-hydroxyphenethyl(trichloromethyl)carbonate **3d\***.



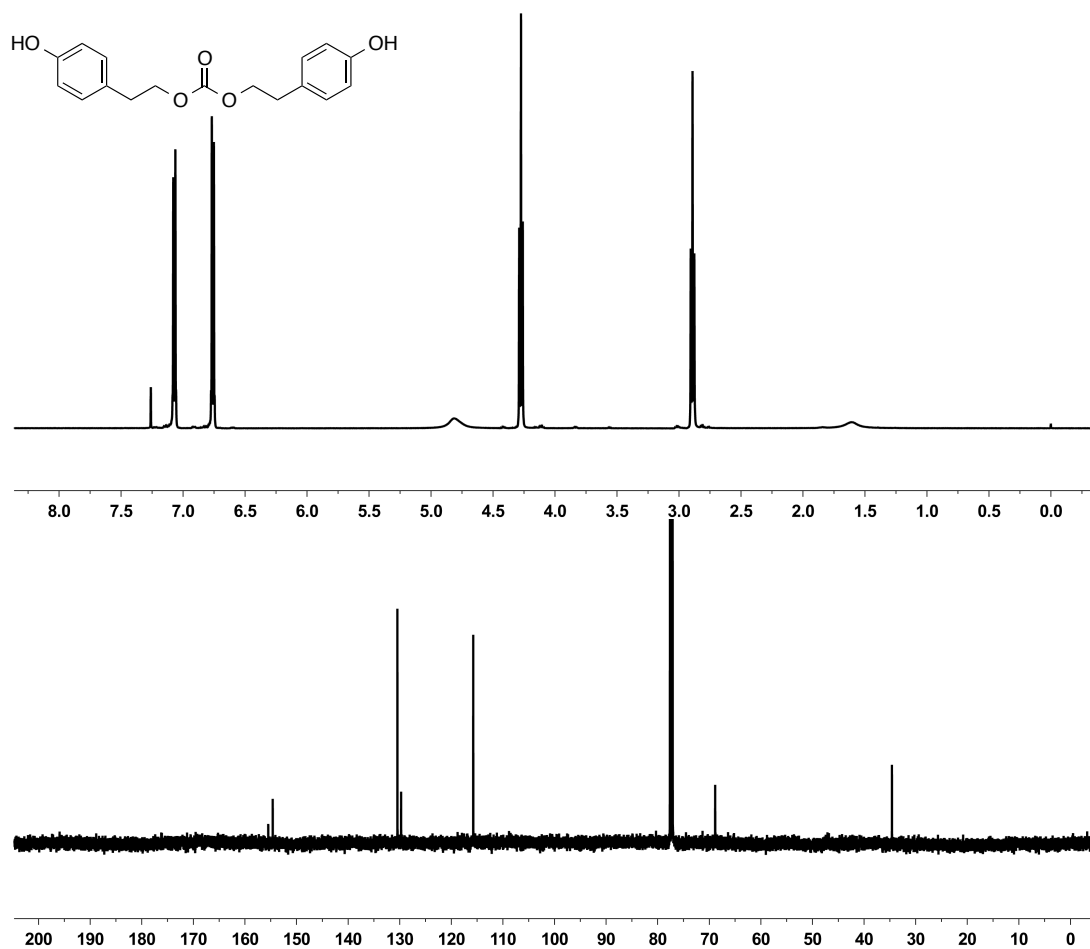


Figure S12: NMR spectra, bis(4-hydroxyphenethyl) carbonate **4a**.

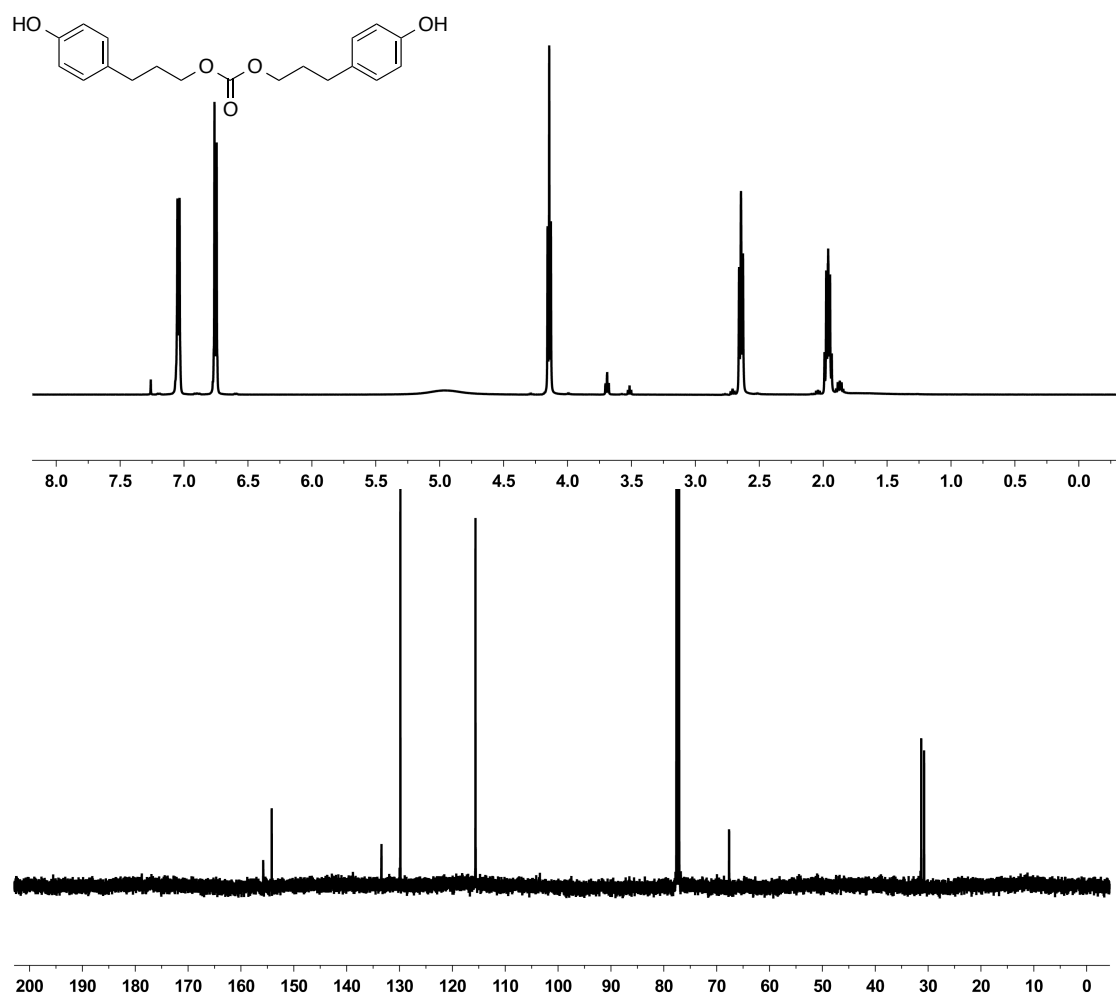


Figure S13: NMR spectra, bis(3-(4-hydroxyphenyl)propyl) carbonate **4b**.

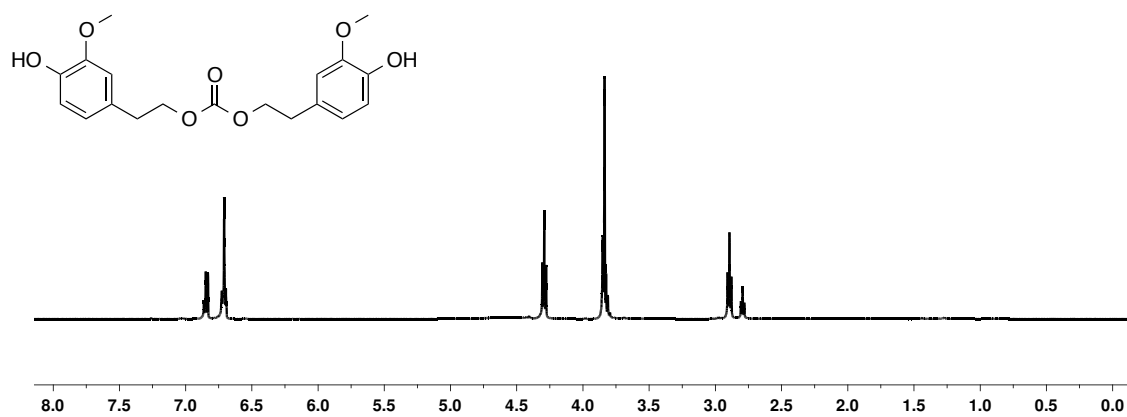


Figure S14: NMR spectra, bis(4-hydroxy-3-methoxyphenethyl) carbonate **4c**.

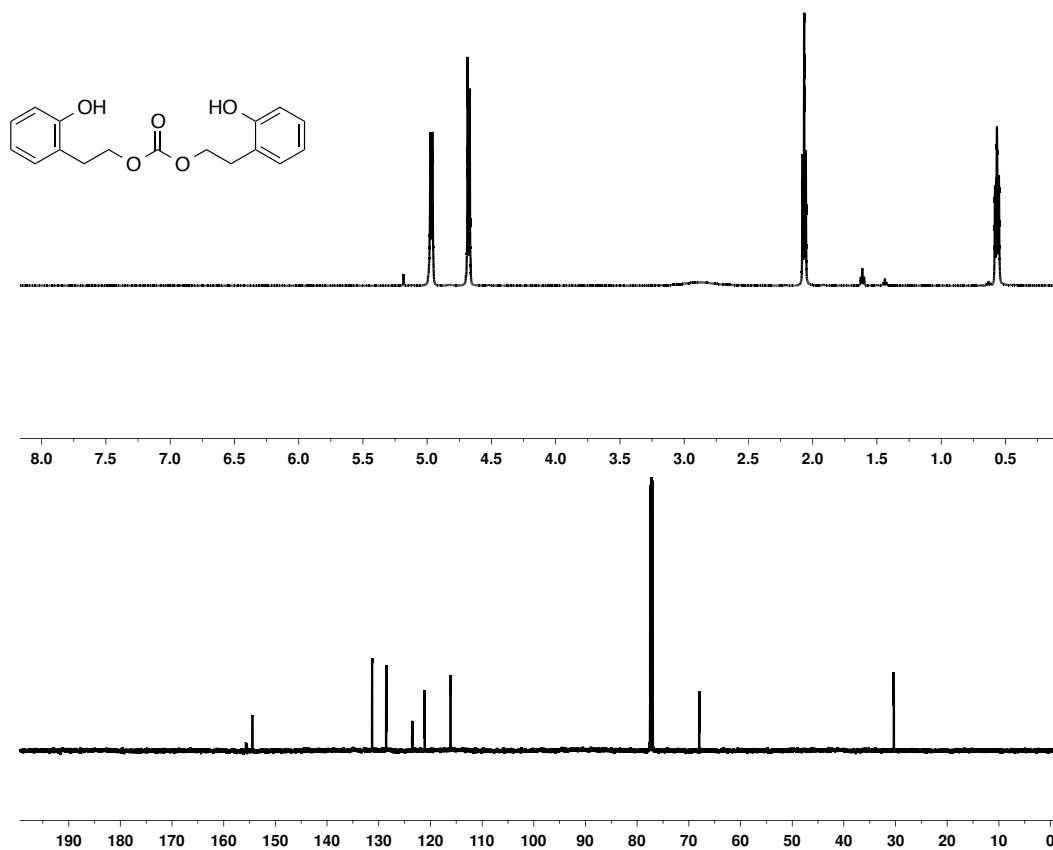


Figure S15: NMR spectra, bis(2-hydroxyphenethyl) carbonate **4d**.

## Supporting Information Chapter 6

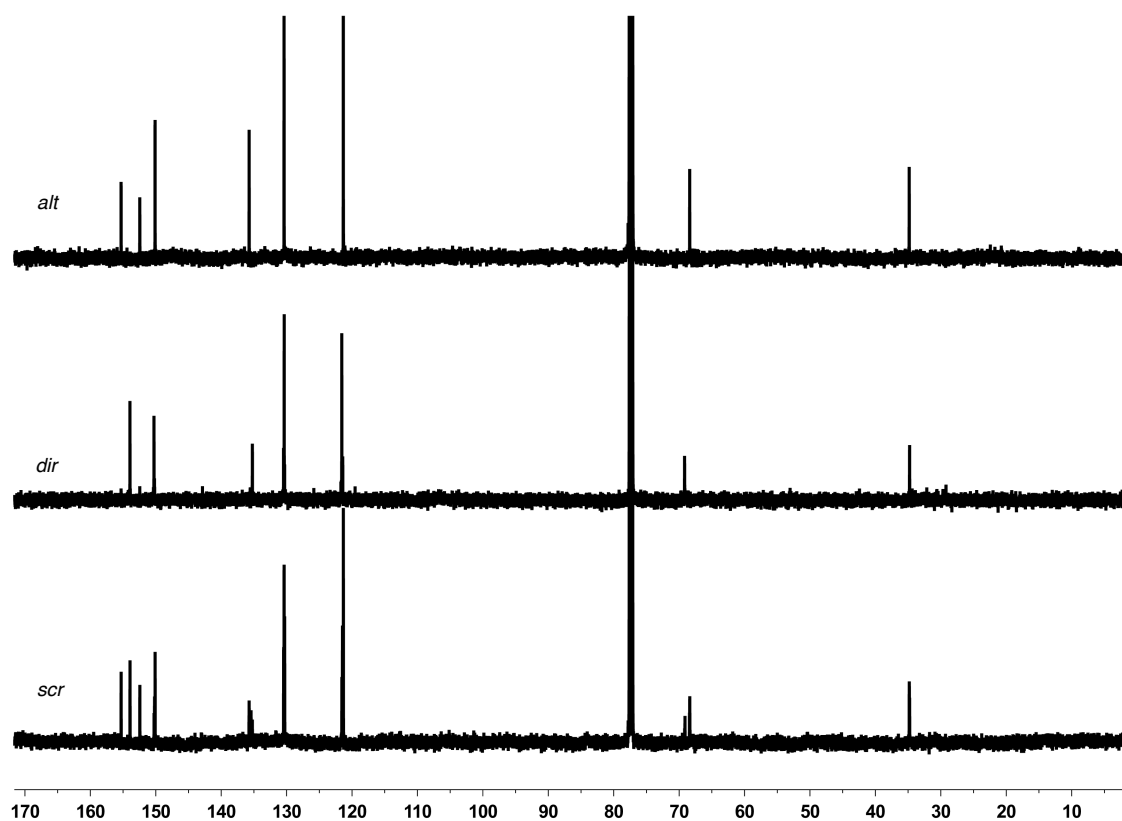


Figure S16:  $^{13}\text{C}$  NMR spectra (126 MHz,  $\text{CDCl}_3$ ) of poly(tyrosol carbonate): (Top) *alt*, (middle) *dir*, (bottom) *scr*. Full spectrum overlay.

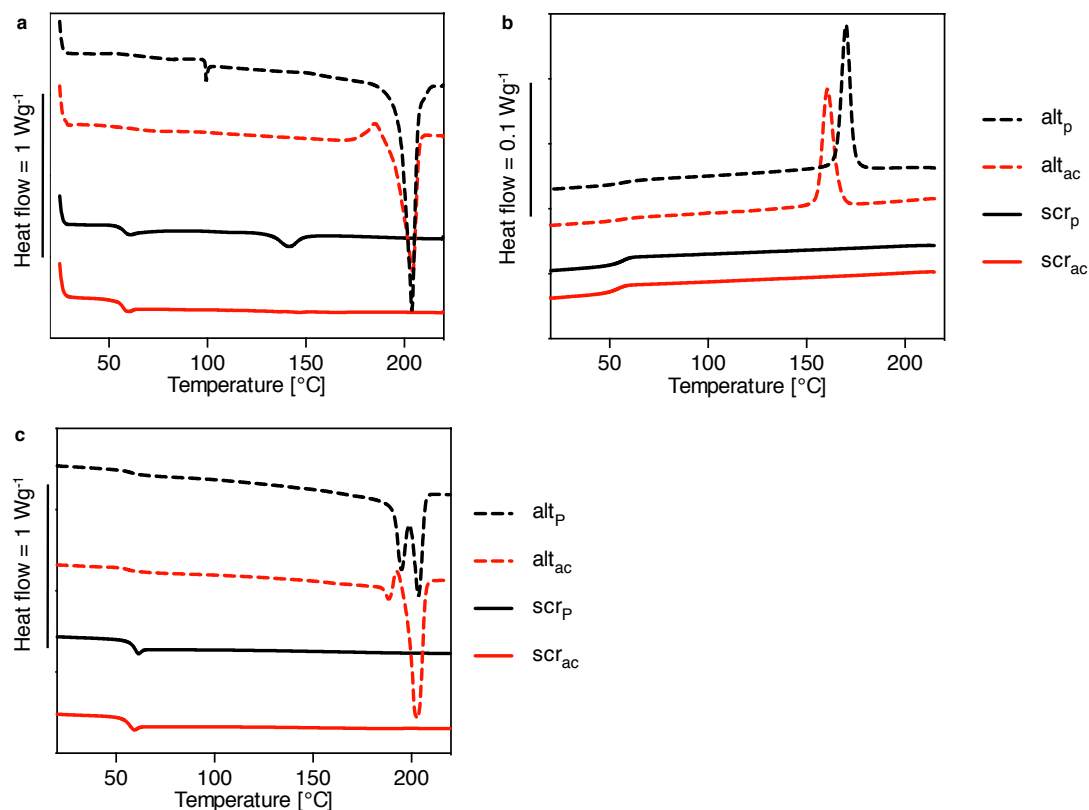


Figure S17: DSC scans of polymer powder and ambient cooled polycarbonate films of *scr* and *alt*: (A) First heating, (B) cooling, (C) second heating. Rate = 10 °C min<sup>-1</sup>, exotherm up.

Table 4: Summary of Thermal and crystalline properties of *scr* and *alt*, controls powder and ambient cooled films.

Polymer	Condition	$T_g$ (°C)	$T_m$ (°C)	$\chi$	Crystallite
		dry	(°C)	(%)	Size (Å)
<i>alt</i>	Powder	-	205	46.3	114
	Ambient	59	205	31.4	218
<i>scr</i>	cool				
	Powder	57	142	1.5	19
	Ambient	56	-	-	-

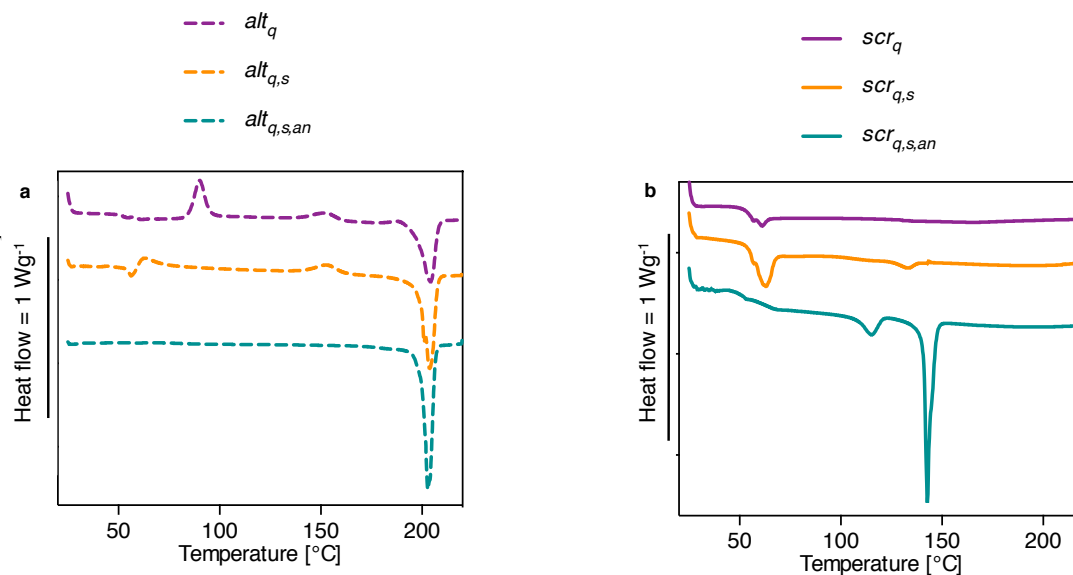


Figure S18: DSC scans of oriented polycarbonate films: (A) *alt*, (B) *scr*. First heating scans of quenched, stretched, stretched & annealed films, rate = 10 °C min<sup>-1</sup>, exotherm up.

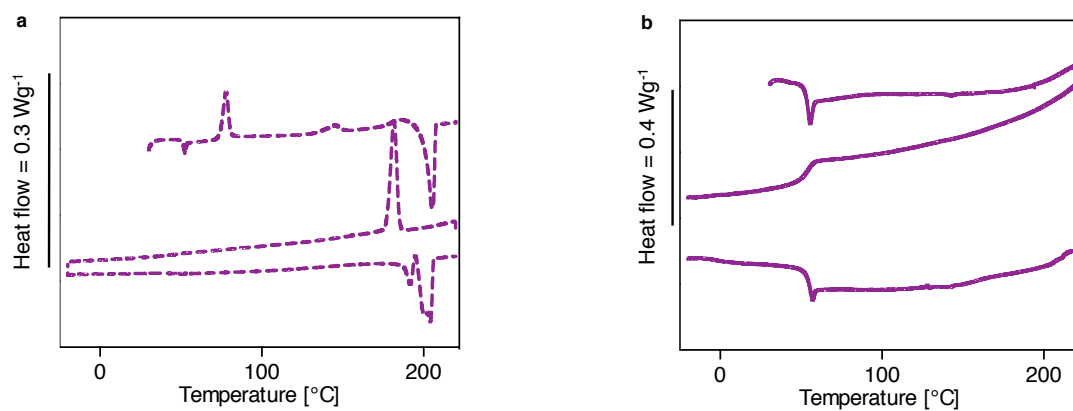


Figure S19: DSC slow scans of quenched polycarbonate films: (A) *alt*, (B) *scr*. First heating, cooling and second heating, rate = 1 °C min<sup>-1</sup>, exotherm up.

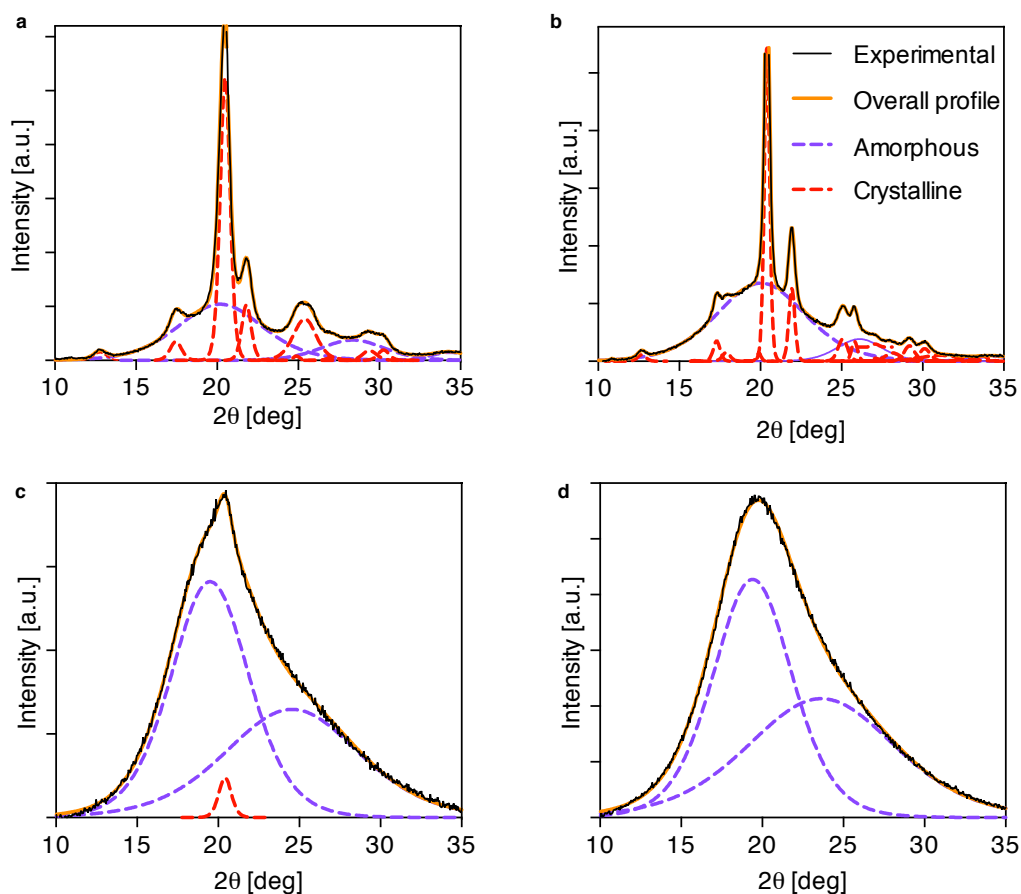


Figure S20: Powder X-ray diffraction patterns of poly(tyrosol carbonate): (Top) *alt*, (bottom) *scr*, (A) and (C) polymer powder, (B) and (D) ambient cooled films.

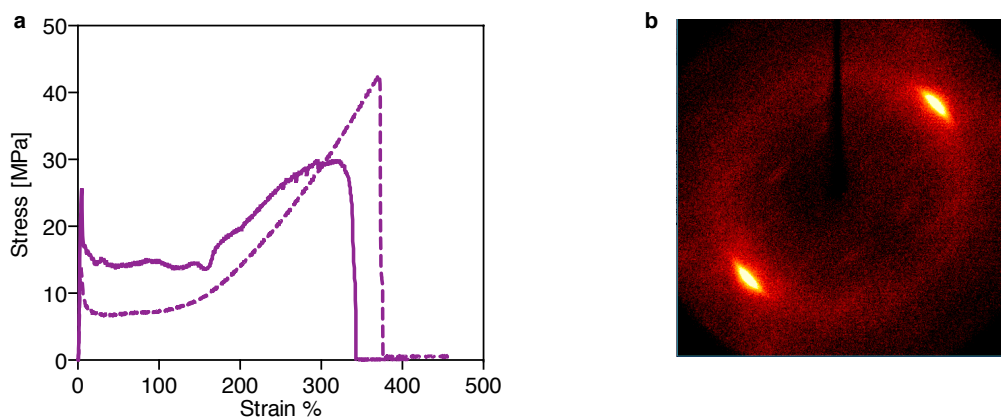


Figure S21: (A) Stress-strain curve of films of *alt* and *scr* at  $T_{g,wet}$ , (B) X-ray diffraction in 2-D of *alt*, quenched and stretched.



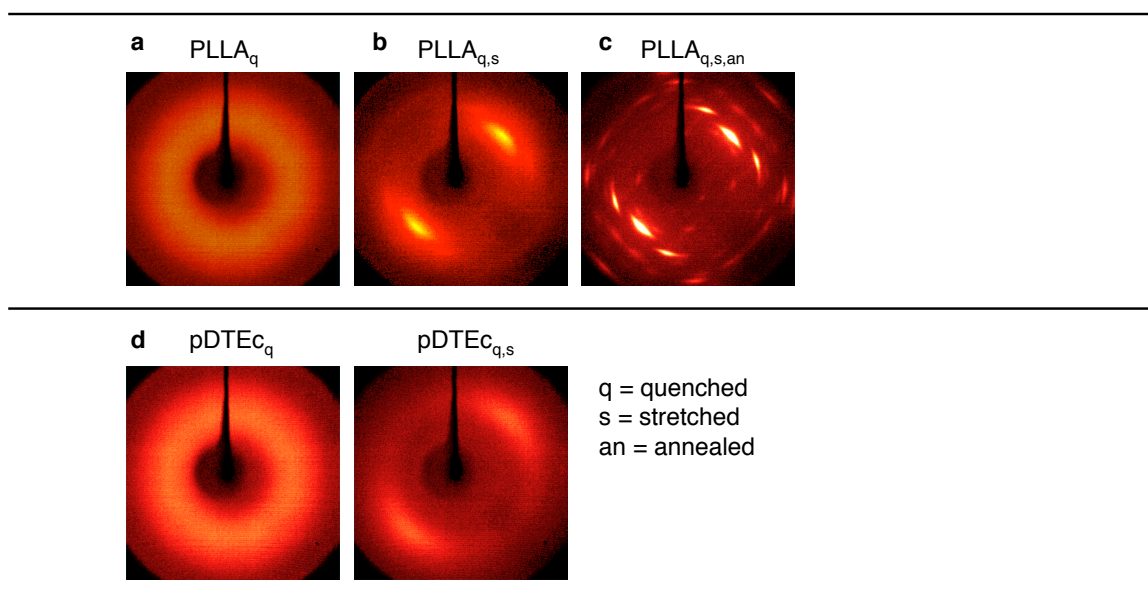


Figure S22: X-ray diffraction in 2-D of films of control polymers: (Top) PLLA, (bottom) poly(DTE carbonate), (A) and (D) quenched, (B) and (E) quenched and stretched, (C) quenched, annealed and stretched.

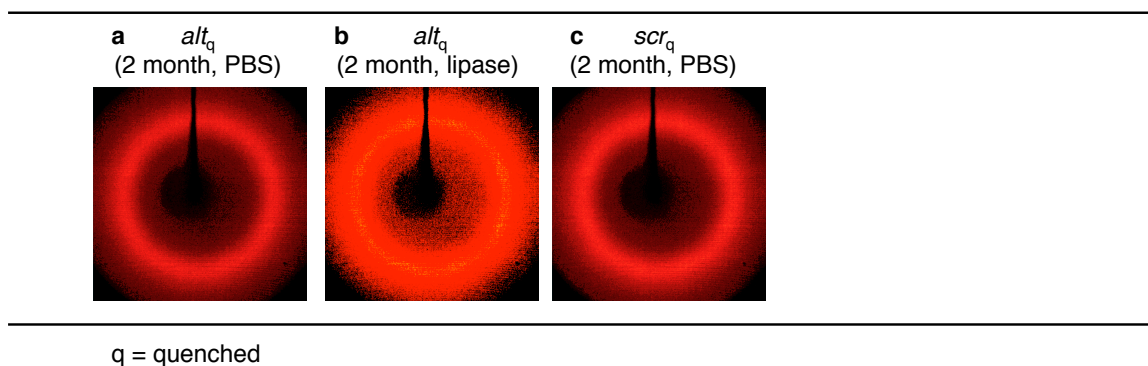


Figure S23: X-ray diffraction in 2-D of quenched films from poly(tyrosol carbonate) over time: (A) *alt*, 2 months in PBS (B) *scr*, 2 months in lipase (C) *scr*, 2 months in PBS.

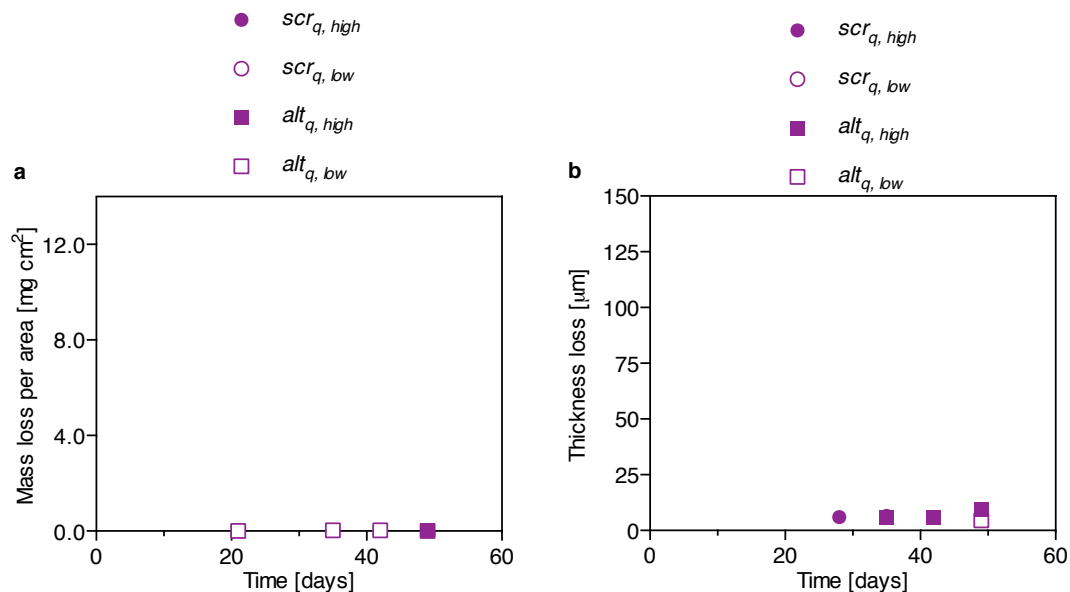


Figure S24: (A) Mass loss per area. (B) Thickness loss, incubation at 37 °C in PBS as control.

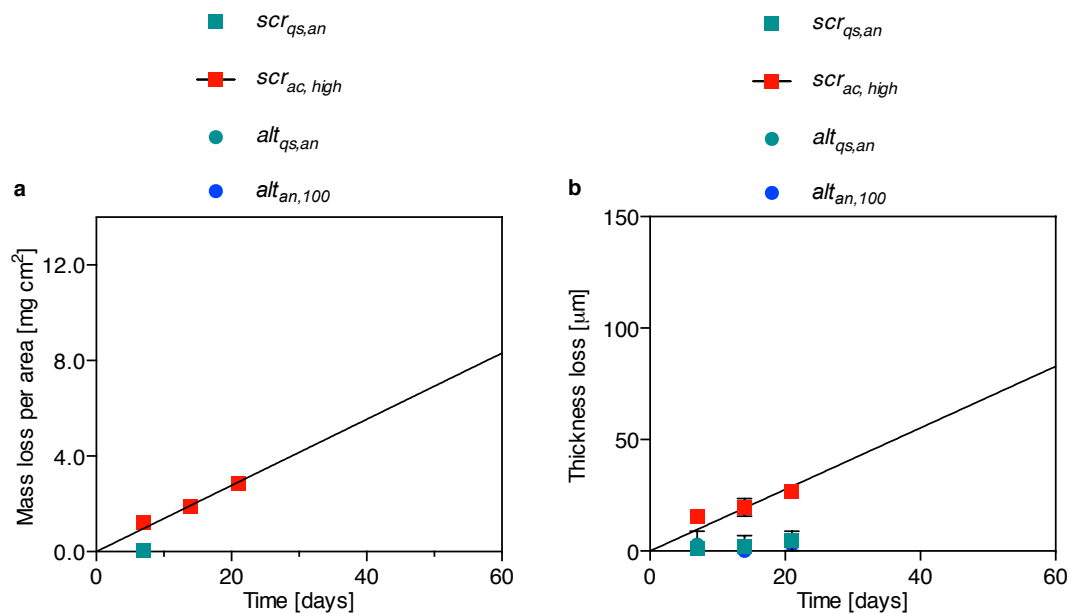


Figure S25: (A) Mass loss per area. (B) Thickness loss of *alt* or *scr* films: quenched, stretched and annealed or ambient cooled in lipase solution incubation at 37 °C in lipase solutions.

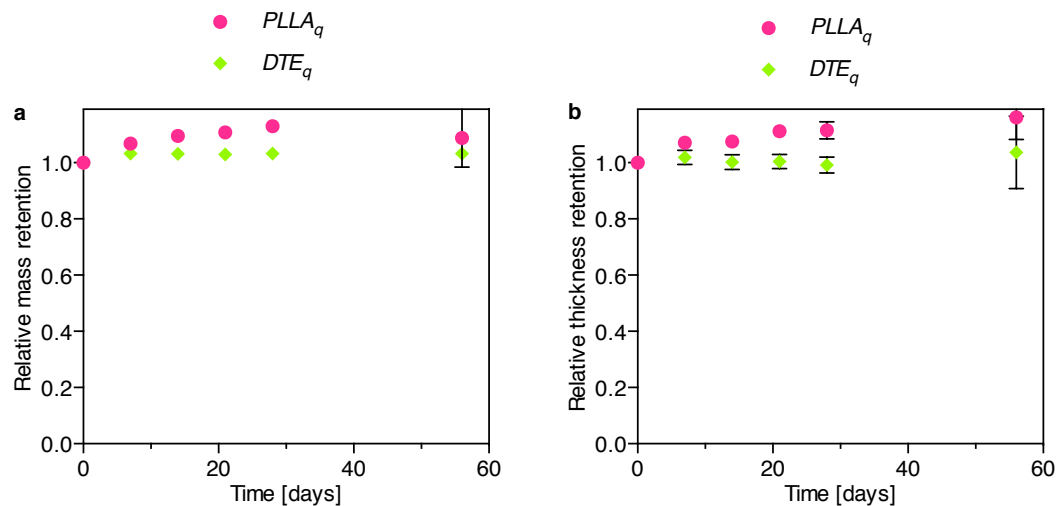


Figure S26: Bioerosion control of quenched, compression molded films from PLLA and poly(DTE carbonate)(A) Relative mass retention. (B) Relative thickness retention at 37 °C in lipase solutions.

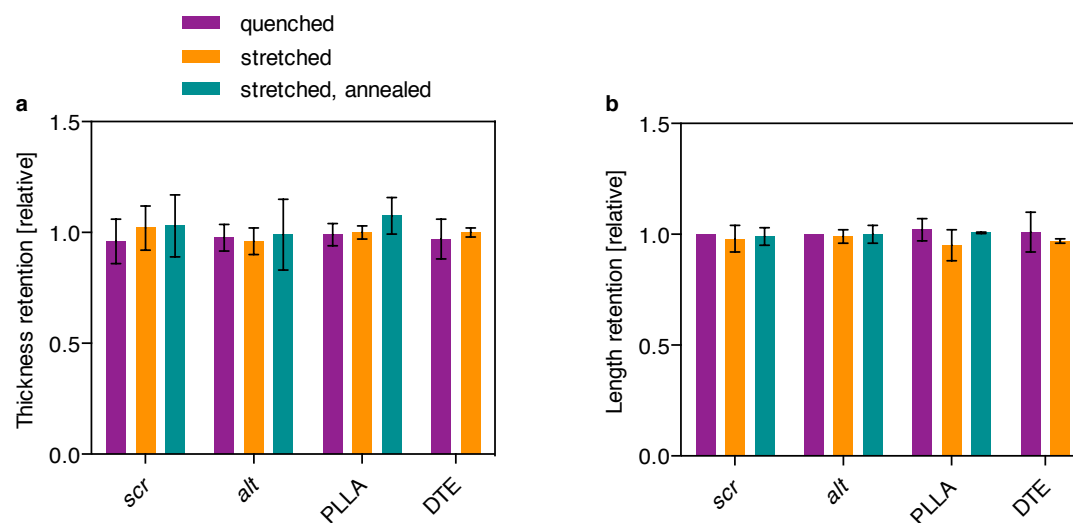


Figure S27: Dimensional stability of *alt* and *scr* polymer films, PLLA, poly(DTE) carbonate controls (A) Retention of thickness, (B) Retention of length cool; after 8 week incubation in PBS at 37 °C.

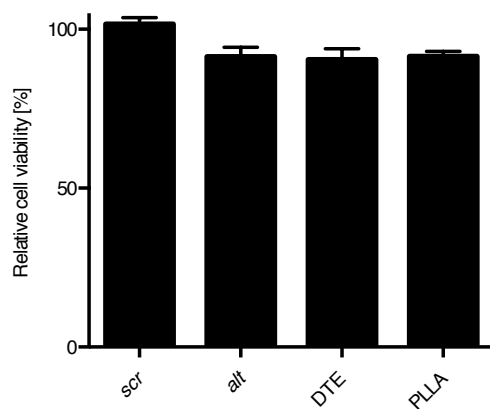


Figure S28: Relative cell viability of polycarbonate films with *alt* or *scr* sequence

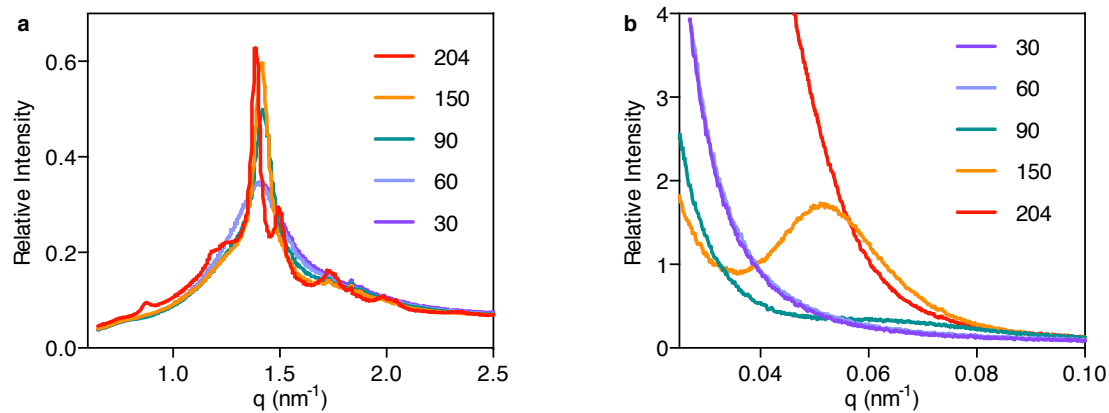


Figure S29: (A) SAXS and (B) WAXS scans of  $alt_q$ , simultaneous experiment during heating, rate =  $10\text{ }^{\circ}\text{C min}^{-1}$ , exotherm up.

## Supporting Information Chapter 7

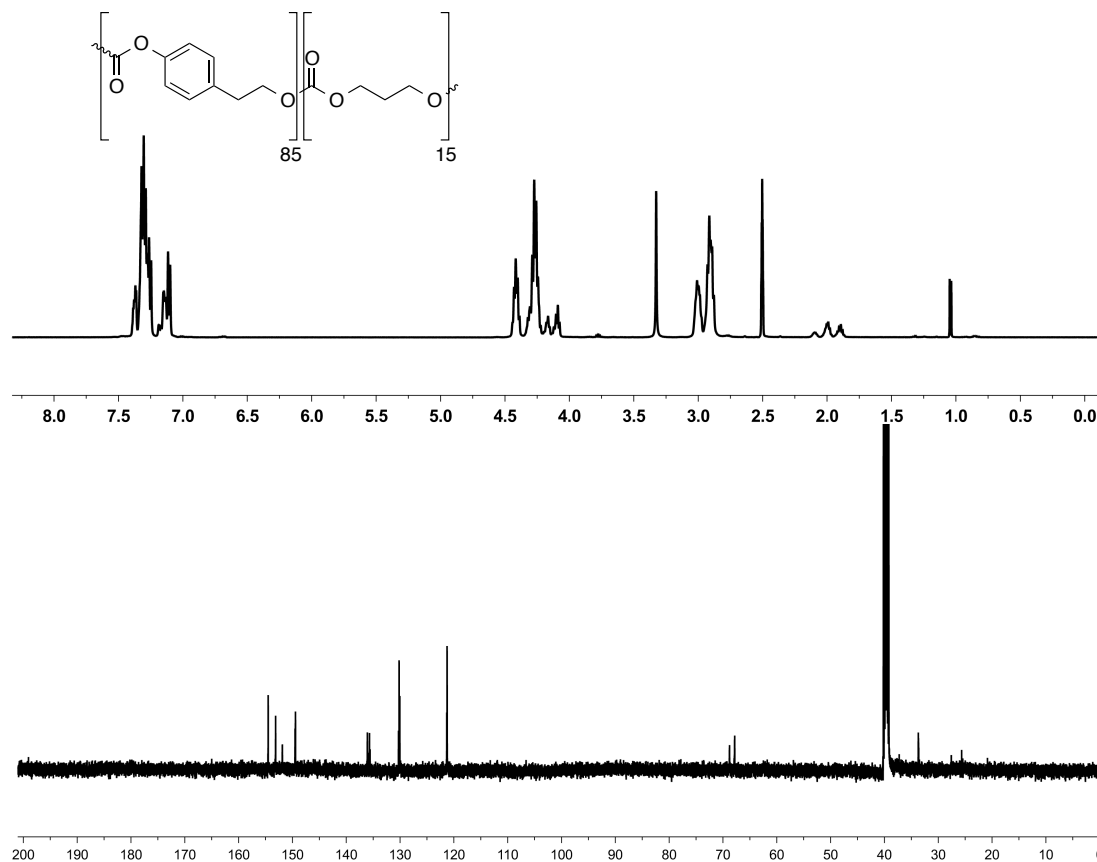


Figure S30:  $^1\text{H}$  NMR (500 MHz,  $\text{DMSO-}d^6$ ) spectrum: poly(tyrosol-*co*-1,3-propanediol carbonate) with 85/15 molar ratio of Ty/PD.

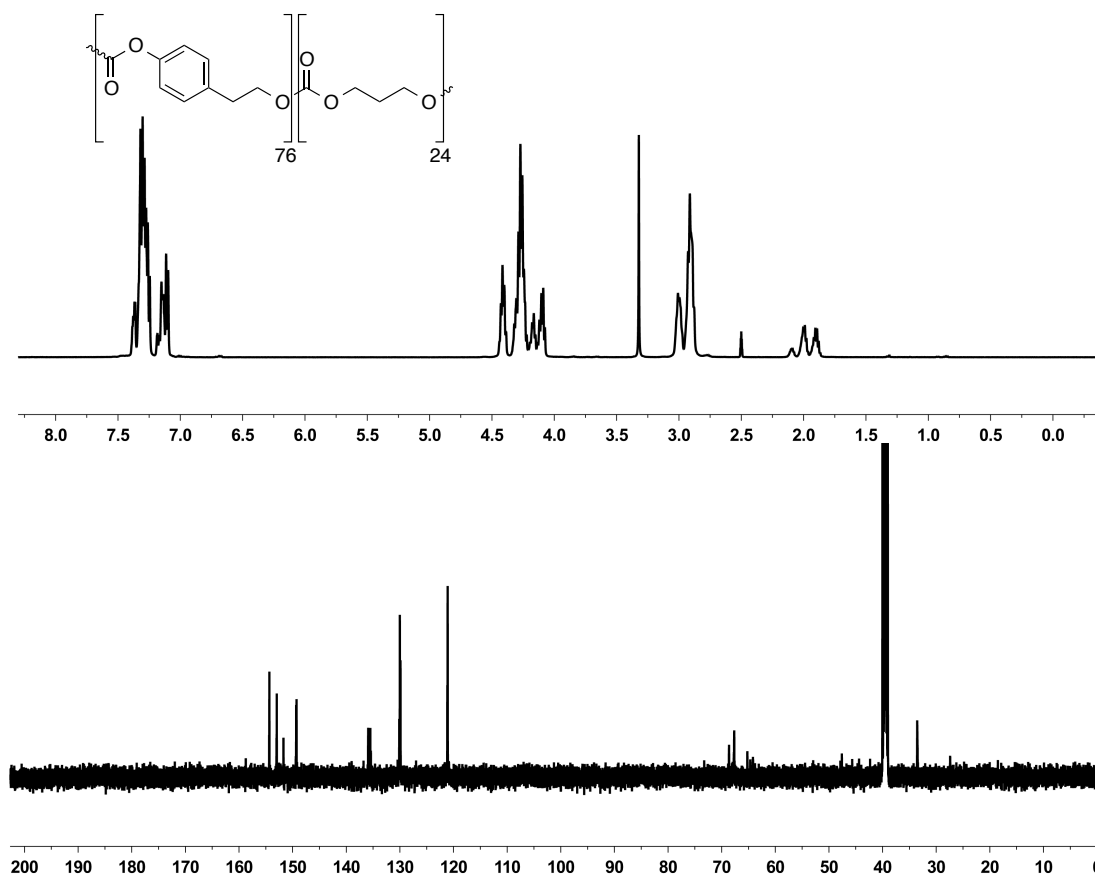


Figure S31:  $^1\text{H}$  NMR (500 MHz,  $\text{DMSO-}d^6$ ) spectrum: poly(tyrosol-co-1,3-propanediol carbonate) with 76/24 molar ratio of Ty/PD.

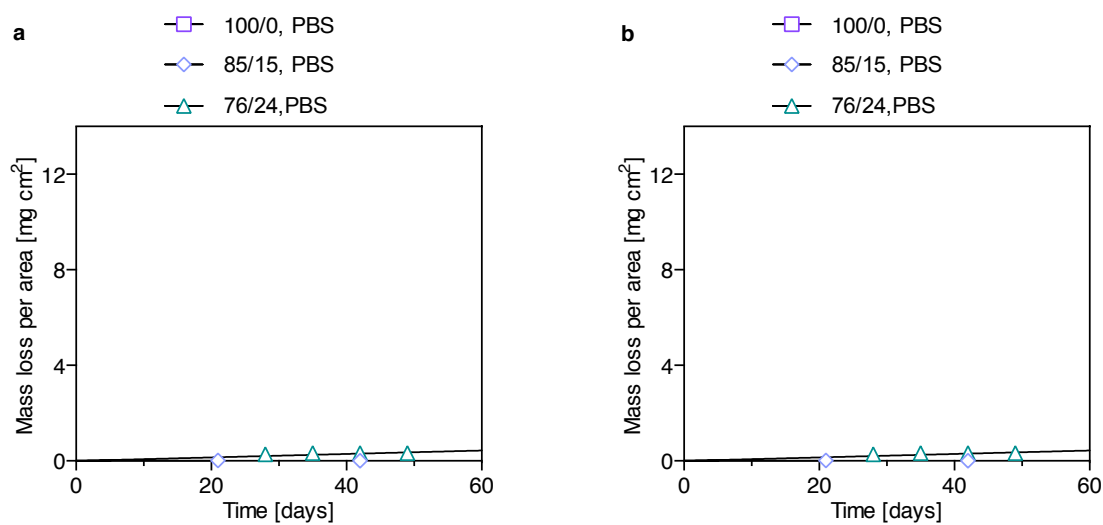


Figure S32: Bioerosion of Ty/PD: (A) Mass loss per area, (B) thickness loss, incubation in PBS at 37 °C.